Design of Mobile Radio Channel Simulators Using the Iterative Nonlinear Least Square Approximation Method with Applications in Vehicle-to-X Communications

Akmal Fayziyev

Design of Mobile Radio Channel Simulators Using the Iterative Nonlinear Least Square Approximation Method with Applications in Vehicle-to-X Communications

Doctoral Dissertation for the Degree *Philosophiae Doctor (PhD)* in
Information and Communication Technology

University of Agder
Faculty of Engineering and Science
2015

Doctoral Dissertations at the University of Agder 104
ISBN: 978-82-7117-790-4
ISSN: 1504-9272

Printed in the Printing Office, University of Agder
Kristiansand

Preface and Acknowledgements

The research work presented in this dissertation was conducted in the Mobile Communications Group, Department of Information and Communication Technology (ICT), University of Agder, Grimstad, Norway.

I would never have been able to finish this dissertation without the guidance of my supervisor, help from friends, and support from my family. I would like to take this opportunity to express my deepest gratitude to all of them.

First, I would like to express my sincere gratitude to my supervisor Prof. Matthias Pätzold for providing an excellent atmosphere for doing research, for his valuable comments, constant support and motivation. His guidance helped me in all the time of research and writing of this dissertation. I could not have imagined having a better advisor and mentor for my PhD.

I would also like to thank Prof. Frank Young Lee and Prof. Andreas Prinz for their advice and feedback, also for many educational and inspiring discussions.

My sincere gratitude goes to the doctoral fellows (present and former) in the Mobile Communications Group and the ICT department, especially to Ali Chelli, Alireza Borhani, Batool Talha, Dmitry Umansky, Gulzaib Rafiq, Meisam Naderi, Nurilla Avazov and Yuanyuan Ma. Without their support and friendship it would have been difficult to complete my PhD studies.

I am also thankful to the project secretary of the Mobile Communications Group, Katharina Pätzold, for her invaluable editorial support, and the coordinators of the PhD programme in the ICT department Trine Tønnessen and Emma Horneman.

I would also like to express my deepest gratitude to my parents, my younger sister and brother. They were always supporting me and encouraging me with their best wishes, they were standing by me throughout my life.

Last but not least, I would like to thank my wife, Nuriza Mirrakhimova, for her unwavering support and belief throughout my PhD studies.

Akmal Fayziyev
February 2015
Grimstad, Norway

Summary

Vehicle-to-X (V2X) communication systems are expected to provide tremendous benefits associated with the safety and traffic efficiency on roads. The successful deployment of emerging technologies like V2X requires channel models accurately representing fading statistics in environments where those technologies are used. The accuracy is, of course, a major concern when adapting or developing a suitable channel model for test and evaluation purposes. However, it is also important to take into account the simplicity of a channel model, which is crucial for efficient numerical computations and computer simulations. Reconciling simplicity and accuracy is a rather complex task to accomplish, which requires sophisticated parameter computation methods. To the best of our knowledge, only a limited number of investigations address the channel modelling and parametrization problems for vehicular propagation scenarios in the literature. In order to fill this gap, we concentrate on the development of new sophisticated channel modelling approaches and efficient parameter computation methods for the design of V2X communication systems in this dissertation.

In general, there are two main applications of channel models: (1) for the design and test of wireless communication systems and (2) for the optimization of existing communication systems. For the design and test purposes, more general statistical models such as Rice and Rayleigh channel models are preferred. Those channel models provide a fundamental insight into propagation phenomena and at the same time they greatly simplify the theoretical and numerical computations to assess the performance of wireless communication systems. For the optimization purposes, however, measurement-based channel models are commonly used. The main advantage of such channel models is that they always accurately reflect the physical reality. In this dissertation, we will focus on the channel models designed for both of those application purposes.

A significant part of this dissertation will be devoted to the thorough analysis and design of Rayleigh and Rice fading channel models. We investigate the correlation properties of those channels assuming asymmetrical shapes of Doppler power spectral densities (PSDs). In fact, this is what we often observe in real-world propagation scenarios. In this regard, we will present an analytical expression for the autocorrelation function (ACF) of Rice processes that captures such realistic scenarios. Another important contribution to this topic is the novel iterative nonlinear least square approximation method for the design of Rice and Rayleigh channel simulators based

on sum-of-sinusoids (SOS), as well as sum-of-cisoids (SOC) approaches. The idea behind the proposed method is very simple. The parameters of the simulation model are extracted from the reference model, such as the stochastic Rice and Rayleigh channel models, by fitting the statistical properties of interest, e.g. the ACF and the probability density function (PDF). We show that the proposed method outperforms several other methods in designing channel simulators with desired distribution and correlation properties. We also show that the proposed method provides a subtle balance between channel model's simplicity and accuracy in designing Rayleigh and Rice channel simulators.

The parametrization is a process of determining the key parameters specifying the channel model. This process has a great influence on the reliability of the developed channel model. It is therefore highly desirable if those parameters are extracted from measurements. In fact, this idea constitutes the fundamental concept behind measurement-based channel modelling approach. The measurement-based models are important in the sense that they can be used for the optimizations of the wireless communication system. Hence, the problem of computing the channel model parameters from the measurements is of special interest. In this regard, we propose iterative nonlinear least square approximation method for the design of measurement-based channel simulators. Through detailed investigations and comparative studies, we demonstrate that the proposed method is highly flexible and outperforms several other conventional methods in terms of reproducing the correlation characteristics obtained from several measurements. In addition, we introduce a new approach for the design of channel models for V2X communications in tunnel environments, where the number of scatterers contributing to the total received power is relatively small.

Contents

List of Figures **xvi**

List of Tables **xvii**

Abbreviations **xix**

1 Introduction **1**

1.1 Channel Modelling Approaches and the State of the Art 1

1.2 Overview of V2X Channels 4

1.3 Motivations and Contributions of the Dissertation 6

1.4 Organization of the Dissertation 8

2 Overview of Rayleigh and Rice Simulation Models for V2X Fading Channels **11**

2.1 Introduction 11

2.2 Rayleigh and Rice Channels 12

2.3 Deterministic SOS Channel Models 14

2.4 Deterministic SOC Channel Models 15

2.5 Chapter Summary and Conclusions 16

3 Principles of Measurement-Based V2X Fading Channels **19**

3.1 Introduction 19

3.2 Channel Measurements 20

3.2.1 Measurement Techniques 20

3.2.2 Stationarity Aspects of the Measured Channels 21

3.3 Channel Model and Modelling Approaches 21

3.3.1 Channel Model for Measurement-Based Scenarios 21

3.3.2 Modelling the TFCF by Using the INLSA Method 22

3.3.3 Modelling the Impulse Response by Using the INLSA Method 24
3.4 Chapter Summary and Conclusion 25

4 Parametrization in Channel Modelling 27
4.1 Introduction 27
4.2 Parameter Computation Methods for SOS Channel Models 28
4.2.1 MEDS 28
4.2.2 LPNM 29
4.2.3 Performance Comparison of the INLSA, MEDS and LPNM 29
4.3 Parameter Computation Methods for SOC Channel Models 30
4.3.1 RSM 30
4.3.2 LPNM 31
4.3.3 Performance Comparison of the INLSA, RSM and LPNM . 31
4.4 Parameter Computation Methods for Measurement-Based Channel Models 32
4.4.1 ESPRIT 32
4.4.2 SAGE 33
4.4.3 Performance Comparison of the INLSA, ESPRIT and SAGE 34
4.5 Chapter Summary and Conclusions 35

5 Summary of Contributions and Outlook 37
5.1 Major Contributions 37
5.2 Outlook 38

References 41

List of Publications 47

A Paper I 49

B Paper II 67

C Paper III 87

D Paper IV 105

E Paper V 121

F Paper VI 137

G Paper VII **157**

List of Figures

1.1 Geometry-Based Channel Modelling. 3
1.2 Measurement-Based Channel Modelling. 3
1.3 V2X communication-example. 5

3.1 Absolute value of the TFCF $|R(\nu', \tau)|$ of the measured channel. . . . 25
3.2 Absolute value of the TFCF $|\tilde{R}(\nu', \tau)|$ of the channel model (simulator). 26

4.1 The ULA with M identical sensors and two subarrays each with $M-1$ elements. 33

A.1 Typical Multipath Propagation Scenario. 53
A.2 Autocovariance function $r^c_{\xi\xi}(\tau)$ of Rice processes $\xi(t)$ for different values of ρ. 58
A.3 ACF $r_{\xi\xi}(\tau)$ of Rice processes $\xi(t)$ for different values of κ. 59
A.4 ACF of Rayleigh processes $r_{\zeta\zeta}(\tau)$ for different values of κ. 59
A.5 ACF $r_{\xi\xi}(\tau)$ of Rice processes $\xi(t)$ for different values of m_α. . . . 60
A.6 ACF $r_{\zeta\zeta}(\tau)$ of Rayleigh processes $\zeta(t)$ for different values of m_α. . 60
A.7 Covariance spectrum $S^c_{\xi\xi}(f)$ of Rice processes $\xi(t)$ for different values of ρ. 61
A.8 Covariance spectrum $S^c_{\xi\xi}(f)$ of Rice processes $\xi(t)$ for different values of κ. 61
A.9 Covariance spectrum $S^c_{\zeta\zeta}(f)$ of Rayleigh processes $\zeta(t)$ for different values of κ. 62
A.10 Covariance spectrum $S^c_{\xi\xi}(f)$ of Rice processes $\xi(t)$ for different values of m_α. 62
A.11 Covariance spectrum $S^c_{\zeta\zeta}(f)$ of Rayleigh $\zeta(t)$ processes for different values of m_α. 63

B.1 Normalized residual error norm $\|\check{R}-R\|_F/\|\check{R}\|_F$ versus the number of propagation paths N. 78
B.2 Absolute value of the normalized TFCF $\left|\check{R}[\nu'_p,\tau_q]\right|$ of the measured channel. 80
B.3 Absolute value of the normalized TFCF $\left|R[\nu'_p,\tau_q]\right|$ of the simulation model with the parameters estimated by using the proposed INLSA-TF method. 80
B.4 Absolute value of the normalized TFCF $\left|R[\nu'_p,\tau_q]\right|$ of the simulation model with the parameters estimated by using the INLSA-T-F method. 81
B.5 Absolute value of the normalized TACFs $\left|\check{r}_{t_k}[\tau_q]\right|$ (measured channel) and $\left|r_{t_k}[\tau_q]\right|$ (simulation model) for different parameter computation methods. 82
B.6 Absolute value of the normalized FCFs $\left|\check{r}_{f'_m}[\nu'_p]\right|$ (measured channel) and $\left|r_{f'_m}[\nu'_p]\right|$ (simulation model) for different parameter computation methods. 82
B.7 Comparison between the scattering functions $\check{S}(\tau',f)$ (measured channel) and $S(\tau',f)$ (simulation model) designed by using the INLSA-TF method. 83
B.8 Comparison between the scattering functions $\check{S}(\tau',f)$ (measured channel) and $S(\tau',f)$ (simulation model) designed by using the INLSA method. 83

C.1 Dimensions of the tunnel. 95
C.2 Measurement configuration in the tunnel. 96
C.3 Absolute value of the TVIR $|h(\tau',t)|$ of the measured channel. . . . 97
C.4 Absolute value of the transfer function $|H(f',t)|$ of the measured channel. 98
C.5 Absolute value of the TFCF $|R(\nu',\tau)|$ of the measured channel. . . . 98
C.6 Absolute value of the TVIR $|h(\tau',t_0)|$ of the measured channel at a fixed point in time $t=t_0$. 99
C.7 Absolute value of the transfer function $|\tilde{H}(f',t)|$ of the channel model (simulator). 100
C.8 Absolute value of the TFCF $|\tilde{R}(\nu',\tau)|$ of the channel model (simulator). 101
C.9 Absolute value of the transfer function $|\tilde{H}(f',t)|$ of the channel model (simulator). 101
C.10 Absolute value of the TFCF $|\tilde{R}(\nu',\tau)|$ of the channel model (simulator). 102

D.1 The ACFs $r_{\mu_i\mu_i}(\tau)$ (reference model) and $\tilde{r}_{\mu_i\mu_i}(\tau)$ (simulation model) for different parameter computation methods (Jakes PSD). 114
D.2 Mean-square error $E_{r_{\mu_i\mu_i}}$ (Jakes PSD). 115
D.3 The ACFs $r_{\mu_i\mu_i}(\tau)$ (reference model) and $\tilde{r}_{\mu_i\mu_i}(\tau)$ (simulation model) for different parameter computation methods (Gaussian PSD). . . . 116
D.4 Mean-square error $E_{r_{\mu_i\mu_i}}$ (Gaussian PSD). 117
D.5 Mean-square error $E_{p_{\mu_i}}$ (Gaussian PSD). 117
D.6 Mean-square error $E_{r_{\mu_i\mu_i}}$, $c_{i,n} = \sigma_0\sqrt{2/N_i}$ with $\sigma_0 = 1$ (Gaussian PSD). 118

E.1 The ACFs $r_{\boldsymbol{\mu}\boldsymbol{\mu}}(\tau)$ (reference model) and $r_{\hat{\boldsymbol{\mu}}\hat{\boldsymbol{\mu}}}(\tau)$ (simulation model) for different different values of κ with $m_\alpha = 0$ and $N = 10$. 130
E.2 The ACFs $r_{\boldsymbol{\mu}\boldsymbol{\mu}}(\tau)$ (reference model) and $r_{\hat{\boldsymbol{\mu}}\hat{\boldsymbol{\mu}}}(\tau)$ (simulation model) for different different values of m_α with $\kappa = 5$ and $N = 10$. 131
E.3 Mean-square error $E_{r_{\boldsymbol{\mu}\boldsymbol{\mu}}}$ of $r_{\hat{\boldsymbol{\mu}}\hat{\boldsymbol{\mu}}}(\tau)$ for different parameter computation methods with $\kappa = 5$ and $m_\alpha = \pi/2$. 131
E.4 The envelope PDF $p_{\boldsymbol{\zeta}}(z)$ (reference model) and $\hat{p}_{\boldsymbol{\zeta}}(z)$ (simulation model) for different parameter computation methods with $\kappa = 5$, $m_\alpha = \pi/2$ and $N = 10$. 132
E.5 Mean-square error E_{p_ζ} of $\hat{p}_{\boldsymbol{\zeta}}(z)$ for different parameter computation methods with $\kappa = 5$ and $m_\alpha = \pi/2$. 132

F.1 Uniform linear array of $M = 6$ identical sensors and subarrays with $m = 5$ required for ESPRIT algorithm. 143
F.2 The ACFs $r_{\mu\mu}(\tau)$ (reference model) and $\tilde{r}_{\mu\mu}(\tau)$ (simulation model) for Scenario I. 149
F.3 The ACFs $r_{\mu\mu}(\tau)$ (reference model) and $\tilde{r}_{\mu\mu}(\tau)$ (simulation model) for Scenario II. 149
F.4 Mean-square error $E_{r_{\mu\mu}}$ of $\tilde{r}_{\mu\mu}(\tau)$ for Scenario II. 150
F.5 Parameter computation time T_c for Scenario II. 150
F.6 The ACFs $r_{\mu\mu}(\tau)$ (reference model) and $\tilde{r}_{\mu\mu}(\tau)$ (simulation model) for Rayleigh distributed and optimized c_n, $N_s = N$. 151
F.7 The ACFs $r_{\mu\mu}(\tau)$ (reference model) and $\tilde{r}_{\mu\mu}(\tau)$ (simulation model) for Rayleigh distributed and optimized c_n, $N_s < N$. 152
F.8 Mean-square error $E_{r_{\mu\mu}}$ of $\tilde{r}_{\mu\mu}(\tau)$ for Rayleigh distributed and optimized c_n. 152

G.1 Normalized residual error norm versus the number of propagation paths N. 167
G.2 Absolute value of the normalized TFCF $\check{R}[\nu'_p, \tau_q]$ of the measured channel. 168
G.3 Absolute value of the normalized TFCF $R[\nu'_p, \tau_q]$ of the simulation model with the parameters estimated by using the proposed INLSA-TF method. 169
G.4 Absolute value of the normalized TFCF $R[\nu'_p, \tau_q]$ of the simulation model with the parameters estimated by using the INLSA-T-F method. 169
G.5 Examples of estimated TACFs. 170
G.6 Examples of estimated FCFs. 170
G.7 Comparison between the scattering functions of the measured channel and the simulation model designed by using the INLSA-TF method. 171
G.8 Comparison between the scattering functions of the measured channel and the simulation model designed by using the original INLSA method. 171

List of Tables

C.1 Parameters of the real-world channel simulator for tunnels. 100

D.1 Parameter computation time (Gaussian PSD). 116

Abbreviations

ACF	autocorrelation function
AOAs	angles of arrival
AODs	angles of departure
AWGN	additive white Gaussian noise
BS	base station
BRSM	basic approach of the Riemann sum method
CBTC	Communications-Based Train Control
CCF	cross-correlation function
CCTV	Closed-Circuit Television
CDF	cumulative distribution function
DPSD	Doppler power spectral density
DSRC	Dedicated Short-Range Communication
EMEDS	extended method of exact Doppler spread
ESPRIT	estimation of signal parameters via rotational invariance techniques
FCF	frequency correlation function
GMEA	generalized method of equal areas
GMEDS	generalized method of exact Doppler spread
GSM	Global System for Mobile
INLSA	iterative nonlinear least square approximation
ITS	Intelligent Transportation Systems
LCR	level-crossing rate
LOS	line-of-sight
LPNM	L_p-norm method
MEA	method of equal areas
MEDS	method of exact Doppler spread
MIMO	multiple-input multiple-output
MMEA	modified method of equal areas

MUSIC	multiple signal classification
NLOS	non-line-of-sight
OFDM	orthogonal frequency-division multiplexing
PDF	probability density function
PSD	power spectral density
RSM	Riemann sum method
SAGE	space-alternating generalized expectation-maximization
SISO	single-input single output
SOC	sum-of-cisoids
SOS	sum-of-sinusoids
V2I	vehicle-to-infrastructure
V2V	vehicle-to-vehicle
TACF	temporal autocorrelation function
TFCF	time-frequency correlation function
TFCM	time-frequency correlation matrix
TVFR	time-variant frequency response
TVIR	time-variant impulse response
WiFi	wireless fidelity
WSSUS	wide-sense stationary uncorrelated scattering

Chapter 1

Introduction

The most important task in the development of wireless communication systems is that of determining the suitable radio signal transmission and processing techniques that allows for an efficient utilization of the available power and frequency resources. Accomplishing this nontrivial task requires various system performance investigations with different communication system settings, modulation schemes and coding techniques. In this regard, realistic channel models become a useful benchmarking tool for such performance investigations. In general, channel modelling is the analytical or statistical representation of the propagation characteristics such as path loss, shadowing and multipath fading. Accordingly, the design of channel models needs to be carried out with emphasis on their ability to reproduce the realistic propagation conditions.

In the last few years, there has been a growing interest in intelligent transportation systems (ITS). This actuates the need for sophisticated channel models for V2X communications that are an essential part of ITS. In this regard, we concentrate on the general concepts in channel modelling and present a brief introduction to V2X communication systems in the remainder of this chapter. This chapter also delineates our motivations for the research presented herein and highlights the major contributions of this dissertation.

1.1 Channel Modelling Approaches and the State of the Art

The fundamental step in the modelling of a wireless channel is the derivation of the baseband representation of the received signal. In essence, this step removes the de-

pendence of the channel from the carrier frequency, which greatly simplifies the task of channel modelling. In the time domain, the received signal will then be represented as a convolution of the transmitted signal and the so-called channel impulse response. The channel impulse response is the wideband representation of the wireless channel and carries all the necessary information to characterize a given wireless propagation environment. Therefore, in this dissertation the term *channel modelling* will refer to the modelling of the impulse response or its Fourier transform, the channel transfer function. It is obvious that those two characteristics of a wireless channel are completely interchangeable and provide exactly the same amount of information.

Over the past few decades, a large variety of channel models have been proposed in the literature [1–6]. A comprehensive overview of the widely used channel models can be found in [7]. These channel models can be classified in many different ways. For instance, we can classify them based on the modelling approach that has been used. With respect to this criterion, we distinguish between two types of channel models, namely *stochastic* and *deterministic* models. The stochastic approach focuses on modelling of the statistical characteristics such as the distribution of the impulse response. Popular examples of the stochastic approach are the geometry-based channel models and the well-known Rayleigh fading channel model. The latter is often considered as a worst-case fading scenario in wireless communications. In Fig. 1.1, we illustrated the methodology behind the stochastic approach in case of the geometry-based channel modelling. In this case, the reference model is determined by performing an ensemble averaging over an infinitely large number of scenarios. It is important to note that the designed reference model is non-realizable as it assumes that the number of scatterers N is infinite. From the reference model, however, we can derive a realizable simulation model by considering only a finite number of scatterers and approximating the statistics of the reference model. The main advantage of the stochastic approach is its computational simplicity. Additionally, the designed channel models using this approach can be utilized for parameter studies. However, it is noteworthy that these channel models are in general not realistic and have a limited confirmation by measurements.

The deterministic modelling approach, in contrast to the stochastic approach, concentrates only on one particular scenario. The measurement-based channel modelling and ray tracing techniques are the most popular examples of the deterministic approach. For example, in case of measurement-based channel modelling, the measurement data corresponding to the particular scenario is used for the derivation of the statistics of interest (see Fig. 1.2). A simulation model is then obtained by

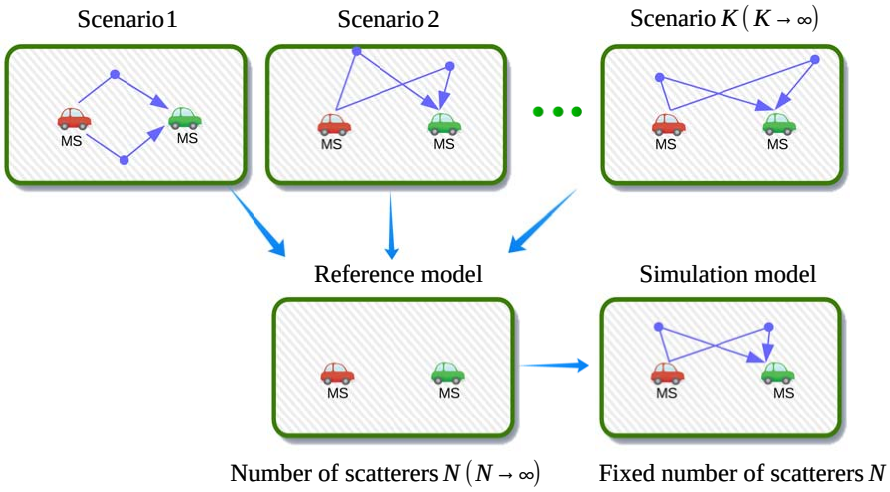

Figure 1.1: Geometry-Based Channel Modelling.

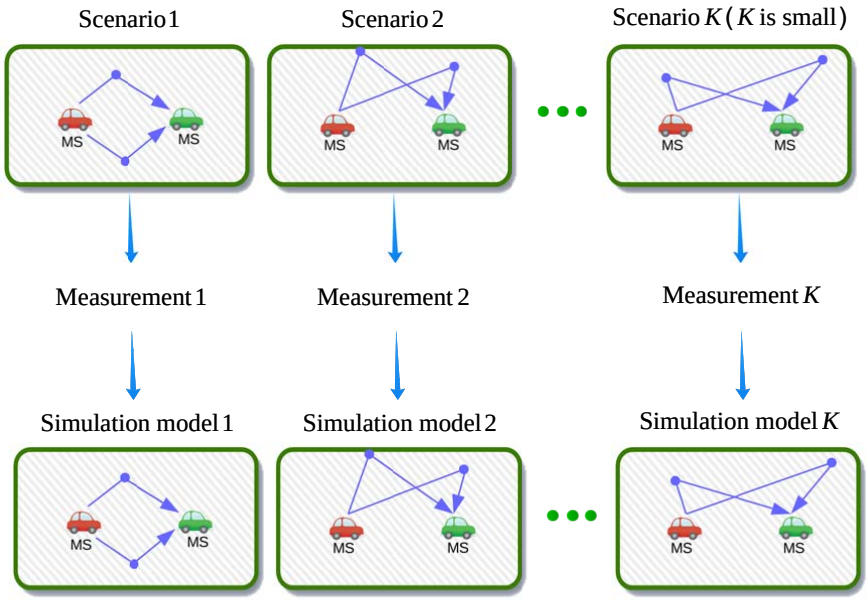

Figure 1.2: Measurement-Based Channel Modelling.

approximating the derived statistics. Taking unpredictable fading behavior into account, for each scenario we end up with a simulation model that is entirely different from any of those for other scenarios. The deterministic approach results in highly realistic simulation models. However, these simulation models are only valid for specific scenarios. This makes them not suitable for parameter studies. Another major disadvantage of the deterministic approach is the time-consuming procedures such as the field measurements (measurement-based modelling) or the topographic data

collection (ray tracing technique).

Unfortunately, there is no standard approach that satisfies all the channel modelling needs. Thus, the selection of a suitable approach is made based on the application purposes of the simulation model. More general stochastic models are considered to be suitable for design and comparison purposes, whereas realistic and site-specific deterministic models are often used for the optimization and deployment of wireless communication systems.

With respect to the type of a wireless channel, we can distinguish between *narrowband* and *wideband* channel models. The development of these types of channel models has been addressed in [8], where the SOS and SOC channel modelling principles have been applied to design a number of channel models that are based on the utilization of Gaussian processes, e.g., Rayleigh, Rice, and Suzuki channel models to name just a few. It has been demonstrated that depending on the chosen parameter computation method, the SOS and SOC channel models allow for an accurate emulation of the channel characteristics. The development of simple and efficient parameter computation methods is therefore essential for these channel models.

1.2 Overview of V2X Channels

One of the most interesting trends in the area of wireless communications is V2X communications proposed for ITS applications. Before we describe the V2X channels, let us first provide some insight into V2X communications. V2X communications for ITS are based on Dedicated Short Range Communication (DSRC), which constitutes a two-way wireless communication technology designed specifically for objects in motion like vehicles [9, 10]. In general DSRC allows vehicles to exchange data with other vehicles and infrastructures, such as road operators and sensors (See Fig. 1.3). It acts similar to the well-known Wi-Fi communication, however, it utilizes specific features enabling efficient networking in environments with high mobility. Owing to their benefits in safety and traveling ease, there has been a significant interest both from research institutes and industry in V2X communications and DSRCs in particular.

The channel is a complex phenomenon and a decisive factor influencing the performance of communication systems. Hence, the development of future V2X communication systems is impossible without thorough investigations of the wireless channel. When considering V2X propagation scenarios from the channel modelling standpoint, we have to distinguish between vehicle-to-vehicle (V2V) and vehicle-to-

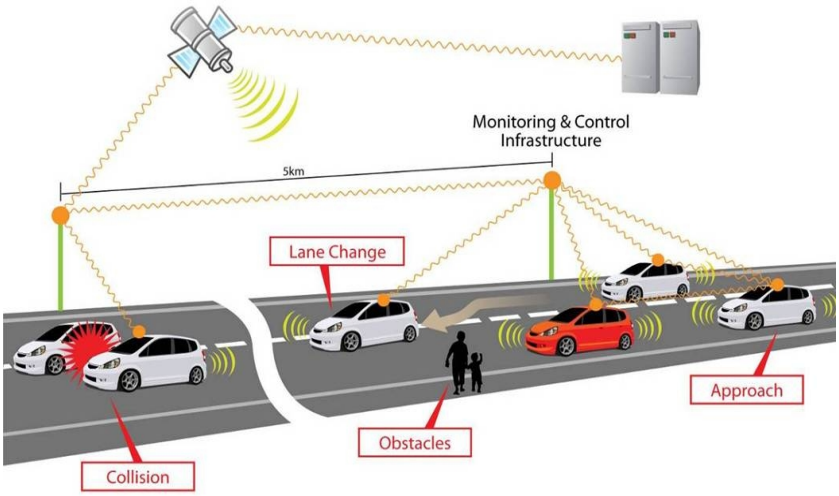

Figure 1.3: V2X communication-example.

infrastructure (V2I) channels. These two channels differ not only from each other, but also from well-studied channels in cellular propagation environments [11]. In cellular propagation scenarios, the base station (BS) is fixed and well elevated. Hence, there are no scatterers in the immediate vicinity of the BS. Moreover, the majority of scatterers around the mobile station are fixed or in relatively slow motion. In V2V communications, however, we observe a completely different behavior of the scatterers. First of all, there are no fixed and elevated elements in such scenarios. Furthermore, both the transmitter and the receiver, as well as the scatterers (other vehicles) are in motion and may be travelling at significantly higher speeds. The number of moving scatterers can vary greatly depending on a variety of important factors, such as the area and the time of the day.

The V2I scenarios combine the characteristics of both V2V and cellular propagation environments. In V2I communications we presume the presence of an access point, which acts like a BS in cellular systems. Therefore, the propagation channel in such scenarios will be quite similar to those in cellular microcell scenarios if the position of the access point antenna is high enough. In this case, the investigations in V2I propagation can benefit from the results and measurements for cellular scenarios collected over the decades. However, in case the access point antenna is fixed at a lower level, we can expect some similarities in V2I and V2V scenarios with significant differences in channel characteristics such as the average Doppler shift and Doppler spread [12].

1.3 Motivations and Contributions of the Dissertation

Channel modelling is not a new area of research in wireless communications. However, emerging technologies, such as V2X communications, motivate researchers to study and develop new channel models. In Section 1.2, we have discussed the major differences between V2X and traditional cellular propagation channels. This implies that we have to consider the channel characteristics specific to V2X propagation environments when designing channel models for such environments. Hence, much attention was devoted to the studies of V2X channels and their characteristics such as path loss, delay spread, Doppler spread, and PDF of the received signal envelope [13–21]. For instance, the authors in [20] reported that the envelope PDF gradually changes from Rice to Rayleigh distribution as the distance between the vehicles increases. The reason for this is that the LOS component disappears at large distances between vehicles and the channel fading becomes more severe. Similar conclusions have also been drawn from the investigations in [21]. These observations motivate us to regard Rayleigh and Rice processes as suitable channel models for the performance analysis of the V2X communication system. In this context, it is important to study the correlation properties and the power spectrum of these processes. Unfortunately, these characteristics of Rice and Rayleigh processes have not been investigated for realistic scattering scenarios up to now.

For the design of Rayleigh and Rice channel models, one can utilize the previously mentioned SOS and SOC modelling approaches. Selecting a proper modelling approach is only the first step of the channel modelling process. As we mentioned earlier in this chapter, the primary objective of the channel modelling process is to reproduce the statistical characteristics of the reference model with an acceptable level of accuracy. Obviously, the reliability of a channel model is greatly improved if the target statistical characteristics are derived from real-world measurements. Nevertheless, that objective is implemented in the second step, which is the process of determining the parameters required for the specification of the channel model. This calls for the need of sophisticated parameter computation methods that allow for a proper reproduction of the desired channel characteristics.

In order to cope with these needs, this dissertation makes the following contributions to the field:

- Deriving an analytical expression for the ACF of Rice processes that takes into account the realistic asymmetrical shapes of Doppler PSDs.

- Propose a novel parameter computation method for the design of measurement-based V2X channel models.
- Modelling the measurement-based V2X channels in different environments, while coping with the problems caused by limited measurements.
- Propose a parameter computation method for the design of SOS channel models.
- Propose a parameter computation method for the design of SOC channel models.
- Provide performance investigations into the proposed methods to verify their validity and their potential for applications to V2X communications.

1.4 Organization of the Dissertation

This dissertation is organized as a collection of six technical papers. The connection between these papers is elaborated. Papers addressing similar topics are collected together to form chapters. The structure of this dissertation is as follows:

- **Chapter 2** presents the Rice and Rayleigh fading channels for V2X communications. In this chapter, we also discuss on two different approaches for the design of Rice and Rayleigh channel simulators, namely the SOS and SOC methods. Furthermore, an overview of Paper I (Appendix A) is presented in this chapter, which addresses the autocorrelation functions (ACFs) of Rice and Rayleigh processes for asymmetrical Doppler PSDs.

- **Chapter 3** deals with the principles of measurement-based channel modelling for V2X communications. After a brief introduction into the field, this chapter sheds light on the major contributions of Papers II and III (Appendices B-C). Those papers deal with different approaches in designing measurement-based channel models.

- **Chapter 4** summarizes the important results presented in Papers IV-VI (Appendices D-F). These papers deal with parametrization problems in SOS, SOC, and measurement-based channel models. Those papers also present different performance studies.

- **Chapter 5** highlights the main contributions of this dissertation. We close this chapter by addressing open problems that require further research and investigations.

Each chapter consists of several sections dealing with the subtopics explored in the chapter. The outline of each chapter has the following organization:

- **Introduction** presents the topic addressed in the chapter and the motivations behind the study of the topic.

- **Section M** presents the discussion of the paper(s) dealing with similar subtopics. Each section has the following structure:

  - Each section begins with a short introduction of the subject.

  - It then provides a problem description and the methods that have been used to solve that particular problem. Furthermore, it emphasizes the differences between the problem addressed in the discussed paper and the papers reviewed in the same chapter.
  - Finally, the most significant findings of the paper(s) are discussed and the importance of the achieved results is highlighted.

- **Chapter Summary and Conclusions** highlights the specific findings of the chapter.

Chapter 2

Overview of Rayleigh and Rice Simulation Models for V2X Fading Channels

2.1 Introduction

Rayleigh and Rice channels are the most widely used and well-established channel models in wireless communications. This is due to the fact that they are relatively easy to describe and can be efficiently modelled for various investigation using computer simulations. Moreover, there are several measurements that confirm Rice and Rayleigh distributions for the received signal amplitude in V2X propagation environments [20, 21]. Taking all the above into account, we feel confident that Rayleigh and Rice channel models can be considered for the performance analysis of V2X communication systems. Hence, an accurate and deep understanding of the correlation properties of these models becomes very important. In particular, the temporal ACF is essential for the design of interleavers, determining the pilot insertion periods and for making several other decisions that have an impact on the performance of communication systems.

Although Rayleigh and Rice channels have been studied for many decades, there are several practical questions that remain unanswered. One deals with the description of the correlation properties of real-world channels. A key limitation in this regard is that most of the previous studies do not take into account the asymmetrical shapes of Doppler PSDs (non-isotropic scattering). In order to fill this gap, this chapter presents the derivation of an envelope ACF for the case of asymmetrical Doppler

PSDs. We also address the modelling of Rayleigh and Rice channel simulators with such Doppler PSDs.

2.2 Rayleigh and Rice Channels

Before proceeding with the derivation of the ACF of Rice processes, we need to recall the definitions of these processes. When considering a multipath propagation, typical phenomena like diffraction, reflection, and scattering lead to a diffusion of the emitted signal into many different components arriving at the receiver with different phases, amplitudes, and delays. The delay differences of these components are often considered to be negligible with respect to the symbol duration. This simplifying assumption allows us to model the channel as a narrowband channel. We often model the narrowband fading channel in the equivalent complex baseband by a complex Gaussian process $\mu(t)$. In fact, the process $\mu(t)$ is represented as a linear combination of two real-valued Gaussian processes, i.e $\mu(t) = \mu_1(t) + j\mu_2(t)$. The complex and zero-mean Gaussian process $\mu(t)$ is considered as a result of the scattering phenomenon. One well-known approach for modelling real-valued Gaussian processes is the Rice method [22, 23]. According to this approach, the Gaussian process $\mu_i(t)$ $(i = 1,2)$ with the PSD $S_{\mu\mu}(f) = S_{\mu_1\mu_1}(f) + S_{\mu_2\mu_2}(f)$ is modelled as

$$\mu_i(t) = \lim_{N_i \to \infty} \sum_{n=1}^{N_i} c_{i,n} \cos\left(2\pi f_{i,n} t + \theta_{i,n}\right) \tag{2.1}$$

where the phases $\theta_{i,n}$ are independent and identically distributed random variables, each having a uniform distribution over $[0, 2\pi)$. The gains $c_{i,n} = 2\sqrt{\Delta f_i S_{\mu_i\mu_i}(f_{i,n})}$ and the frequencies $f_{i,n} = n \cdot \Delta f_i$ are constant quantities. In this case, the parameter Δf_i is selected in such a way that $f_{i,n}$ covers the whole relevant spectrum. The Jakes PSD is often selected for characterizing the Doppler PSD of the scattered component $\mu(t)$. The Jakes PSD can be expressed as follows

$$S_{\mu_i\mu_i}(f) = \begin{cases} \frac{\sigma_0^2}{\pi f_{\max}\sqrt{1-(f/f_{\max})^2}}, & |f| \leq f_{\max}, \\ 0, & |f| > f_{\max}, \end{cases} \tag{2.2}$$

where $f_{\max}$ is the maximum Doppler frequency. Applying the inverse Fourier transform to the Jakes PSD $S_{\mu\mu}(f)$ results in the following ACF for the Gaussian pro-

cess $\mu(t)$

$$r_{\mu\mu}(f) = 2\sigma_0^2 J_0(2\pi f_{\max}\tau) \tag{2.3}$$

where $J_0(\cdot)$ is the zeroth-order modified Bessel function of the first kind.

In some scenarios, we receive a superposition of the scattered components and the LOS component at the receiver. In order to take into account the LOS propagation component, we introduce a time-variant deterministic process $m(t)$, i.e. $m(t) = \rho e^{j(2\pi f_\rho t + \theta_\rho)}$, where ρ, f_ρ and θ_ρ denote the amplitude, the Doppler frequency, and the phase of the LOS component, respectively. The resulting complex Gaussian process in this case is denoted by $\mu_\rho(t)$, where $\mu_\rho(t) = \mu(t) + m(t)$.

As we know, the Rice process $\xi(t)$ is obtained by taking the absolute value of the Gaussian process $\mu_\rho(t)$ as

$$\xi(t) = |\mu_\rho(t)| = |\mu(t) + m(t)|. \tag{2.4}$$

Similarly, the Rayleigh process $\zeta(t)$ is obtained by taking the absolute value of $\mu(t)$ and represented as follows

$$\zeta(t) = |\mu(t)| = |\mu_1(t) + j\mu_2(t)|. \tag{2.5}$$

The processes $\xi(t)$ and $\zeta(t)$ follow the Rice and Rayleigh distributions, respectively. When it comes to the derivation of the ACFs of the Rice and Rayleigh processes, we are faced with a complex problem. Therefore, only a limited number of solutions dealing with this problem are available in the literature [8, 24, 25]. Unfortunately, these solutions only deal with simplistic scenarios where the underlying Gaussian processes are uncorrelated. In Paper I, we tried to fill this gap by obtaining an analytical expression for the ACF of Rice processes that captures asymmetrical shapes of Doppler PSDs. The description of the Gaussian processes $\mu(t)$ is the starting point for the derivation of these ACFs. Although the inphase $\mu_1(t)$ and the quadrature $\mu_2(t)$ components of the process $\mu(t)$ are often assumed to be uncorrelated, this is not in agreement with real-world situations in V2X scenarios. Therefore, we considered a case where $\mu_1(t)$ and $\mu_2(t)$ are allowed to be correlated. For the sake of simplicity in deriving the solution for the ACF of Rice and Rayleigh processes, it is assumed that the LOS component is time-invariant. Analytical expressions are then presented for the ACF of both Rice and Rayleigh processes. In fact, the ACF of the Rayleigh process has been derived from that of the Rice process as a special case. The expression is quite general and can be used for the analysis of both correlated

and uncorrelated cases of inphase and quadrature components.

2.3 Deterministic SOS Channel Models

The implementation of a fading channel by using the method described in (2.1) requires the summation of an infinite number of harmonic functions, which makes it non-realizable. However, for simulation purposes, we do not necessarily need to consider an infinite number of components. The results in [8, 26] demonstrated that the desired statistical properties can be accurately described even with a very low number of harmonic functions. Moreover, an excellent accuracy in the modelling of such statistics as the ACF, spectral characteristics, and the envelope PDF can be achieved in a simpler, deterministic manner [26] which is referred to as a deterministic channel modelling principle. According to that principle, the real-valued Gaussian process is denoted by

$$\tilde{\mu}_i(t) = \sum_{n=1}^{N_i} c_{i,n} \cos(2\pi f_{i,n} t + \theta_{i,n}). \tag{2.6}$$

In the above equation, all model parameters are constant quantities. Hence, $\tilde{\mu}_i(t)$ is a deterministic process. In this case, we obtain a complex-valued deterministic Gaussian process $\tilde{\mu}(t)$ represented as follows

$$\tilde{\mu}(t) = \tilde{\mu}_1(t) + j\tilde{\mu}_2(t). \tag{2.7}$$

We apply the terms *reference model* and *simulation model* to distinguish between the channel models derived from $\mu(t)$ and $\tilde{\mu}(t)$, respectively. Deterministic Rice and Rayleigh processes can be modelled according to

$$\tilde{\xi}(t) = |\tilde{\mu}(t) + m(t)| = |\tilde{\mu}_\rho(t)| \tag{2.8}$$

and

$$\tilde{\zeta}(t) = |\tilde{\mu}(t)| = |\tilde{\mu}_1(t) + j\tilde{\mu}_2(t)| \tag{2.9}$$

respectively.

The closed-form expression for the ACF $\tilde{r}_{\mu_i\mu_i}(\tau)$ of the deterministic process $\tilde{\mu}_i(t)$ can be expressed as [8, p. 103]

$$\tilde{r}_{\mu_i\mu_i}(\tau) = \sum_{n=1}^{N_i} \frac{c_{i,n}^2}{2} \cos(2\pi f_{i,n}\tau). \tag{2.10}$$

The Fourier transform of the ACF $\tilde{r}_{\mu_i\mu_i}(\tau)$ results in the following expression for the PSD of $\tilde{\mu}_i(t)$

$$\tilde{S}_{\mu_i\mu_i}(f) = \sum_{n=1}^{N_i} \frac{c_{i,n}^2}{4} \left[\delta(f - f_{i,n}) + \delta(f + f_{i,n})\right]. \tag{2.11}$$

Note that the ACF and the PSD of the simulation model are completely characterized by the gains and the Doppler frequencies. It should also be mentioned that the PSD $\tilde{S}_{\mu_i\mu_i}(f)$ is a symmetrical PSD.

When dealing with SOS channel simulators, the processes $\tilde{\mu}_1(t)$ and $\tilde{\mu}_2(t)$ are often assumed to be uncorrelated, i.e. the Doppler PSD $\tilde{S}_{\mu\mu}(f)$ of $\tilde{\mu}(t)$ also has a symmetrical shape (isotropic scattering). This assumption limits the application of the SOS-based approach to channel modelling under isotropic scattering conditions.

2.4 Deterministic SOC Channel Models

An alternative way of approximating the Gaussian process $\mu(t)$ is based on the SOC model. In the deterministic SOC model, the complex Gaussian process $\tilde{\mu}(t)$ is represented by a finite sum of complex sinusoids as

$$\tilde{\mu}(t) = \tilde{\mu}_1(t) + j\tilde{\mu}_2(t) = \sum_{n=1}^{N} c_n e^{j(2\pi f_n t + \theta_n)}. \tag{2.12}$$

Similar to the deterministic scenario in Section 2.3, the parameters of the SOC model in (2.12) are considered to be constant quantities. The corresponding envelope processes $\tilde{\xi}(t)$ and $\tilde{\zeta}(t)$ are derived from the deterministic SOC process $\tilde{\mu}(t)$ in (2.8) and (2.9), respectively.

The correlation properties of this model have been investigated in [27], where the ACF $\tilde{r}_{\mu\mu}(\tau)$ of $\tilde{\mu}(t)$ is found to be equal to

$$\tilde{r}_{\mu\mu}(\tau) = \sum_{n=1}^{N} c_n^2 e^{j2\pi f_n \tau}. \tag{2.13}$$

Note that the ACF $\tilde{r}_{\mu\mu}(\tau)$ of the deterministic SOC process $\tilde{\mu}(t)$ is in general complex. This implies that the real-valued Gaussian processes $\tilde{\mu}_1(t)$ and $\tilde{\mu}_2(t)$ are correlated. Hence, the PSD $\tilde{S}_{\mu\mu}(f)$ of the designed process $\tilde{\mu}(t)$ has an asymmetrical

shape, which can also be seen from the following expression of $\tilde{S}_{\mu\mu}(f)$

$$\tilde{S}_{\mu\mu}(f) = \sum_{n=1}^{N_i} c_{i,n}^2 \delta(f - f_{i,n}). \tag{2.14}$$

It is noteworthy that under the certain conditions, the SOC model can also be used for designing the Gaussian processes with symmetrically shaped PSDs [8].

When the model parameters are properly computed, both the SOS and SOC models will result in a process with the desired statistical properties. In [28], the authors demonstrated that the SOC-based approach is more preferable for the modelling and simulation of realistic non-isotropic scattering conditions, while the SOS approach is the better choice if isotropic scattering scenarios are considered. Another decisive feature of the SOC model is its similarity to the physical wave propagation, which makes the model quite handy in the development of measurement-based V2X channel simulators. Owing to these advantages, the SOC model has been adopted for validation purposes in Paper I. The derived analytical expression for the ACF of the reference Rice process $\xi(t)$ has been validated by using the SOC approach. In Paper I, we considered propagation environments with both isotropic and non-isotropic scattering conditions. In our investigations, the well-known von Mises distribution has been used for the angles of arrival (AOAs). The reason for this is, the von Mises distribution includes a uniform distribution as a special case and therefore can be used for the simulation of isotropic and non-isotropic scattering scenarios. The derived expression for the ACF allowed us to analyze the different factors affecting the correlation behavior of fading channels, such as the LOS component, angular spread and mean AOA. The impact of the angular spread and the mean AOA was much more significant if there was no LOS component. The results in Paper I demonstrate that the coherence time of the channel increases with an increase in the angular spread, whereas an increase in the mean AOA causes the channel to change faster. The detailed results are included in Appendix A.

2.5 Chapter Summary and Conclusions

In this chapter we studied narrowband Rice and Rayleigh channel models. The chapter started with an overview of the recent results obtained in various V2X measurement campaigns. Based on those results, Rice and Rayleigh fading channels have been chosen as appropriate models to describe the fading behavior in V2X scenar-

ios. These channel models are described by a complex Gaussian process. Therefore, we adopted Rice's method for modelling real-valued Gaussian processes. We also discussed the correlation properties as well as the PSD of the Gaussian process. The formal description of Rayleigh and Rice channel models was then provided by means of the Gaussian process.

It should be mentioned that in Rice's method, the number of harmonic functions used to generate the Gaussian process is infinite, which makes it impossible to implement in computer simulations. In this connection, we further continued with the description of the deterministic SOS and SOC models for simulation purposes. The ACF and the PSDs of deterministic Gaussian processes obtained by using the SOS as well as the SOC approaches are also provided.

The asymmetrical shape of the PSDs is often observed in real-world V2X channels. Therefore, the derivation of the ACF of Rice processes for such scenarios was the aim of Paper I. We have already mentioned that the SOC approach is better suited for the design of channel models that can capture non-isotropic scattering conditions. This was the decisive factor in selecting the SOC model for validating the obtained analytical expressions in that paper. The derived ACF was then utilized for various investigations into the temporal behavior of the fading channel in different scenarios. The corresponding conference paper can be found in Appendix A.

Chapter 3

Principles of Measurement-Based V2X Fading Channels

3.1 Introduction

For the efficient development of ITS many aspects of the V2X propagation mechanisms must be investigated. The wave propagation is a complex mechanism that strongly depends on the propagation environment. The propagation scenarios in V2X communication differ substantially from those in well-investigated cellular systems. Consequently, V2X communications need to be treated in a different way and the channel models should capture inherent aspects of V2X propagation scenarios. One way of accomplishing this task is using the measurements in channel modelling.

In the introduction, we mentioned two different approaches in channel modelling, namely deterministic and stochastic approaches. The measurement-based channel modelling is one of the widely used implementations of the deterministic approach. Generally speaking, the term *measurement-based* implies that some or all of the parameters characterizing the selected channel model have been derived from measurements [29]. Making use of this kind of approach allows us to emulate important and unique channel properties that are specific to a given scenario.

In this chapter, we first discuss the fundamental concepts of measurement-based channel modelling. Then, we provide an outline of the adopted measurement-based channel model. We will show how this channel model can be designed by using two different approaches.

3.2 Channel Measurements

The properties of a propagation channel determine the ultimate performance limits of a wireless communication system. Unfortunately, we cannot do much about the channel itself. Nevertheless, we can improve the system performance by properly designing the transmitter and the receiver, which requires detailed investigations into the propagation environments. This is usually done with the help of channel measurements.

3.2.1 Measurement Techniques

The channel measurements are often provided in the form of a measured impulse response or equivalently the channel transfer function. The process of measuring the impulse response is known as channel sounding.

The fundamental idea behind channel sounding is quite simple: the channel is excited by a periodic test signal, which is observed by the receiver and stored; from the knowledge of the transmitted and the received signal, the time-variant impulse response or the transfer function is obtained depending on whether the analysis was in the time or the frequency domain. There are three major techniques to implement the channel sounder, i.e., pulse sounding, correlation, and frequency sweep techniques [30]. For the measurements used in this dissertation, the sliding correlation technique is chosen within the Propsound CS^{TM} channel sounder by Elektrobit described in [31]. The channel sounder measures the impulse response, which in general is represented as a convolution of the channel impulse response with the impulse response of the sounder [2, p. 150]. Whereas, the impulse response of the channel sounder itself is the convolution of the transmitted pulse shape and the impulse response of the filter implemented at the receiver. In channel sounding based on correlation techniques, the receiver filter is a matched filter implying that the impulse response of the channel sounder is the ACF of the transmitted sounding pulses. The pseudo noise sequences in such channel sounders are used as transmitted pulses. Thus, the sounding pulses should have an ACF that is a good approximation of the delta function, which allows for a direct derivation of the true channel impulse response.

3.2.2 Stationarity Aspects of Measured Channels

When dealing with measurement-based channel modelling, we often make wide-sense stationarity (WSS) and uncorrelated scattering (US) assumptions about the physical channel. These assumptions allow us to simplify the representation and derivation of the channel's correlation properties [2, p. 109]. The stationarity aspects of fading channels have been the topic of many studies [32–34]. Generally speaking, the WSS assumption implies that the statistical properties of the channel do not change with time. According to the mathematical definition, WSS has to be fulfilled for any arbitrary time [35, p. 388]. However, this is not possible in reality. The WSS assumption can only be applied for a limited observation time interval. Therefore, a quasi-stationarity interval, over which the statistics of the channel do not change noticeably, is often defined. Similarly, in the frequency domain, the US condition implies that the FCF depends only on the frequency difference and not on the absolute frequency.

The measurement-based channel models developed in this dissertation presume both WSS and US assumptions simultaneously. The reason for this is that the measurements are limited by the bandwidth of the channel sounder. By imposing such assumptions, we can obtain the correlation properties by time and frequency averaging from the time and frequency limited transfer function.

3.3 Channel Model and Modelling Approaches

3.3.1 Channel Model for Measurement-Based Scenarios

The presence of scatterers in the propagation environment distorts the transmitted signal energy in amplitude, phase, and time. It also results in multiple versions of the transmitted signal which arrive at the receiver antenna with different delays. The random phase and amplitudes of the different multipath components result in fluctuations of the received signal strength. In order to take into account all these characteristics of the multipath propagation phenomenon, the following model for the impulse response is often considered in measurement-based channel modelling

$$h(\tau',t) = \sum_{n=1}^{N} c_n e^{j(2\pi f_n t + \theta_n)} \delta(\tau' - \tau'_n). \tag{3.1}$$

where N denotes the number of paths with different propagation delays τ'_n. The parameters c_n, f_n, and θ_n are the path gains, Doppler frequencies, and phases, respectively, which are associated with the nth propagation path. The model in 3.1 has a fairly generic structure and is referred to as the Rayleigh-fading model. This channel model can also be represented in terms of the transfer function, which is derived as the inverse Fourier transform of $h(\tau',t)$ with respect to τ'.

$$H(f',t) = \sum_{n=1}^{N} c_n e^{j(2\pi f_n t - 2\pi f' \tau'_n + \theta_n)}. \tag{3.2}$$

It can be easily shown that the time-frequency correlation function (TFCF) of the channel model in (3.2) is represented as follows

$$R(\nu',\tau) = \sum_{n=1}^{N} c_n^2 e^{j2\pi(\tau'_n \nu' - f_n \tau)} \tag{3.3}$$

where τ and ν' denote the time-lag and frequency-lag, respectively. The Rayleigh-fading model has successfully been deployed in Papers II and III for the design of measurement-based V2X channel models for different propagation scenarios.

3.3.2 Modelling the TFCF by Using the INLSA Method

The primary goal of channel modelling consists in generating the realizations of the channel functions such as the impulse response and transfer function with the desired statistical properties. The properties of interest can be any of the important first- or second-order characteristics, e.g. the PDF and the TFCF. In the measurement-based channel modelling approach, the properties of the channel model are matched to those of the measured channel functions by applying proper parameter computation methods. A variety of methods dealing with the parametrization problem can be found in the literature [36–42]. However, most of those methods are relatively difficult to implement or not accurate enough in the sense that the obtained channel model characteristics differ substantially from the desired ones. To cope with this problem, we proposed a new efficient method for designing the measurement-based channel models in Paper II. The proposed iterative nonlinear least-square approximation (INLSA) method is based on optimization techniques and computes the channel model parameters by fitting the statistics of the model to that of the measured channel in an iterative manner. One useful feature of the channel model described in (3.2) is

that it allows us to distinguish between different propagation components and treat them separately. To demonstrate this, we consider the TFCF $\check{R}(\nu',\tau)$ derived from the measurement data. In this case, the primary goal of the parameter computation method is to determine the channel model parameters $\mathbb{P} = \{c_n, f_n, \tau'_n\}$ such that a good fitting between the TFCFs of the channel model $R(\nu',\tau)$ and the measured channel $\check{R}(\nu',\tau)$ is achieved. For accomplishing this task, the INLSA method requires arbitrarily chosen initial values for the sets of parameters $\{f_n\}$ and $\{\tau'_n\}$. At every iteration i $(i = 0,1,2,...)$, the INLSA method determines the channel model parameters separately for each path l $(l = 1,2,...,N)$. This is done by using the auxiliary error function $Y_l^{(i)}(\nu',\tau)$ as follows

$$Y_l^{(i)}(\nu',\tau) = \check{R}(\nu',\tau) - \sum_{n=1,n\neq l}^{N} \left(c_n^{(i)}\right)^2 e^{j2\pi(\tau_n'^{(i)}\nu' - f_n^{(i)}\tau)} \tag{3.4}$$

$$c_l^{(i+1)} = \arg\min_{c_l} \left\| Y_l^{(i)}(\nu',\tau) - c_l^2 e^{j2\pi(\tau_l'^{(i)}\nu' - f_l^{(i)}\tau)} \right\|_F \tag{3.5}$$

$$f_l^{(i+1)} = \arg\min_{f_l} \left\| Y_l^{(i)}(\nu',\tau) - \left(c_l^{(i+1)}\right)^2 e^{j2\pi(\tau_l'^{(i)}\nu' - f_l\tau)} \right\|_F \tag{3.6}$$

$$\tau_l'^{(i+1)} = \arg\min_{\tau'_l} \left\| Y_l^{(i)}(\nu',\tau) - \left(c_l^{(i+1)}\right)^2 e^{j2\pi(\tau'_l\nu' - f_l^{(i+1)}\tau)} \right\|_F \tag{3.7}$$

As we mentioned earlier, the parameter computation process described in (3.4), (3.5), (3.6) and (3.7) is implemented for each path l $(l = 1,2,...,N)$ separately, which completes the current iteration. The model error $E(\mathbb{P}) = \left\|\check{R} - R\right\|_F$ needs to be reevaluated in the end of each iteration. After this, the iteration index is increased by one (i.e., $i+1 \rightarrow i$) and the parameter computation process is repeated. The iterations continue until the relative change in the model error $E(\mathbb{P})$ drops below the predefined threshold level ε.

It is easy to show that the optimization problem given in (3.5) results in the following closed-form solution

$$c_l^{(i+1)} = \sqrt{\frac{\mathrm{Re}\left\{\mathbf{y}_l^{(i)}\right\}^T \mathrm{Re}\left\{\mathbf{p}_l^{(i)}\right\} + \mathrm{Im}\left\{\mathbf{y}_l^{(i)}\right\}^T \mathrm{Im}\left\{\mathbf{p}_l^{(i)}\right\}}{\left(\mathbf{p}_l^{(i)}\right)^H \mathbf{p}_l^{(i)}}} \tag{3.8}$$

where the symbol $\mathbf{y}_l^{(i)}$ refers to a column vector containing the elements of the error function $Y_l^{(i)}(\nu',\tau)$. Similarly, the symbol $\mathbf{p}_l^{(i)}$ represents the column vector formed

by using the exponential function $e^{j2\pi(\tau_l'^{(i)}\nu' - f_l^{(i)}\tau)}$. The operators $\{\cdot\}^T$ and $\{\cdot\}^H$ denote the transpose and complex-conjugate transpose, respectively.

In contrast to the far more complex parallel optimization of the model parameters, the INLSA method is an efficient solution to the channel model parametrization problem. The INLSA method achieves a high level of accuracy in approximating the TFCF of the measured channel, which has been proven by computer simulations in Paper II. In that paper, we applied the proposed method to the V2I measurement data collected in urban areas. We assessed the method's performance by comparing the TFCF of the simulation model with that of the measured channel. A comparison was also made with respect to the scattering functions generated by the designed channel model and the measured channel. In both cases, the INLSA approach demonstrated an excellent agreement between the designed and measured channel functions.

3.3.3 Modelling the Impulse Response by Using the INLSA Method

As we mentioned earlier in this chapter, channel measurements are often limited by the parameters of the channel sounder. A common way of estimating the correlation properties of the measured channel is the time and frequency averaging. However, when we try to estimate those properties from the measurement, which are limited in the time and/or frequency domain, we encounter an estimation error. This results in an inaccurate modelling of the physical channel statistics, which is highly undesirable. In [43] and [44], the authors developed improved methods for estimating the ACF and the FCF from limited measurements, respectively. These methods utilize the appropriate kernel function to enhance the estimation quality.

In Paper III, we presented an alternative solution to this problem. By observing the measured impulse response, we selected the dominant paths and determined the corresponding propagation delays. In our simulation model, these paths are referred to as channel gains. The channel gains (selected paths) are modelled as a superposition of several propagation components, each described by its own parameters (path gains, Doppler frequencies, and phases). These parameters are obtained by fitting the channel gains of the simulation model to the measured impulse response at the corresponding fixed propagation delays. For computing the parameters, we extended the INLSA method to the modelling of the channel gains. This is easily done by using the channel gains of the channel model and the measured channel in the parameter computation procedure described in the previous section. In this case,

the auxiliary model error norm and the error function must be modified accordingly. The computed parameters of the channel gains together with the propagation delays are then used to simulate the channel impulse response beyond the measured time limits. Eventually, the simulations are used to compute the TFCF and mitigate the estimation error.

Our investigations demonstrated that insufficient measurements can greatly affect the measured TFCF. For instance, this effect becomes apparent from the triangular shape of the TFCF in the direction of τ in Fig 3.1. In Fig 3.2, it has been shown that the proposed approach easily handles the effects caused by insufficient measurements and eliminates the triangular shape.

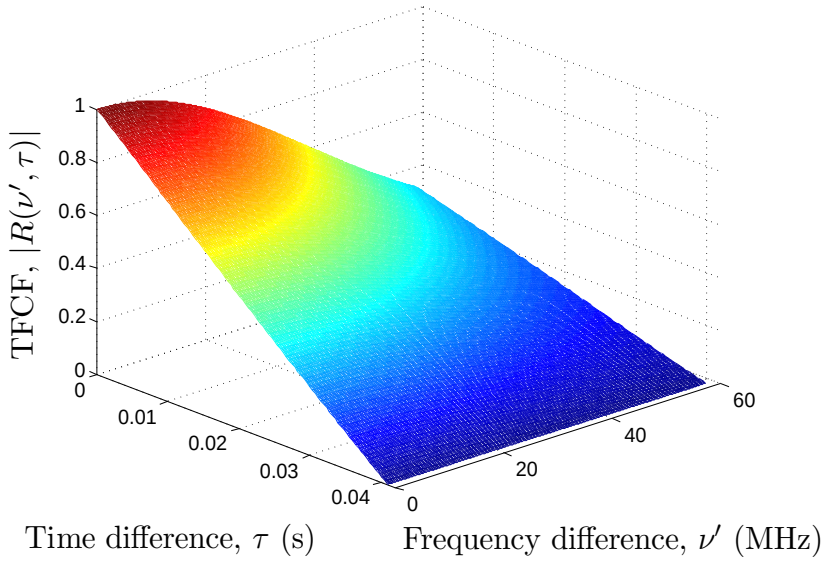

Figure 3.1: Absolute value of the TFCF $|R(\nu',\tau)|$ of the measured channel.

3.4 Chapter Summary and Conclusion

In this chapter, the principles of measurement-based channel modelling were addressed. We also discussed the Rayleigh-fading model that is used in our measurement-based channel modelling analysis. A novel parameter computation method was proposed for the design of measurement-based channel simulators (see Paper II). In fact, the application of this method is not limited to the design of the desired statistical properties. Evidence of this has been demonstrated by applying the method to the design of the channel impulse response (see Paper II). Finally, we highlighted the TFCF estimation problem and presented an efficient way of dealing with it.

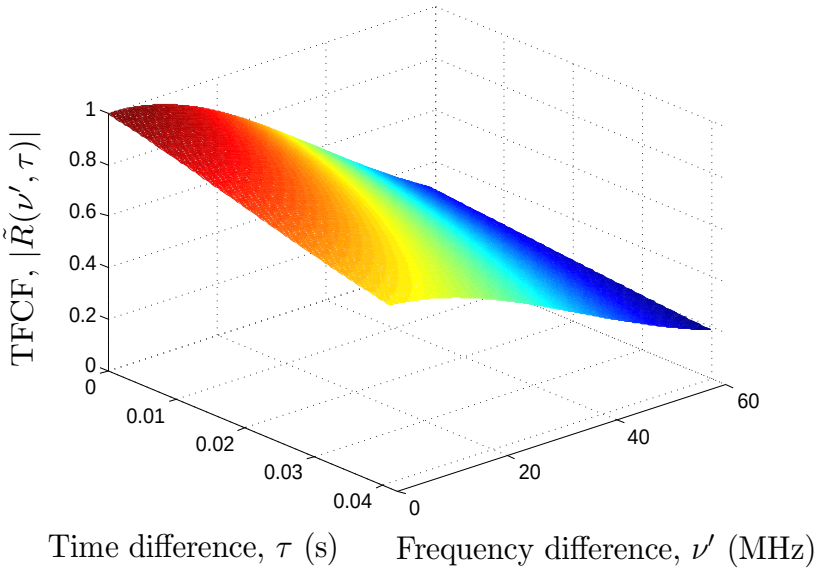

Figure 3.2: Absolute value of the TFCF $|\tilde{R}(\nu', \tau)|$ of the channel model (simulator).

Chapter 4

Parametrization in Channel Modelling

4.1 Introduction

This chapter deals with the parametrization of narrowband and wideband channel models discussed previously. Accordingly, this chapter presents extensions of the highly flexible parameter computation method described in Paper II for the design of SOS and SOC channel simulators as well as it provides corresponding performance evaluations.

Generally speaking, the parametrization is the most significant part in the channel modelling process. Once the channel model has been selected, the problem consists in finding the parameters that specify the model. In SOS and SOC models these are the path gains, Doppler frequencies, and the phases. In case of the adopted wideband Rayleigh-fading model for measurement-based scenarios, additional parameters, i.e., the propagation delays should be determined. In order to exploit the advantages of each channel model, one must carefully determine the model parameters. The literature includes numerous parameter computation methods for SOS channel models with different degrees of accuracy, such as those developed in [26, 45–47]. In contrast to SOS channel models, there are relatively fewer parameter computation methods proposed for the design of SOC channel simulators. However, because of the similarities in the model structure, some methods for SOS models can be extended to SOC channel models. Examples are the extended method of exact Doppler spread (EMEDS) [48], the generalized method of equal areas (GMEA) [49], and the L_p-norm method (LPNM) [26]. Beyond that, there are other methods that are

explicitly developed for SOC channel modelling, such as the Riemann sum method (RSM) [50]. While the methods mentioned above are computationally attractive, they do not always provide sufficient accuracy or require high implementation cost. In particular, the LPNM method, which is the most accurate one for the modelling of SOS and SOC channel models, has a relatively high computational complexity [8]. This fact motivated us to design simpler methods with a degree of accuracy similar to that of LPNM.

When it comes to measurement-based channel modelling, one can benefit from the methods designed for parameter estimation purposes. There exist two main approaches in parameter estimation: subspace-based and maximum likelihood-based methods. The most popular subspace-based methods are the multiple signal classification (MUSIC) [39] and estimation of signal parameters via rotational invariance techniques (ESPRIT) [36, 51], whereas the space-alternating generalized expectation-maximization (SAGE) [40] algorithm is the most widely used maximum likelihood-based method. These methods, however, have not yet been analyzed from the channel modelling perspective. In order to fill this gap, we investigate the application potential of these methods for measurement-based channel modelling.

4.2 Parameter Computation Methods for SOS Channel Models

In this section, we concentrate on the parametrization of SOS channel models. As noted previously, SOS channel models are explicitly used to emulate mobile radio channels under isotropic scattering conditions. In this regard, we extend the INLSA method for the design of SOS channel models and compare its performance to those of the method of exact Doppler spread (MEDS) [47] and LPNM [26] in Paper IV.

4.2.1 MEDS

The MEDS, in the case of the Jakes PSD, computes the parameters $c_{i,n}$ and $f_{i,n}$ of the SOS model as [47]

$$c_{i,n} = \sigma_0 \sqrt{\frac{2}{N_i}} \tag{4.1}$$

and

$$f_{i,n} = f_{\max} \sin\left[\frac{\pi}{2N_i}\left(n - \frac{1}{2}\right)\right] \tag{4.2}$$

respectively, for all $n = 1,2,\ldots,N_i$ $(i = 1,2)$. If we apply the MEDS in connection with the Gaussian PSD, then the gains $c_{i,n}$ are again computed according to (4.1). However, the Doppler frequencies $f_{i,n}$ should now be computed by solving the following equation

$$\frac{2n-1}{2N_i} - \mathrm{erf}\left(\frac{f_{i,n}}{f_c}\sqrt{\ln 2}\right) = 0 \tag{4.3}$$

for all $n = 1,2,\ldots,N_i$ $(i = 1,2)$, where $\mathrm{erf}(\cdot)$ denotes the error function.

4.2.2 LPNM

With respect to the LPNM, the parameters of the SOS channel model are determined in a way that minimized the following L_p-norm

$$E^{(p)}_{r_{\mu_i\mu_i}} := \left\{ \frac{1}{\tau_{\max}} \int_0^{\tau_{\max}} |r_{\mu_i\mu_i}(\tau) - \tilde{r}_{\mu_i\mu_i}(\tau)|^p d\tau \right\}^{1/p} \tag{4.4}$$

where $\tilde{r}_{\mu_i\mu_i}(\tau)$ and $r_{\mu_i\mu_i}(\tau)$ denote the ACFs of the simulation model and the reference model, respectively. The parameter $\tau_{\max}$ determines the interval $[0,\tau_{\max}]$ over which the approximation $\tilde{r}_{\mu_i\mu_i}(\tau) \approx r_{\mu_i\mu_i}(\tau)$ is carried out. It is important to mention that, according to the results presented in [8, Sec. 5.1.6], the LPNM provides an optimal set of parameters for the approximation of $r_{\mu_i\mu_i}(\tau)$.

4.2.3 Performance Comparison of the INLSA, MEDS and LPNM

The aim of the SOS approach is to model the Gaussian processes with the desired statistical characteristics. As we know, the Gaussian process is completely characterized by its mean value and ACF. Hence, it appears natural to compute the SOS model parameters by fitting the ACF of this model to that of the reference model. In Paper IV, the model parameters are calculated as minimizing arguments of the error norm between the ACFs of the SOS model and the reference process. We derive a closed-form solution for computing the optimal path gains, whereas the Doppler frequencies must be computed numerically by solving a nonlinear optimization problem. Since the phases have no impact on the ACF of the SOS process, they are not included in the parameter computation process.

The performance analysis of the INLSA method in comparison with other conventional parameter computation methods is one of the objectives of Paper IV. In this regard, we compare the performance of the INLSA method with the LPNM and

MEDS. The performance comparisons have been made with respect to the accuracy in approximating the reference ACFs. In Paper IV, we deal with isotropic scattering scenarios. With this in mind, the ACFs corresponding to the Jakes and Gaussian PSDs have been selected as reference ACFs. As expected, the INLSA method significantly outperformed the MEDS in the approximation of both ACFs. Furthermore, we demonstrated that the INLSA provides a performance similar to the LPNM in fitting the reference ACFs yet with significantly lower implementation complexity. This makes the INLSA approach an obvious choice for the design of SOS channel simulators, especially if implementation complexity matters.

4.3 Parameter Computation Methods for SOC Channel Models

As in the case of SOS channel models, most standard methods for the design of SOC channel simulators put emphasis on approximating the ACF of the reference model. Examples are the LPNM [26] and RSM [50]. Although one has to deal with complex ACFs in SOC channel models, this does not complicate the parameter computation process in any sense. The flexibility of the INLSA method, originally proposed in Paper II, allows us to easily extend it to the design of SOC processes with the desired correlation properties, which is the main objective of Paper V.

4.3.1 RSM

The RSM, as originally introduced in [50], suggests to determine the gains c_n and AOAs α_n as

$$c_n = \sigma_{\boldsymbol{\mu}} \sqrt{\frac{g_{\boldsymbol{\alpha}}(\alpha_m)}{\sum_{m=1}^{N} g_{\boldsymbol{\alpha}}(\alpha_m)}} \tag{4.5}$$

and

$$\alpha_n = \frac{\pi}{N}\left(n - \frac{1}{2}\right) \tag{4.6}$$

respectively, for all $n = 1, 2, \ldots, N$. The function $g_{\boldsymbol{\alpha}}(\alpha)$ designates the even part of the distribution of the AOA α. For the von Mises distribution of AOAs, we can

represent $g_{\boldsymbol{\alpha}}(\alpha)$ as

$$g_{\boldsymbol{\alpha}}(\alpha) = \frac{e^{\kappa\cos(\alpha - m_\alpha)}}{2\pi I_0(\kappa)} \cdot \cosh(\kappa \sin(\alpha)\sin(m_\alpha)) \tag{4.7}$$

where $\alpha \in [-\pi, \pi)$ and $I_0(\cdot)$ denotes the zeroth-order modified Bessel function of the first kind. The parameter $m_\alpha \in [-\pi, \pi)$ is the mean AOA and $\kappa > 0$ controls the angular spread. Note that the Doppler frequencies f_n of the SOC model presented in (2.12) can be computed as $f_n = f_{\max}\cos(\alpha_n)$, where $f_{\max}$ represents the maximum Doppler frequency.

4.3.2 LPNM

In Paper V, we consider two versions of the LPNM, one with fixed gains (LPNM I) and another one with optimized gains (LPNM II). In the LPNM I, the path gains c_n are assumed to be equal and computed according to the following formula

$$c_n = \sigma_{\boldsymbol{\mu}} \sqrt{1/N} \tag{4.8}$$

for all $n = 1, 2, \ldots, N$.

The Doppler frequencies f_n are then computed by minimizing the L_p-norm

$$E_{r_{\mu\mu}}^{(p)} := \left\{ \frac{1}{\tau_{\max}} \int_0^{\tau_{\max}} |r_{\mu\mu}(\tau) - \tilde{r}_{\mu\mu}(\tau)|^p d\tau \right\}^{1/p} \tag{4.9}$$

where $\tau_{\max}$ determines the interval $[0, \tau_{\max}]$ over which the approximation $\tilde{r}_{\mu\mu}(\tau) \approx r_{\mu\mu}(\tau)$ is performed. According to the LPNM II, both parameters are computed by minimizing the L_p-norm in (4.9). In Paper IV, the LPNM I and LPNM II are used to determine the target performance in designing the envelope PDF and the ACF of the complex-valued Gaussian process, respectively.

4.3.3 Performance Comparison of the INLSA, RSM and LPNM

In Paper V, we propose the iterative nonlinear approximation method for the design of SOC channel models. From Section 2.4, we know that the ACF of the SOC model is represented as a sum of N exponential components, each characterized by the corresponding path gains and Doppler frequencies. In this case, we implement

almost the same procedure as in Paper IV, i.e., we determine the model parameters by minimizing the error norm between the ACFs of the SOC and the reference models. These parameters, which correspond to different exponential components, are computed separately and in an iterative manner. We provide an analytical expression for the computation of the path gains, whereas the Doppler frequencies are again computed numerically by solving the nonlinear optimization problem as in Paper IV.

In Paper V, we also provide performance comparisons of the INLSA method with the well-known methods for the design of SOC channel models, i.e., the LPNM and the RSM. In fact, we consider two different versions of the LPNM discussed in Section 4.3.2. In our investigations, it has been assumed that the AOAs follow the von Mises distribution. Such an assumption allows us to simulate both isotropic and non-isotropic scattering conditions. We demonstrated that the INLSA method is superior to the RSM, and its performance is very close to the LPNM I and LPNM II in approximating the envelope PDF and the ACF, respectively. This makes the INLSA an excellent method for the design of SOC channel simulators.

4.4 Parameter Computation Methods for Measurement-Based Channel Models

The estimation of signal parameters is essential in many practical applications. For instance, the estimation of AOAs is of crucial importance for radars, sonars, and in seismology. The parameter estimation techniques, such as ESPRIT, MUSIC and SAGE, are the classical methods for solving such estimation problems. These methods can be easily extended to measurement-based channel modelling, which has been demonstrated by our investigations in Paper VI.

4.4.1 ESPRIT

In Paper VI, we selected the ESPRIT technique for the performance investigations. This technique relies on the assumption of the uniformly spaced antenna array. For the sake of exposition, we consider a uniform linear array (ULA) antenna structure with M-elements and a steering vector represented in the following form

$$\boldsymbol{a}(\nu_n) = [1 \;\; e^{j\nu_n} \;\; e^{j2\nu_n} \;\; \cdots \;\; e^{j(M-1)\nu_n}]^T, \; n = 1,2,\ldots,N \tag{4.10}$$

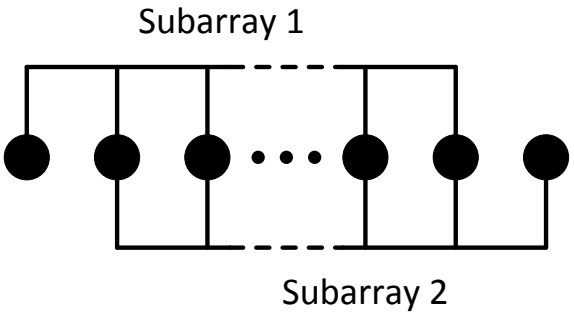

Figure 4.1: The ULA with M identical sensors and two subarrays each with $M-1$ elements.

where the parameter N refers to the number of propagation paths. The spatial frequencies ν_n are related to AOAs θ_n as $\nu_n = -\pi \sin\theta_n$. It is important to mention that ESPRIT requires the condition $N < M$ to be fulfilled [52]. For the ESPRIT scenario in Fig. 4.1, the relation between outputs of subarrays can be represented in terms of the $N \times N$ diagonal matrix $\mathbf{\Phi}$

$$\mathbf{\Phi} = \text{diag}[e^{j\nu_1}, e^{j\nu_2}, \ldots, e^{j\nu_N}]. \tag{4.11}$$

Since the diagonal elements of $\mathbf{\Phi}$ represent the estimates of $e^{j\nu_n}$, the problem of determining the AOAs can be reduced to that of finding $\mathbf{\Phi}$. In general, this is done by exploiting the eigenstructure of the received signal covariance matrix. One way to implement this concept is presented in Paper VI, where the ESPRIT technique is utilized for computing the channel model parameters.

4.4.2 SAGE

The SAGE algorithm is known to have several advantages over the ESPRIT technique. For instance, the SAGE algorithm does not require multiple antenna elements to resolve the parameters corresponding to different signal components. Moreover, it can be utilized for computing not only the AOAs but also any other parameter of interest. In order to explain the concepts behind the SAGE algorithm, we consider the following widely used data model in signal processing

$$x(t) = \sum_{n=1}^{N} s_n(t) + n(t) = \sum_{n=1}^{N} c_n e^{j(2\pi f_{\max}\cos(\alpha_n)t + \theta_n)} + n(t) \tag{4.12}$$

where $n(t)$ is an additive white Gaussian noise process. The parameter N corresponds to the total number of signal components. The gains c_n, AOAs α_n, and phases θ_n are used to describe the nth component of the received signal $s(t)$. In this case, the primary goal of the SAGE algorithm is to determine the set $\mathbb{P}_n = \{\tilde{c}_n, \tilde{\alpha}_n, \tilde{\theta}_n\}$ of the computed values for the parameters c_n, α_n, and θ_n. To accomplish this goal, the SAGE algorithm requires the initial set $\mathbb{P}'_n$, e.g., $\mathbb{P}'_n = \{0,0,0\}$ for $n = 1,2,\ldots,N$. For a given $\mathbb{P}'_n$, the estimate of each signal component is obtained as follows

$$\tilde{s}_n(t) = x(t) - \sum_{l=1, l\neq n}^{N} \tilde{c}_l e^{j(2\pi f_{\max}\cos(\tilde{\alpha}_l)t + \tilde{\theta}_l)}. \tag{4.13}$$

An update procedure is then carried out to compute the new set of parameters $\mathbb{P}''_n$ corresponding to $\tilde{s}_n(t)$. This procedure consists of the following steps

$$\tilde{\alpha}''_l = \arg\max_{\tilde{\alpha}_l} \left\{ |z(\tilde{\alpha}_l, \tilde{\theta}'_l)| \right\} \tag{4.14}$$

$$\tilde{\theta}''_l = \arg\max_{\tilde{\theta}_l} \left\{ |z(\tilde{\alpha}''_l, \tilde{\theta}_l)| \right\} \tag{4.15}$$

$$\tilde{c}''_l = \frac{1}{T} |z(\tilde{\alpha}''_l, \tilde{\theta}''_l)| \tag{4.16}$$

where T represents the maximum time for which $x(t)$ is evaluated and

$$z(\tilde{\alpha}_l, \tilde{\theta}_l) = \int_0^T \tilde{s}_n(t) e^{-j(2\pi f_{\max}\cos(\tilde{\alpha}_l)t + \tilde{\theta}_l)} dt. \tag{4.17}$$

After finding $\mathbb{P}''_n$ for $n = 1,2,\ldots,N$, the log-likelihood function L should be evaluated as

$$L = \frac{1}{\sigma_N} \left[2 \int_0^T Re\{\tilde{s}^*(t) x(t)\} dt - \int_0^T \tilde{s}^2(t) dt \right] \tag{4.18}$$

where $Re\{\cdot\}$ and $||\cdot||$ denote the real part and the norm of the argument, respectively. The update procedure is carried out iteratively until L reaches its maximum.

4.4.3 Performance Comparison of the INLSA, ESPRIT and SAGE

In order to highlight the usefulness of the INLSA method proposed in Paper II, we compare the performance of this method with other methods that can be used for measurement-based channel modelling, such as the ESPRIT and the SAGE. These

methods are originally proposed for estimating the channel parameters, i.e., determining the AOAs, path gains and other relevant parameters. The parameter estimation problem differs significantly from the parameter computation problem in channel modelling. When estimating the parameters, the simplicity of the method and the accuracy of certain channel characteristics are usually not very important. However, these items are crucial for the parametrization problem in channel modelling. In this regard, we study selected parameter estimation methods together with the INLSA method from the perspective of channel modelling in Paper VI.

Concerning the measurements, we have to be aware of the fact that measured impulse responses also carry undesired contributions. These are mainly the interference from other signal sources and most commonly additive white Gaussian noise. In order to emulate such conditions, we assume in Paper VI that the synthetic impulse response is affected by the noise process. Accordingly, the noise is modelled as a white Gaussian process. The synthetic channel model itself is designed as an SOC process. Then, we compare the performance of the SAGE, ESPRIT, and INLSA methods with respect to their capability to approximate the synthetic channel model's correlation properties. The investigations are carried out for two scenarios, one with equal gains and another one with Rayleigh distributed gains in a synthetic channel model. We demonstrate that the INLSA is more advantageous than the ESPRIT and the SAGE in approximating the ACFs of measured channels. Hence, it is better suited for channel modelling purposes, especially if the ACF needs to be modelled properly.

4.5 Chapter Summary and Conclusions

We have introduced extensions of the INLSA method originally proposed in Paper II for the development of SOS and SOC channel models. We have shown that the INLSA approach is very useful for the modelling of both SOS and SOC mobile fading channels. We came to this conclusion through thorough investigations and comparisons with the other highly accurate parameter computation methods in the relevant application fields. We also addressed the parametrization problem in measurement-based channel modelling, where we studied the potential applications of the INLSA method together with the SAGE and ESPRIT methods for such types of channel modelling. Investigations were performed assuming that the measured (synthetic) channel is corrupted by additive white Gaussian noise. From Paper VI, it can be concluded that the flexibility of the proposed INLSA method allows its efficient application to modelling channels based on measurements.

Chapter 5

Summary of Contributions and Outlook

5.1 Major Contributions

This dissertation dealt with the exploration of various aspects of channel modelling for V2X communications. The topics covered parametrization aspects ranging from deterministic Rice and Rayleigh fading channels in V2X communications under different propagation conditions to measurement-based channel models. In the following, the contributions of this doctoral dissertation are summarized.

- An analytical expression for the ACFs of Rice and Rayleigh processes has been derived. The correlation properties of those channels were investigated for realistic asymmetrical Doppler PSDs. Investigations were performed by analyzing the impact of different factors, such as the Rice factor, angular spread, and mean AOA, on the ACF.

- A novel iterative method has been presented for the design of measurement-based channel models for V2X communications. It was shown that the new approach allows us to model accurately the desired statistical characteristics of a measured channel.

- We have extended the INLSA method for scenarios where the measured impulse responses are limited in time. It has been shown that the INLSA approach can efficiently be utilized to mitigate the ACF estimation error in such scenarios.

- We extended the INLSA approach for the design of SOS channel simulators. It has been shown that the novel approach is an excellent choice for the design of Gaussian processes under isotropic scattering conditions.

- In order to accommodate asymmetric propagation conditions and demonstrate the flexibility of the INLSA method, we have also extended the method to the design of SOC channel simulators. We demonstrated that the statistical properties of the reference Gaussian process, such as the ACF and the envelope PDF, can be well approximated if the INLSA method is used.

- The necessity of the performance evaluation in the design and development of measurement-based channel models motivated us to analyze the performance of the INLSA method in comparison with well-known methods, such as the SAGE and the ESPRIT. Once again, the results proved the efficiency, accuracy and the superiority of the INLSA method to the conventional methods.

5.2 Outlook

This dissertation studied parametrization issues in the modelling of various V2X fading channels considering different propagation conditions. The statistical characterization of channel models and the performance analysis of various parameter computation methods were also addressed. However, there are still unsolved problems, which will be described in the following:

- In this dissertation, we derived the ACF of the reference Rice processes. A similar derivation should be implemented for the simulation model.

- The entire channel models presented in this dissertation consider a single antenna at both the transmitter and the receiver side. The parameter computation method can be extended to the design of channel models considering multiple antennas at the transmitter and/or the receiver.

- The performance analysis of the INLSA method for MIMO scenarios should be implemented.

- Moreover, in this dissertation we focused on channel models in two-dimensional environments. Further research is necessary to create channel models for three-dimensional scenarios.

- Hybrid channel models, capturing all the advantages of deterministic and stochastic modelling approaches, should be developed.
- The measurement-based channel models designed in this dissertation rely on the WSSUS assumption. These models can be expanded by considering realistic non-stationary scenarios.

REFERENCES

[1] G. Acosta-Marum and M. A. Ingram, "Six time- and frequency-selective empirical channel models for vehicular wireless LANs," *IEEE Veh. Technol. Mag.*, vol. 2, no. 4, pp. 4–11, Dec. 2007.

[2] A. F. Molisch, *Wireless Communications*, 2nd ed. Chichester, England: John Wiley & Sons, 2010.

[3] I. Ivan *et al.*, "Influence of propagation channel modeling on V2X physical layer performance," in *Proc. 4th European Conference on Antennas and Propagation, EuCAP 2010*, Apr. 2010, pp. 1–5.

[4] A. G. Burr, "Capacity bounds and estimates for the finite scatterers MIMO wireless channel," *IEEE J. Select. Areas Commun.*, vol. 21, no. 5, pp. 812–818, Jun. 2003.

[5] M. Debbah and R. Müller, "MIMO channel modeling and the principle of maximum entropy," *IEEE Trans. Inform. Theory*, vol. 51, no. 5, pp. 1667–1690, May 2005.

[6] J. P. Kermoal *et al.*, "A stochastic MIMO radio channel model with experimental validation," *IEEE J. Select. Areas Commun.*, vol. 20, no. 6, pp. 1211–1226, Aug. 2002.

[7] P. Almers *et al.*, "Survey of channel and radio propagation models for wireless MIMO systems," *EURASIP Journal on Wireless Communications and Networking*, vol. 2007, pp. Article ID: 19070, 19 pages, 2007.

[8] M. Pätzold, *Mobile Radio Channels*, 2nd ed. Chichester: John Wiley & Sons, 2011, 583 pages.

[9] D. Jiang *et al.*, "Design of 5.9 GHz DSRC-based vehicular safety communication," *Wireless Communications*, vol. IEEE 13, no. 5, pp. 36–43, 2006.

[10] D. B. Kenney, "Dedicated short-range communications (DSRC) standards in the United States," *Proceedings of the IEEE*, vol. 99, no. 7, pp. 1162–1182, Jul. 2011.

[11] A. Chelli, "Channel modelling and system performance analysis of vehicle-to-vehicle communication systems," Ph.D. dissertation, University of Agder, Norway, 2013.

[12] C. F. Mecklenbräucker *et al.*, "Vehicular channel characterization and its implications for wireless system design and performance," *Proceedings of the IEEE*, vol. 99, no. 7, pp. 1189–1212, Jul. 2011.

[13] A. F. Molisch, F. Tufvesson, J. Karedal, and C. F. Mecklenbräucker, "Propagation aspects of vehicle-to-vehicle communications - an overview," in *IEEE Radio and Wireless Symposium, RWS '09*. San Diego, CA, USA, Jan. 2009, pp. 179–182.

[14] A. Paier *et al.*, "First results from car-to-car and car-to-infrastructure radio channel measurements at 5.2GHz," in *Proc. 18th IEEE Int. Symp. on Personal, Indoor and Mobile Radio Communications, PIMRC 2007*, Sept 2007, pp. 1–5.

[15] A. F. Molisch, F. Tufvesson, J. Karedal, and C. F. Mecklenbräucker, "A survey on vehicle-to-vehicle propagation channels," *IEEE Wireless Communications*, vol. 16, no. 6, pp. 12–22, Dec. 2009.

[16] L. Bernado *et al.*, "In-tunnel vehicular radio channel characterization," in *Proc. IEEE 73rd Vehicular Technology Conference, IEEE VTC 2011-Spring*, May 2011, pp. 1–5.

[17] ——, "Delay and Doppler spreads of nonstationary vehicular channels for safety-relevant scenarios," *IEEE Trans. Veh. Technol.*, vol. 63, no. 1, pp. 82–93, Jan. 2014.

[18] J. Maurer, T. Fügen, and W. Wiesbeck, "Narrow-band measurement and analysis of the inter-vehicle transmission channel at 5.2 GHz," in *Proc. IEEE 55th Vehicular Technology Conference, IEEE VTC 2002-Spring*, vol. 3, 2002, pp. 1274–1278.

[19] J. Kunisch and J. Pamp, "Wideband car-to-car radio channel measurements and model at 5.9 GHz," in *Proc. IEEE 68th Veh. Technol. Conf., IEEE VTC'08-Fall*. Calgary, Canada, Sep. 2008.

[20] L. Cheng *et al.*, "Mobile vehicle-to-vehicle narrow-band channel measurement and characterization of the 5.9 GHz dedicated short range communication

(DSRC) frequency band," *IEEE J. Select. Areas Commun.*, vol. 25, no. 8, pp. 1501–1516, Oct 2007.

[21] I. Sen and D. W. Matolak, "Vehicle-vehicle channel models for the 5-GHz band," *IEEE Trans. Intell. Trans. Sys.*, vol. 9, no. 2, pp. 235–245, Jun. 2008.

[22] S. O. Rice, "Mathematical analysis of random noise," *Bell Syst. Tech. J.*, vol. 23, pp. 282–332, Jul. 1944.

[23] ——, "Mathematical analysis of random noise," *Bell Syst. Tech. J.*, vol. 24, pp. 46–156, Jan. 1945.

[24] R. Price, "A note on the envelope and phase-modulated components of narrow-band Gaussian noise," *IRE Trans. Inf. Theory*, vol. 1, no. 2, pp. 9–13, Sep. 1955.

[25] C. Iskander and P. T. Mathiopoulis, "Analytical envelope correlation and spectrum of maximal-ratio combined fading signals," *IEEE Trans. Veh. Technol.*, vol. 54, no. 1, pp. 399–404, Jan. 2005.

[26] M. Pätzold, U. Killat, F. Laue, and Y. Li, "On the statistical properties of deterministic simulation models for mobile fading channels," *IEEE Trans. Veh. Technol.*, vol. 47, no. 1, pp. 254–269, Feb. 1998.

[27] C. A. Gutiérrez, A. Melendez, A. Sandoval, and H. Rodriguez, "On the autocorrelation ergodic properties of sum-of-cisoids Rayleigh fading channel simulators," in *Proc. of 11th European Wireless Conference, EW 2007, Vienna, Austria*, Apr. 2011, pp. 1–6.

[28] M. Pätzold and B. Talha, "On the statistical properties of sum-of-cisoids-based mobile radio channel simulators," in *Proc. 10th International Symposium on Wireless Personal Multimedia Communications, WPMC 2007*. Jaipur, India, Dec. 2007, pp. 394–400.

[29] D. Umansky, "Measurement-based channel simulation models for mobile communication systems," Ph.D. dissertation, University of Agder, Kristiansand, 2010.

[30] T. S. Rappaport, *Wireless Communications: Principles and Practice*. Upper Saddle River, New Jersey: Prentice-Hall, 1996.

[31] Propsound CS, "Propsound CS - Multi-dimensional Channel Sounder," [online], http://www.anite.com/propsim (Accessed: 30 September 2013).

[32] P. A. Bello, "Characterization of randomly time-variant linear channels," *IEEE Trans. Commun. Syst.*, vol. 11, no. 4, pp. 360–393, Dec. 1963.

[33] D. Umansky and M. Pätzold, "Stationarity test for wireless communication channels," in *Proc. IEEE Global Communications Conference, IEEE GLOBECOM 2009*. Honolulu, Hawaii, USA, Nov./Dec. 2009.

[34] G. Matz, "On non-WSSUS wireless fading channels," *IEEE Trans. Wireless Commun.*, pp. 2465–2478, Sep. 2005.

[35] A. Papoulis and S. U. Pillai, *Probability, Random Variables and Stochastic Processes*, 4th ed. New York: McGraw-Hill, 2002.

[36] R. Roy and T. Kailath, "ESPRIT-estimation of signal parameters via rotational invariance techniques," *IEEE Trans. Acoust., Speech, Signal Processing*, vol. 37, no. 7, pp. 984–995, Jul. 1989.

[37] M. Haardt and J. A. Nossek, "Unitary ESPRIT: how to obtain increased estimation accuracy with a reduced computational burden," *IEEE Trans. Signal Process.*, vol. 43, no. 5, pp. 1232–1242, May 1995.

[38] M. Feder and E. Weinstein, "Parameter estimation of superimposed signals using the EM algorithm," *IEEE Trans. Acoust., Speech, and Signal Processing*, vol. 36, no. 4, pp. 477–489, Aug. 1988.

[39] R. O. Schmidt, "Multiple emitter location and signal parameter estimation," *IEEE Trans. Antennas Propag.*, vol. AP-34, no. 3, pp. 276–280, Mar. 1986.

[40] B. H. Fleury, M. Tschudin, R. Heddergott, D. Dahlhaus, and K. I. Pedersen, "Channel parameter estimation in mobile radio environments using the SAGE algorithm," *IEEE J. Select. Areas Commun.*, vol. 17, no. 3, pp. 434–450, Mar. 1999.

[41] C. B. Ribeiro, E. Ollila, and V. Koivunen, "Stochastic maximum likelihood method for propagation parameter estimation," in *Proc. 15th IEEE Int. Symp. Personal, Indoor and Mobile Radio Commun., PIMRC 2004*, vol. 3, Sept. 2004, pp. 1839–1843.

[42] D. Umansky and M. Pätzold, "Design of measurement-based wideband mobile radio channel simulators," in *Proc. 4th IEEE International Symposium on Wireless Communication Systems, ISWCS 2007, Trondheim, Norway*, Oct. 2007, pp. 229–235.

[43] A. Chelli and M. Pätzold, "An improved method for estimating the time ACF of a sum of complex plane waves," in *Proc. IEEE GLOBECOM 2010*. Miami, Florida, USA, Dec. 2010, DOI 10.1109/GLOCOM.2010.5683495.

[44] ——, "An improved method for estimating the frequency correlation function," in *Proc. 2012 IEEE Wireless Communications and Networking Conference, WCNC 2012*. Paris, France, Apr. 2012, pp. 1054–1059.

[45] M. Pätzold, U. Killat, and F. Laue, "A deterministic model for a shadowed Rayleigh land mobile radio channel," in *Proc. 5th IEEE Int. Symp. Personal, Indoor and Mobile Radio Commun., PIMRC'94*. The Hague, The Netherlands, Sep. 1994, pp. 1202–1210.

[46] ——, "A deterministic digital simulation model for Suzuki processes with application to a shadowed Rayleigh land mobile radio channel," *IEEE Trans. Veh. Technol.*, vol. 45, no. 2, pp. 318–331, May 1996.

[47] M. Pätzold, U. Killat, F. Laue, and Y. Li, "A new and optimal method for the derivation of deterministic simulation models for mobile radio channels," in *Proc. IEEE 46th Veh. Technol. Conf., VTC'96*, vol. 3. Atlanta, Georgia, USA, Apr./May 1996, pp. 1423–1427.

[48] B. O. Hogstad, M. Pätzold, N. Youssef, and D. Kim, "A MIMO mobile-to-mobile channel model: Part II – The simulation model," in *Proc. 16th IEEE Int. Symp. on Personal, Indoor and Mobile Radio Communications, PIMRC 2005*, vol. 1. Berlin, Germany, Sep. 2005, pp. 562–567.

[49] C. A. Gutiérrez and M. Pätzold, "The generalized method of equal areas for the design of sum-of-cisoids simulators for mobile Rayleigh fading channels with arbitrary Doppler spectra," *Wireless Communications and Mobile Computing*, 2011, published online, DOI 10.1002/wcm.1154.

[50] ——, "The Riemann sum method for the design of sum-of-cisoids simulators for Rayleigh fading channels in non-isotropic scattering environments," in *Proc.*

IEEE Workshop on Mobile Computing and Network Technologies, WMCNT 2009. St. Petersburg, Russia, Oct. 2009.

[51] A. Paulraj, R. Roy, and T. Kailath, "A subspace rotation approach to signal parameter estimation," in *Proceedings of the IEEE*, vol. 74, no. 7, Jul. 1986, pp. 1044–1046.

[52] H. Krim and M. Viberg, "Two decades of array signal processing," *IEEE Signal Processing Magazine*, vol. 13, no. 4, pp. 67–94, Jul. 1996.

Appendices A–G

List of Publications

The purpose of this preface is to record all the articles that are outcomes of the research work carried out by the author of this dissertation.

The list of publications consists of submitted and already published papers. First, the next section lists those articles which are briefly discussed in Chapters 2–5 of this dissertation and are replicated in Appendices A–F. Thereafter, the subsequent section details those papers which are published within the framework of this doctoral thesis, however they are not addressed in this dissertation.

Articles Included in this Dissertation

Those articles which are included in Appendices A–F of this dissertation are tabulated as follows:

Paper I A. Fayziyev, M. Pätzold and N. Youssef, "On the autocorrelation function of Rice processes for unsymmetrical Doppler power spectral densities," in *Proc. IEEE International Conference on Advanced Technologies for Communications, ATC 2010*, Ho Chi Minh City, Vietnam, Oct. 2010, pp. 139 – 144.

Paper II A. Fayziyev and M. Pätzold, "An improved iterative nonlinear least square approximation method for the design of SISO wideband mobile radio channel simulators," in *REV Journal on Electronics and Communications*, vol. 1, no. 1-2, pp. 19 – 25, January – June, 2012.

Paper III A. Fayziyev, M. Pätzold, E. Masson, Y. Cocheril and M. Berbineau, "A measurement-based channel model for vehicular communications in

tunnels," in *Proc. Wireless Communication and Network Conference, WCNC 2014*, Istanbul, Turkey, Apr. 2014, pp. 128 – 133.

Paper IV A. Fayziyev and M. Pätzold, "The design of sum-of-sinusoids channel simulators using the iterative nonlinear least square approximation method," *Proc. 20th International Conference on Software, Telecommunications and Computer Networks, SoftCOM 2012*, Split, Croatia, Sep. 2012.

Paper V A. Fayziyev and M. Pätzold, "The design of sum-of-cisoids channel simulators using the iterative nonlinear least square approximation method," *Proc. IEEE International Conference on Advanced Technologies for Communications, ATC 2013*, Ho Chi Minh City, Vietnam, Oct. 2013, pp. 511 – 515.

Paper VI A. Fayziyev and M. Pätzold, "The Performance of the INLSA in Comparison with the SAGE and ESPRIT Algorithms," in *Proc. IEEE International Conference on Advanced Technologies for Communications, ATC 2014*, Ho Chi Minh City, Vietnam, Oct. 2014, pp. 332 – 337.

In the next section, those papers are listed which have not been reproduced in this paper collection.

Articles Not Included in this Dissertation

The article pointed out in the following is also published during this PhD study and carry equal importance as the ones mentioned in the previous section. However, to reduce the overlap between the articles making up the final manuscript, it is not addressed in this dissertation.

Paper VII A. Fayziyev and M. Pätzold, "An improved iterative nonlinear least square approximation method of the design of measurement-based wideband mobile radio channel simulators," *Proc. IEEE International Conference on Advanced Technologies for Communications, ATC 2011*, Da Nang, Vietnam, Oct. 2011, pp. 106 – 111.

Appendix A

Paper I

Title:	On the Autocorrelation Function of Rice Processes for Unsymmetrical Doppler Power Spectral Densities
Authors:	**Akmal Fayziyev**[1], Matthias Pätzold[1] and Neji Youssef[2]
Affiliations:	[1]University of Agder, Faculty of Engineering and Science, P. O. Box 509, NO-4898 Grimstad, Norway [2]Ecole Supérieure des Communications de Tunis, 2083 EL Ghazala, Ariana, Tunisia
Conference:	*IEEE International Conference on Advance Technologies for Communications, ATC 2010*, Ho Chi Minh City, Vietnam, Oct. 2010.

On the Autocorrelation Function of Rice Processes for Unsymmetrical Doppler Power Spectral Densities

Akmal Fayziyev[1] and Matthias Pätzold[1] and Neji Youssef[2]
[1]Faculty of Engineering and Science, University of Agder,
P.O. Box 509, NO-4898 Grimstad, Norway
E-mails: {akmal.fayziyev, matthias.paetzold}@uia.no
[2]Ecole Supérieure des Communications de Tunis,
2083 EL Ghazala, Ariana, Tunisia
E-mail:neji.youssef@supcom.rnu.tn

***Abstract* — In this paper, we derive an analytical expression for the autocorrelation function (ACF) of Rice processes in the general case of unsymmetrical Doppler power spectral densities. This expression, which is obtained based on the multidimensional Gaussian distribution approach, is shown to cover the ACF of Rayleigh processes as a special case. Various numerical examples are presented to illustrate the impact of the channel parameters on the ACF. Computer simulations, considering the von Mises distribution for the angle of arrivals, are also performed to check the validity of the analytical result. Finally, the analysis of the covariance spectrum is addressed.**

***Index Terms* — Rice processes, sum-of-cisoids, non-isotropic scattering, autocorrelation function, power spectral density, covariance spectrum**

I. INTRODUCTION

When dealing with the multipath propagation scenarios, the received signal often consists of the coherent and diffuse components. In such scenarios, the simplest Rice and Rayleigh processes are used to characterize the properties of the received signal envelope for relatively small areas. Several measurement and analytical results support this approach [1, 2].

In this respect, the knowledge of the correlation properties and power spectrum of Rice and Rayleigh processes is of crucial interest. Several approaches have been proposed for the derivation of the envelope ACF [3–5]. In [3], the author described the properties of the envelope correlation functions and presented comparisons of the envelope and complex ACFs for both Rayleigh and Rice fading channels. Exact analytical expressions of the envelope ACF have been derived for Rayleigh and Rice fading channels. Another related work in [4] deals with the ACF and the covariance spectrum analysis of Rayleigh fading channels under isotropic scattering, implying that the Doppler power spectral density (DPSD) has a symmetrical shape. Similar studies could be found in [5], where the authors obtained the exact analytical expression for the envelope ACF of Rayleigh, Rice and Nakagami fading channels by using the theory of multidimensional Gaussian distribution. In [5], also approximations to the envelope power spectrum are presented for Rayleigh and Nakagami fading channels. Some results dealing with the correlation properties of the envelope with unsymmetrical DPSD (non-isotropic scattering) have been discussed in [6]. However, to the best of our knowledge no results dealing with the envelope power spectrum and ACF in non-isotropic scattering can be found in the literature for Rice fading channels.

The main objective of this paper is to present a novel approach and fundamental results on the statistical properties of the received signal envelope. In this connection, an exact analytical expression is obtained for the ACF of Rice processes. The ACF of the Rayleigh process is derived as a special case of the Rice process. The correctness of all the theoretical results is confirmed by computer simulations using the sum-of-cisoids (SOC) principle [7], considering the von Mises distribution of AOAs. Moreover, the impact of the Rice factor and several other important parameters on the ACF and the covariance spectrum is studied.

The rest of the paper is organized as follows. Section II contains the review of the typical propagation scenario. Based on this scenario, the ACF of Rice and Rayleigh processes are derived in Section III. In Section IV, we introduce an SOC-

based channel simulator for Rice and Rayleigh fading channels. Numerical examples and results verification are combined into Section V. Finally, Section VI concludes this work.

II. Review of Rice Processes

Typical propagation scenario corresponding to Rice multipath environment is illustrated in Fig. A.1. We assume that both the transmitter and the receiver are equipped with single omnidirectional antennas, the transmitter is fixed while the receiver is moving along the direction of the vector $\overrightarrow{v}$.

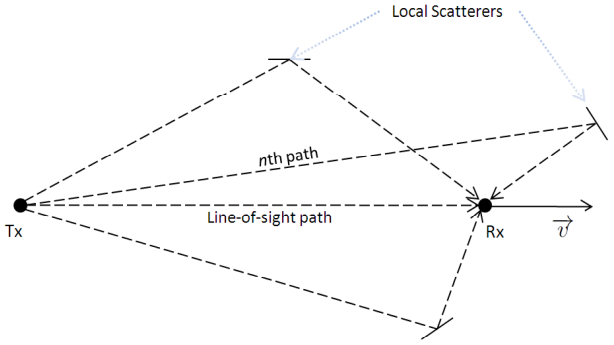

Figure A.1: Typical Multipath Propagation Scenario.

If the channel is frequency-nonselective, the received signal over this scenario can be represented as a delayed version of the transmitted signal multiplied by a complex stochastic process. This stochastic process is the superposition of the line-of-sight component with the diffuse component. The latter component accounts for the sum of the scattered components and is often described by a zero-mean complex Gaussian process [8]

$$\mu(t) = \mu_1(t) + j\mu_2(t) \tag{A.1}$$

where $\mu_1(t)$ and $\mu_2(t)$ are real-valued zero-mean Gaussian processes with a variance σ_0^2. The ACF $r_{\mu\mu}(\tau)$ of $\mu(t)$ is in general complex and has the form

$$\begin{aligned} r_{\mu\mu}(\tau) &= r_{\mu_1\mu_1}(\tau) + r_{\mu_2\mu_2}(\tau) + j[r_{\mu_1\mu_2}(\tau) - r_{\mu_2\mu_1}(\tau)] \\ &= 2[r_{\mu_1\mu_1}(\tau) + j r_{\mu_1\mu_2}(\tau)] \end{aligned} \tag{A.2}$$

For simplicity, the line-of-sight component of the received signal is assumed to be time-invariant and is described by

$$m = m_1 + jm_2 = \rho e^{j\theta_\rho} \tag{A.3}$$

where ρ and θ_ρ denote the amplitude and the phase, respectively. In this connection, we introduce a further complex Gaussian process with time-invariant mean m

$$\mu_\rho(t) = \mu_{\rho_1}(t) + j\mu_{\rho_2}(t) = \mu(t) + m \tag{A.4}$$

Now, the Rice process can be obtained from (A.4), according to

$$\xi(t) = |\mu(t) + m| \tag{A.5}$$

The Rayleigh process is a special case of the Rice process and is obtained from (A.5) by setting the amplitude of the line-of-sight component equal to zero, i.e., $\rho = 0$. That is

$$\zeta(t) = |\mu(t)| = |\mu_1(t) + j\mu_2(t)| \tag{A.6}$$

III. Derivation of the ACF of Rice processes

The ACF of the Rice process $\xi(t)$ is defined as

$$r_{\xi\xi}(\tau) = E\{\xi(t)\xi(t+\tau)\} \tag{A.7}$$

For any fixed time instant $t = t_0$, the ACF $r_{\xi\xi}(\tau)$ can be written as

$$r_{\xi\xi}(\tau) = E\left\{\sqrt{(\mu_{\rho_1}^2 + \mu_{\rho_2}^2)(\mu_{\rho_1}'^2 + \mu_{\rho_2}'^2)}\right\} \tag{A.8}$$

where $\mu_{\rho_i} = \mu_i(t_0) + m_i$ and $\mu'_{\rho_i} = \mu_i(t_0+\tau) + m_i$ are Gaussian random variables with mean m_i. Equation (A.8) can be further put into form of the fourfold integral

$$\begin{aligned} r_{\xi\xi}(\tau) = &\int_0^\infty \int_0^\infty \int_0^\infty \int_0^\infty \sqrt{(x_1^2 + x_2^2)(x_1'^2 + x_2'^2)} \\ &\times p_{\mu_{\rho_1}\mu_{\rho_2}\mu'_{\rho_1}\mu'_{\rho_2}}(x_1, x_2, x_1', x_2')dx_1dx_2dx_1'dx_2' \end{aligned} \tag{A.9}$$

where $p_{\mu_{\rho_1}\mu_{\rho_2}\mu'_{\rho_1}\mu'_{\rho_2}}(\cdot,\cdot,\cdot,\cdot)$ denotes the joint probability density function (PDF) of $\mu_{\rho_1}, \mu_{\rho_2}, \mu'_{\rho_1}$, and μ'_{ρ_2} and can be obtained from the multivariate Gaussian distribution [9]. It is shown in the appendix that this PDF is given by

$$
\begin{aligned}
&p_{\mu_{\rho_1}\mu_{\rho_2}\mu'_{\rho_1}\mu'_{\rho_2}}(x_1,x_2,x'_1,x'_2) = \frac{1}{4\pi^2 D} e^{-\frac{1}{D}\rho^2(\sigma_0^2 - r_{\mu_1\mu_1}(\tau))} \\
&\times e^{-\frac{\sigma_0^2}{2D}(x_1^2+x_2^2+x'^2_1+x'^2_2)} \\
&\times e^{-\frac{1}{2D}(2r_{\mu_1\mu_1}(\tau)(x_1x'_1+x_2x'_2)+2r_{\mu_1\mu_2}(\tau)(x_1x'_2-x_2x'_1))} \\
&\times e^{\frac{1}{D}r_{\mu_1\mu_1}(\tau)(\rho\cos\theta_\rho(x_1+x'_1)+\rho\sin\theta_\rho(x_2+x'_2))} \\
&\times e^{\frac{1}{D}r_{\mu_1\mu_2}(\tau)(\rho\cos\theta_\rho(x_2-x'_2)+\rho\sin\theta_\rho(x'_1-x_1))}
\end{aligned} \tag{A.10}
$$

By transforming Cartesian coordinates into polar coordinates according to

$$
\begin{aligned}
x_1 &= z\cos\theta, \qquad x_2 = z\sin\theta, \\
x'_1 &= z'\cos\theta', \qquad x'_2 = z'\sin\theta'
\end{aligned} \tag{A.11}
$$

and then performing the integration with respect to z' and θ' using [10, Eq. 6.631(1)] and [10, Eq. 3.338(4)], respectively, we get the following expression for the desired ACF

$$
\begin{aligned}
r_{\xi\xi}(\tau) \;=\; & \frac{1}{4\pi\sigma_0^2}\sqrt{\frac{2\pi D}{\sigma_0^2}} e^{-\frac{\sigma_0^2 - r_{\mu_1\mu_1}(\tau)}{D}\rho^2} \times \int_0^\infty \int_{-\pi}^{\pi} z^2 e^{-\frac{\sigma_0^2}{2D}z^2 + \frac{C_2\cos\theta + C_3\sin\theta}{D}z} \\
& \times {}_1F_1\left(\frac{3}{2}, 1; \frac{(B_0 z - C_0)^2 + (B_1 z - C_1)^2}{2\sigma_0^2 D}\right) dz\, d\theta
\end{aligned} \tag{A.12}
$$

where ${}_1F_1(\cdot,\cdot;\cdot)$ is the confluent hypergeometric function.

Furthermore, in (A.12)

$$
\begin{aligned}
C_0 &= (\sigma_0^2 - r_{\mu_1\mu_1}(\tau))\rho\cos\theta_\rho - r_{\mu_1\mu_2}(\tau)\rho\sin\theta_\rho \\
C_1 &= (\sigma_0^2 - r_{\mu_1\mu_1}(\tau))\rho\sin\theta_\rho + r_{\mu_1\mu_2}(\tau)\rho\cos\theta_\rho \\
C_2 &= (\sigma_0^2 - r_{\mu_1\mu_1}(\tau))\rho\cos\theta_\rho + r_{\mu_1\mu_2}(\tau)\rho\sin\theta_\rho \\
C_3 &= (\sigma_0^2 - r_{\mu_1\mu_1}(\tau))\rho\sin\theta_\rho - r_{\mu_1\mu_2}(\tau)\rho\cos\theta_\rho \\
B_0 &= r_{\mu_1\mu_1}(\tau)\cos\theta + r_{\mu_1\mu_2}(\tau)\sin\theta \\
B_1 &= r_{\mu_1\mu_1}(\tau)\sin\theta - r_{\mu_1\mu_2}(\tau)\cos\theta
\end{aligned} \tag{A.13}
$$

Unfortunately, there is no closed-form solution for the double integral involved in (A.12). Considerable simplifications, however, can be made for the Rayleigh process. For this case, we can come to the well-known closed-form solution [11]

$$r_{\zeta\zeta}(\tau) = \sigma_0^2 \frac{\pi}{2} F\left(-\frac{1}{2}, -\frac{1}{2}; 1; \frac{r_{\mu_1\mu_1}^2(\tau) + r_{\mu_1\mu_2}^2(\tau)}{\sigma_0^2}\right) \tag{A.14}$$

where $F(\cdot,\cdot;\cdot;\cdot)$ is the hypergeometric function. We should mention that, although, the formula for the ACF we could obtain is not in closed form, it has a lower numerical computation complexity in comparison with the one reported in [5].

IV. The Simulation Model

As a suitable method to model the underlying complex Gaussian process with given correlation properties, the SOC-principle can be considered [7]. The simulation model $\hat{\xi}(t)$ can be acquired from the reference model given in (A.5) by substituting the underlying Gaussian process $\mu(t)$ with one that is obtained from the SOC-based model

$$\hat{\xi}(t) = |\hat{\mu}_\rho(t)| = |\hat{\mu}(t) + m| \tag{A.15}$$

In this case, the complex process $\hat{\mu}(t) = \hat{\mu}_1(t) + j\hat{\mu}_2(t)$ can be written as

$$\hat{\mu}(t) = \sum_{n=1}^{N} c_n e^{j(2\pi f_n t + \phi_n)} \tag{A.16}$$

In (A.16), N denotes the number of complex sinusoids (cisoids), c_n is the gain, f_n is the Doppler frequency, and ϕ_n is the phase of the n-th cisoid of the process $\hat{\mu}(t)$. The Doppler frequency can also be represented in terms of AOA α_n of the scattered component as $f_n = f_{\max}\cos\alpha_n$, where $f_{\max}$ is the maximum Doppler frequency. The SOC-model assumes that the gains c_n and frequencies f_n are constant, while the phases ϕ_n are independent, identically distributed (i.i.d) random variables, each having a uniform distribution over $[-\pi, \pi)$. In [7], it has been shown that, by choosing the parameters appropriately, a very good approximation can be achieved in such way that the statistical properties of $\hat{\mu}(t)$ are very close to those of $\mu(t)$.

In this simulation model, the ACF $r_{\hat{\mu}_i\hat{\mu}_i}(\tau)$ of $\hat{\mu}_i(t)$ $i = 1,2$ as well as the cross-correlation function $r_{\hat{\mu}_1\hat{\mu}_2}(\tau)$ are given by [7]

$$r_{\hat{\mu}_i\hat{\mu}_i}(\tau) = \sum_{n=1}^{N} \frac{c_n^2}{2}\cos(2\pi f_n \tau) \tag{A.17}$$

and

$$r_{\hat{\mu}_1\hat{\mu}_2}(\tau) = \sum_{n=1}^{N} \frac{c_n^2}{2} \sin(2\pi f_n \tau) \tag{A.18}$$

respectively. When dealing with SOC-method, the determination of appropriate quantities for the parameters c_n and f_n (or α_n) is required. Several parameter computation methods for both isotropic and non-isotropic scattering appear in the literature [12–15]. For the purpose of simulating Rice process with unsymmetrical PSD, the basic approach of the Riemann sum method (BRSM), described in [14], has been selected.

V. Numerical Results

In order to test and evaluate the obtained results, it is necessary to specify the scattering conditions. For our purposes, the well-known von Mises distribution for the AOA α_n is adopted. The von Mises PDF was proposed in [16], and is given by

$$p_\alpha(\alpha) = \frac{\exp[\kappa \cos(\alpha - m_\alpha)]}{2\pi I_0(\kappa)} \tag{A.19}$$

where $I_0(\cdot)$ is the modified Bessel function of order zero, $\alpha \in [-\pi, \pi)$, $m_\alpha \in [-\pi, \pi)$ denotes the mean AOA, and κ is a parameter determining the angular spread. It can easily be verified that in case of $\kappa = 0$, (A.19) reduces to the uniform distribution of the AOAs. In [16], it has been shown that the ACF of a complex envelope $r_{\mu\mu}(\tau)$ can be represented as

$$r_{\mu\mu}(\tau) = \frac{\sigma_\mu I_0(\sqrt{\kappa^2 - 4\pi^2 f_{\max}^2 \tau^2 + j4\pi\kappa \cos(m_\alpha) f_{\max} \tau})}{I_0(\kappa)} \tag{A.20}$$

Similarly, in case of $\kappa = 0$, (A.20) simplifies to the well-known Clarke's isotropic scattering form, i.e., $r_{\mu\mu}(\tau) = \sigma_\mu J_0(2\pi f_{\max}\tau)$, where $J_0(\cdot)$ is the zeroth order Bessel function of the first kind.

In this section, for the purpose of demonstrating the correctness we compare the ACF with corresponding simulation ACF determined for Rice and Rayleigh processes. Both symmetrical and unsymmetrical DPSDs for the underlying Gaussian processes are considered. For obtaining the simulation ACFs, the number of cisoids $N = 100$ and $N = 50$ are used for Rayleigh and Rice processes, respectively. We set the maximum Doppler frequency to $f_{\max} = 91$ Hz and the power of the sum of scattered components to $\sigma_\mu^2 = 2\sigma_0^2 = 2$. Since θ_ρ has no impact on the correlation

properties of the received signal envelope we will keep it constant ($\theta_\rho = 0$) throughout the simulations.

Of particular interest is the impact of the Rice factor on the correlation properties of the envelope. When the scattered power is fixed to σ_μ^2, this impact can be studied by comparing the curves obtained for various values of ρ.

In Fig. A.2, the autocovariance function of Rice processes $r^c_{\xi\xi}(\tau) = r_{\xi\xi}(\tau) - m_\xi^2$ is illustrated. Here, m_ξ^2 denotes the squared mean of the Rice process. From that figure, we observe that the local amplitudes increase with ρ.

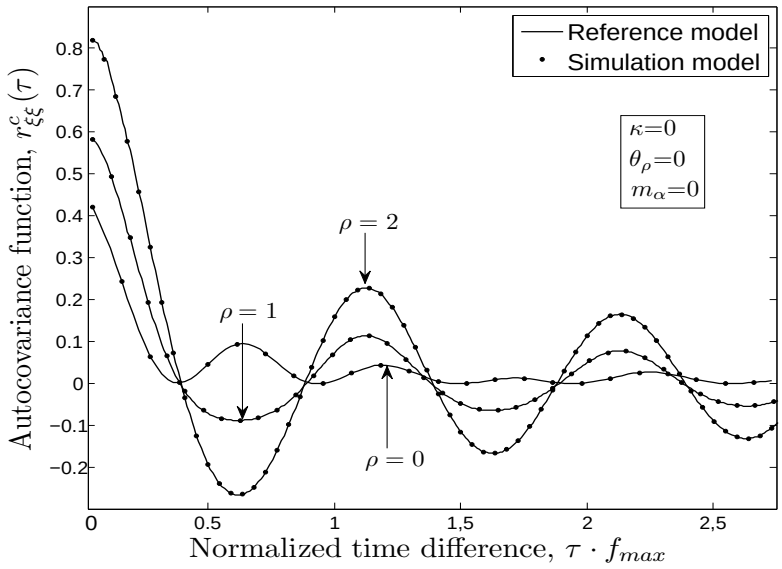

Figure A.2: Autocovariance function $r^c_{\xi\xi}(\tau)$ of Rice processes $\xi(t)$ for different values of ρ.

The parameters κ and m_α have an impact on the channel scattering conditions, as well as on the correlation properties of the envelope. In Figs. A.3 and A.4, the ACF of Rice and Rayleigh processes is depicted for different values of κ, when $m_\alpha = 0$. It can easily be seen from figures that the local amplitudes increase with the von Mises distribution parameter κ. The similar behavior can be noticed for the ACF of Rayleigh processes (see Fig. A.4). We also plot the curves illustrating the impact of m_α on the correlation properties of the envelope in Figs. A.5 and A.6, for Rice and Rayleigh processes, respectively. As it is readily apparent in the graphs, m_α has significant impact on the correlation properties of the received signal envelope.

In the following, we will focus on the analysis of the envelope covariance spectrum $S^c_{\xi\xi}(f)$, which is defined as the Fourier transform of the autocovariance function $r^c_{\xi\xi}(\tau)$. From Fig. A.7, we observe that nonzero Rice factor results in a second peak

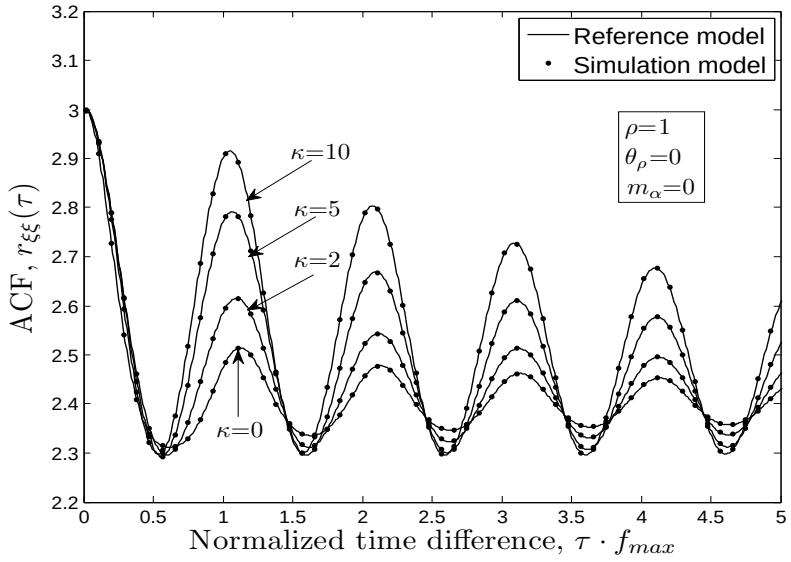

Figure A.3: ACF $r_{\xi\xi}(\tau)$ of Rice processes $\xi(t)$ for different values of κ.

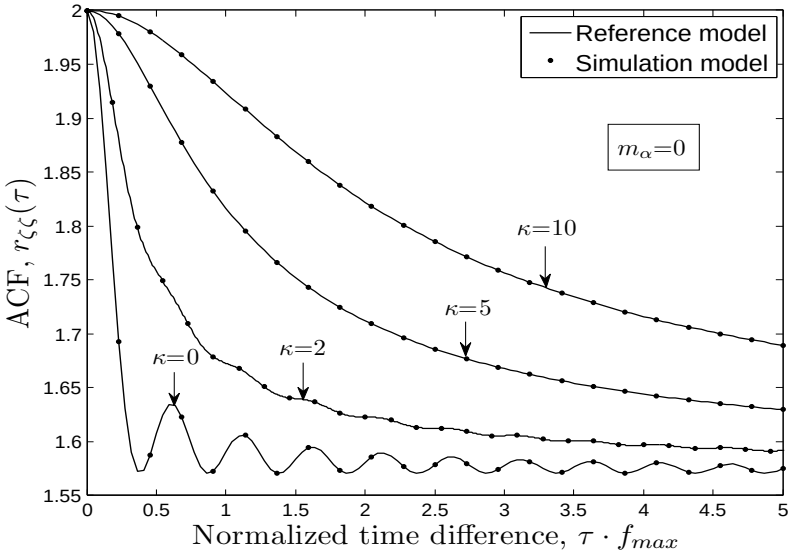

Figure A.4: ACF of Rayleigh processes $r_{\zeta\zeta}(\tau)$ for different values of κ.

located at $f_{\max}$. Further, any increase in the value of ρ causes higher power allocation around the frequency $f_{\max}$, whereas the total power in the frequency range $f_{\max} < f \leq 2f_{\max}$ becomes smaller. The cut-off frequency remains constant for all values of ρ and located at $2f_{\max}$. However, we note from the inspection of Figs. A.8 and A.9 that at high values of κ the cut-off frequency is shifted and is seen to be smaller than $2f_{\max}$. It is evident from visual inspection of the plots illustrated in

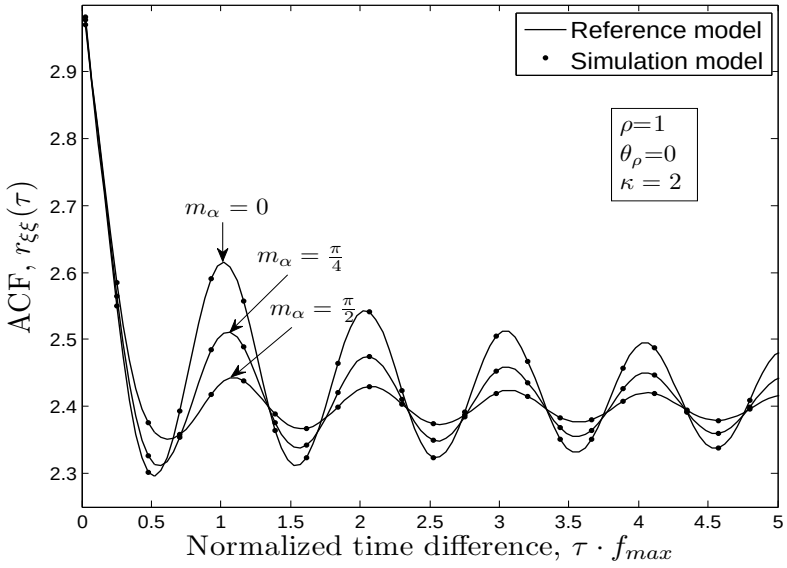

Figure A.5: ACF $r_{\xi\xi}(\tau)$ of Rice processes $\xi(t)$ for different values of m_α.

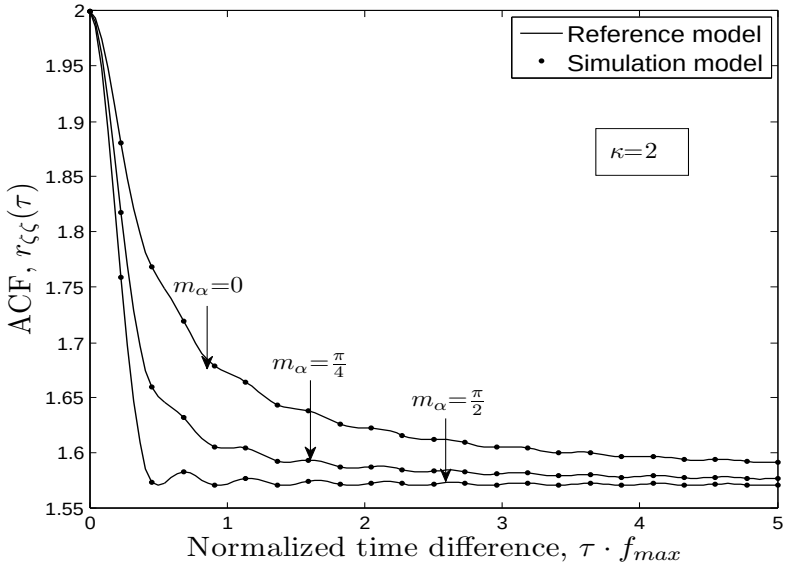

Figure A.6: ACF $r_{\zeta\zeta}(\tau)$ of Rayleigh processes $\zeta(t)$ for different values of m_α.

Figs. A.10 and A.11, that m_α has no impact on the cut-off frequency. However, m_α significantly affects the power allocation at low frequencies.

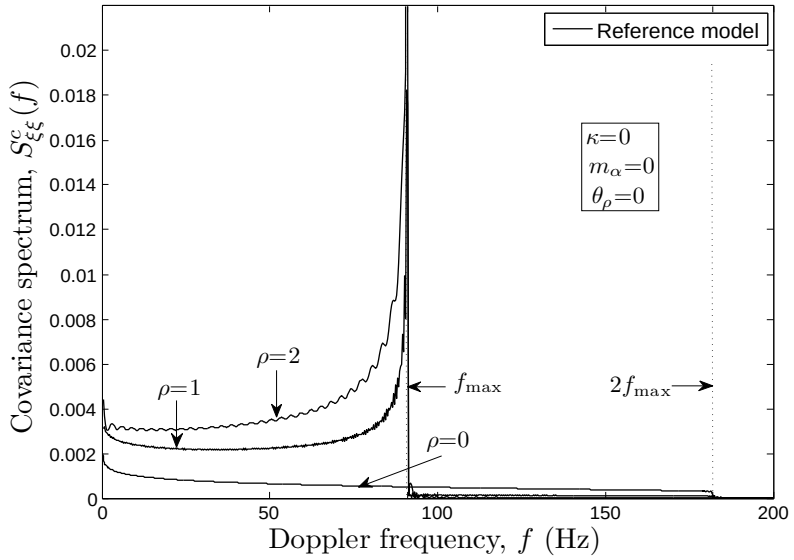

Figure A.7: Covariance spectrum $S^c_{\xi\xi}(f)$ of Rice processes $\xi(t)$ for different values of ρ.

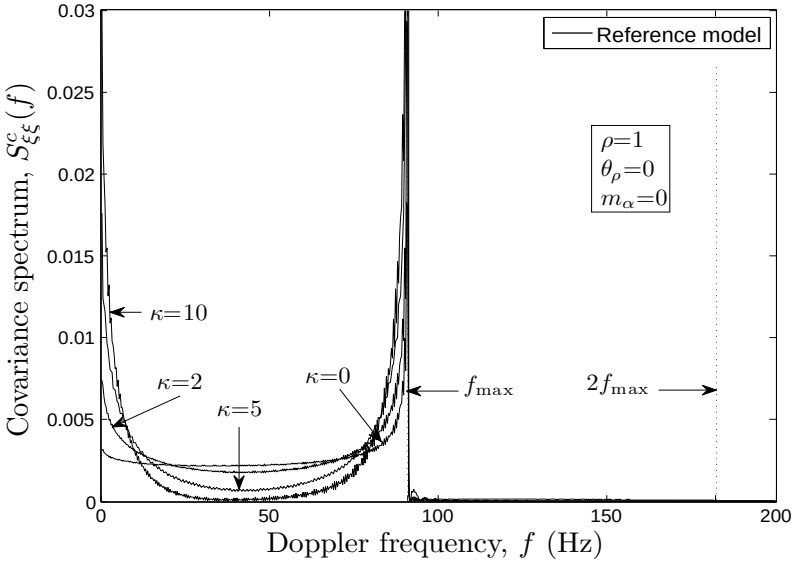

Figure A.8: Covariance spectrum $S^c_{\xi\xi}(f)$ of Rice processes $\xi(t)$ for different values of κ.

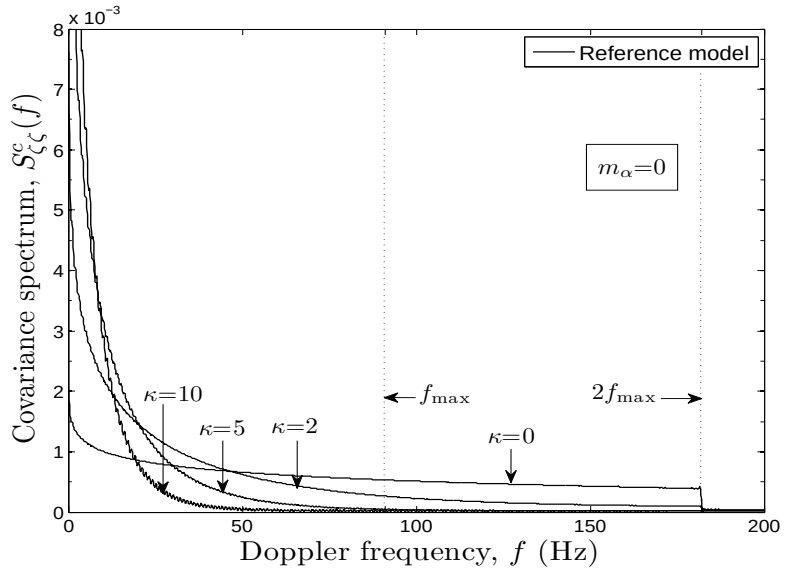

Figure A.9: Covariance spectrum $S^c_{\zeta\zeta}(f)$ of Rayleigh processes $\zeta(t)$ for different values of κ.

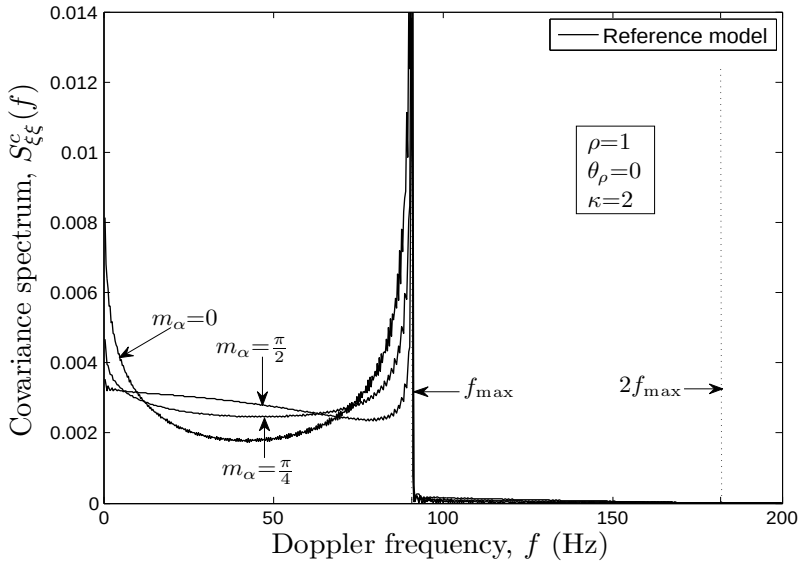

Figure A.10: Covariance spectrum $S^c_{\xi\xi}(f)$ of Rice processes $\xi(t)$ for different values of m_α.

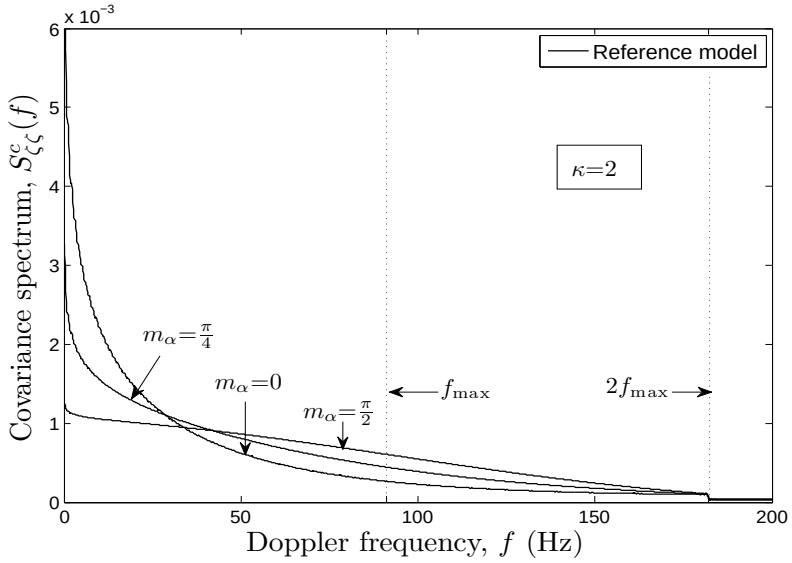

Figure A.11: Covariance spectrum $S^c_{\zeta\zeta}(f)$ of Rayleigh $\zeta(t)$ processes for different values of m_α.

VI. Conclusion

In this paper, a new improper integral form expression is presented for the ACF of the Rice process. This result is obtained by applying the multidimensional Gaussian distribution approach. The Rayleigh process is also considered as a special case. Obtained results are verified by computer simulations using the SOC-based channel simulator for Rice fading channels. The results impressively show the excellent accordance between the reference model and the simulation model. The acquired expressions for the ACF can be easily implemented in simulation platforms and used for the laboratory analysis of mobile communication systems. Moreover, the impact of the Rice factor and the parameters of von Mises distribution on the ACF and covariance spectrum has been analyzed for symmetrical and unsymmetrical DPSD cases. Graphically illustrated simulation results indicate that the Rice factor and the distribution of the AOAs have a significant influence on the correlation properties of the Rice process, as well as on the spectrum.

APPENDIX A.A

In this appendix, we derive the joint PDF of $\mu_{\rho_1}, \mu_{\rho_2}, \mu'_{\rho_1}$, and μ'_{ρ_2} using the multivariate Gaussian distribution formula. Namely,

$$p_{\mu_{\rho_1}\mu_{\rho_2}\mu'_{\rho_1}\mu'_{\rho_2}}(x_1,x_2,x'_1,x'_2) = \frac{1}{4\pi^2\sqrt{\det \mathbf{C}_{\mu_\rho}}} \times e^{-\frac{1}{2}(\mathbf{x}-\mathbf{m}_{\mu_\rho})^{\mathrm{T}}\mathbf{C}^{-1}_{\mu_\rho}(\mathbf{x}-\mathbf{m}_{\mu_\rho})} \tag{A.21}$$

where

$$\mathbf{x} = \begin{pmatrix} x_1 \\ x_2 \\ x'_1 \\ x'_2 \end{pmatrix}, \quad \mathbf{m}_{\mu_\rho} = \begin{pmatrix} E\{\mu_{\rho_1}\} \\ E\{\mu_{\rho_2}\} \\ E\{\mu'_{\rho_1}\} \\ E\{\mu'_{\rho_2}\} \end{pmatrix} = \begin{pmatrix} m_1 \\ m_2 \\ m_1 \\ m_2 \end{pmatrix} \tag{A.22}$$

and $\det \mathbf{C}_{\mu_\rho}$ ($\mathbf{C}^{-1}_{\mu_\rho}$) denotes the determinant (inverse) of the covariance matrix $\mathbf{C}_{\mu_\rho}$ the elements of which are given by

$$C_{\mu_{\rho_i}\mu_{\rho_j}} = E\{(\mu_{\rho_i} - m_{\mu_{\rho_i}})(\mu_{\rho_j} - m_{\mu_{\rho_j}})\}, \ \forall i,j = 1,2,3,4 \tag{A.23}$$

For our scenario, the covariance matrix $\mathbf{C}_{\mu_\rho}$ has the form

$$\mathbf{C}_{\mu_\rho} = \begin{pmatrix} \sigma_0^2 & 0 & r_{\mu_1\mu_1}(\tau) & r_{\mu_1\mu_2}(\tau) \\ 0 & \sigma_0^2 & -r_{\mu_1\mu_2}(\tau) & r_{\mu_1\mu_1}(\tau) \\ r_{\mu_1\mu_1}(\tau) & -r_{\mu_1\mu_2}(\tau) & \sigma_0^2 & 0 \\ r_{\mu_1\mu_2}(\tau) & r_{\mu_1\mu_1}(\tau) & 0 & \sigma_0^2 \end{pmatrix} \tag{A.24}$$

The determinant of the covariance matrix $\mathbf{C}_{\mu_\rho}$ is given by

$$\det \mathbf{C}_{\mu_\rho} = [\sigma_0^4 - r^2_{\mu_1\mu_1}(\tau) - r^2_{\mu_1\mu_2}(\tau)]^2 \tag{A.25}$$

Inserting (A.25), (A.24) and (A.22) into (A.21) results, after some algebraic operations, in the following expression for the joint PDF $p_{\mu_{\rho_1}\mu_{\rho_2}\mu'_{\rho_1}\mu'_{\rho_2}}(x_1,x_2,x'_1,x'_2)$

$$p_{\mu_{\rho_1}\mu_{\rho_2}\mu'_{\rho_1}\mu'_{\rho_2}}(x_1,x_2,x'_1,x'_2) = \frac{1}{4\pi^2 D} e^{-\frac{1}{D}\rho^2(\sigma_0^2 - r_{\mu_1\mu_1}(\tau))} \times e^{-\frac{\sigma_0^2}{2D}(x_1^2+x_2^2+x'^2_1+x'^2_2)} \times e^{-\frac{1}{2D}2r_{\mu_1\mu_1}(\tau)(x_1x'_1+x_2x'_2)+2r_{\mu_1\mu_2}(\tau)(x_1x'_2-x_2x'_1)}$$

$$\times e^{\frac{1}{D} r_{\mu_1\mu_1}(\tau)(\rho\cos\theta_\rho(x_1+x_1')+\rho\sin\theta_\rho(x_2+x_2'))}$$
$$\times e^{\frac{1}{D} r_{\mu_1\mu_2}(\tau)(\rho\cos\theta_\rho(x_2-x_2')+\rho\sin\theta_\rho(x_1'-x_1))} \quad \text{(A.26)}$$

where D can be obtained from (A.25) as

$$D = \sigma_0^4 - r_{\mu_1\mu_1}^2(\tau) - r_{\mu_1\mu_2}^2(\tau) \quad \text{(A.27)}$$

REFERENCES

[1] S. Rice, "Statistical properties of a sine wave plus random noise," *Bell Syst. Tech. J.*, vol. 27, no. 1, pp. 109–157, Jan. 1948.

[2] H. W. Nylund, "Characteristics of small-area signal fading on mobile circuits in the 150 mhz band," *IEEE Trans. Veh. Technol.*, vol. 17, no. 1, pp. 24–30, 1968.

[3] E. Mondre, "Complex and envelope covariance for Rician fading communication channels," *IEEE Trans. Commun. Tech.*, vol. 19, no. 1, pp. 80–84, Feb 1971.

[4] R. Price, "A note on the envelope and phase-modulated components of narrowband Gaussian noise," *IRE Trans. Inf. Theory*, vol. 1, no. 2, pp. 9–13, Sep. 1955.

[5] C. Iskander and P. T. Mathiopoulis, "Analytical envelope correlation and spectrum of maximal-ratio combined fading signals," *IEEE Trans. Veh. Technol.*, vol. 54, no. 1, pp. 399–404, Jan. 2005.

[6] C. A. Gutiérrez and M. Pätzold, "The Reimann sum method for the design of sum-of-cisoids simulators for Rayleigh fading channels in non-isotropic scattering environments," in *Proc. IEEE Workshop on Mobile Computing and Network Technologies, WMCNT*, Dec. 2009.

[7] M. Pätzold and B. Talha, "On the statistical properties of sum-of-cisoids-based mobile radio channel models," in *Proc. 10th Int. Symp. WPMC, Jaipur, India*, Dec. 2007, pp. 394–400.

[8] M. Pätzold, *Mobile Fading Channels*. Chichester: John Wiley & Sons, 2002.

[9] A. Papoulis and S. Pillai, *Probability, Random Variables and Stochastic Processes*. New York: McGraw-Hill, 2004.

[10] I. S. Gradshteyn and I. Ryzhik, *Table of Integrals, Series, and Products*. 6th ed. New York: Academic, 2000.

[11] W. B. Davenport and W. L. Root, *An Introduction to the Theory of Random Signals and Noise*. Piscatway, NJ:IEEE Press, 1987.

[12] M. Pätzold and N. Youssef, "Modelling and simulation of direction-selective and frequency-selective mobile radio channels," *Int. J. Electron. Commun.*, vol. AEÜ-55, no. 6, pp. 433–442, Nov. 2001.

[13] C. A. Gutiérrez and M. Pätzold, "Sum-of-sinusoids-based simulation of flat-fading wireless propagation channels under non-isotropic scattering conditions," in *Proc. 50th IEEE Global Communications Conference (Globecom2007)*, Washington DC, Dec. 2007, pp. 3842–3846.

[14] C. A. Gutiérrez, *Channel Simulation Models for Mobile Broadband Communication Systems, Doctoral Dissertations at the University of Agder*. Krisiansand, Norway: University of Agder, 2009.

[15] M. Pätzold, U. Killat, F. Laue, and Y. Li, "A new and optimal method for the derivation of deterministic simulation models for mobile radio channels," in *Proc. IEEE Veh. Technol. Conf., VTC'96*, Atlanta, Georgia, Apr./May. 1996, pp. 1423–1427.

[16] A. Abdi, A. J. Barger, and M. Kaveh, "A parametric model for the distribution of the angle of arrival and the associated correlation function and power spectrum at the mobile station," *IEEE Trans. Veh. Technol.*, vol. 51, no. 3, pp. 550–560, May 2002.

Appendix B

Paper II

Title:	An Improved Iterative Nonlinear Least Square Approximation Method for the Design of SISO Wideband Mobile Radio Channel Simulators
Authors:	**Akmal Fayziyev** and Matthias Pätzold
Affiliation:	University of Agder, Faculty of Engineering and Science, P. O. Box 509, NO-4898 Grimstad, Norway
Journal:	*REV Journal on Electronics and Communications*.

An Improved Iterative Nonlinear Least Square Approximation Method for the Design of SISO Sideband Mobile Radio Channel Simulators

Akmal Fayziyev and Matthias Pätzold
Faculty of Engineering and Science, University of Agder,
P.O. Box 509, NO-4898 Grimstad, Norway
E-mails: {akmal.fayziyev, matthias.paetzold}@uia.no

***Abstract* — In this paper, we present an improved version of the iterative nonlinear least square approximation (INLSA) method for designing measurement-based single-input single-output (SISO) wideband channel simulators. The proposed method aims to fit the time-frequency correlation function (TFCF) of the simulation model to that of a measured channel. The parameters of the simulation model are determined iteratively by minimizing the Frobenius norm, which serves as a measure for the fitting error. In contrast to the original INLSA method, the proposed approach provides a unique optimized set of model parameters, which guarantees a quasi-perfect fitting with respect to the TFCF. We analyze the performance of the proposed method in terms of the goodness of fit to the measured data. The investigations will be carried out with respect to the TFCF and the scattering function. We demonstrate that the proposed approach is a powerful tool for the design of measurement-based wideband channel simulators, which are important for the performance evaluation of mobile communication systems under real-world propagation conditions.**

***Index Terms* — Wideband channel modelling, multipath propagation, parameter computation, measurement data, time-frequency correlation function, scattering function**

I. INTRODUCTION

The reliability and the maximum achievable data rate of a communication system are heavily dependent on the characteristics of the propagation channel. Hence, during the design and test phase, it is of utmost importance to have a realistic channel model to begin with. A lot of research attention has been devoted to the development of channel models the statistics of which matches very closely that of a real propagation environment. The most recent comprehensive survey on existing modeling approaches is reported in [1, 2].

In general, sophisticated channel models are based on wideband scenarios, which incorporate the frequency selectivity of the physical channel. A widely used approach to develop wideband channel models is to represent the time-variant transfer function by a finite sum of multipath propagation components [3, 4]. The efficient development of wideband channel models relies on a sophisticated method for determining the primary model parameters, which are the path gains, Doppler frequencies, and propagation delays. Hence, advanced and efficient parameter computation methods are required to accurately estimate these model parameters from the measured channels. In last couple of decades, various high resolution parameter estimation methods have been proposed to derive the reference models [5–8]. These methods can also be used as parameter computation techniques for designing measurement-based channel simulators. In [5], e.g., the multiple signal classification (MUSIC) algorithm has been applied for delay estimation. A joint angle and delay estimation (JADE) technique is proposed in [9]. A direction-of-arrival estimation method using the estimation of signal parameters via rotational invariance techniques (ESPRIT) algorithm has been discussed in [6]. The unitary ESPRIT has been proposed in [10] to improve the estimation accuracy of the ESPRIT algorithm. The ESPRIT method has further been extended in [11] to enable a joint delay and azimuth estimation, while the unitary ESPRIT technique has been used in [12] to perform a joint azimuth and elevation estimation. An application of the unitary ESPRIT algorithm to wideband channel measurements is presented in [13]. Owing to the high implementation complexity of the aforementioned methods, maximum-likelihood-based algorithms are preferable for solving the channel parameter estimation problem. These include the expectation maximization [7] and the space alternating generalized expectation maximization (SAGE) [8] algorithms. Particularly the SAGE algorithm is widely used for channel parameter estimation due to its excellent performance in most scenarios. However, the SAGE algorithm often requires a large amount of specular

components, which makes the estimation process relatively complex. In [14], the authors reported a initialization sensitivity problem of the SAGE algorithm. Several approaches have been proposed in [14–17] to mitigate the drawbacks of this algorithm. In [17], the authors proposed the iterative nonlinear least square approximation (INLSA) method for the design of measurement-based wideband channel simulators. The authors showed that the INLSA algorithm provides a good match to empirical data by keeping the complexity lower than that of the SAGE algorithm. The INLSA algorithm has further been refined in [18].

In this paper, we extend the INLSA method to allow a joint estimation of the primary model parameters. The INLSA algorithm is based on the expectation maximization approach [7]. In order to reduce the computational cost, the INLSA algorithm computes the maximum-likelihood estimates of the channel model parameters iteratively. The iterative approach, however, may lead to a poor modeling of the TFCF of the measured channel at the origin. The value at the origin of the TFCF is of crucial importance for computing the characteristic quantities describing the statistics of the fading channel, such as the probability density function of the envelope, the level-crossing rate, and the average duration of fades. The original INLSA method [17] offers two alternatives for optimizing the simulation model parameters. The first alternative computes the path gains together with the Doppler frequencies by modeling the measured temporal autocorrelation function (TACF), and then computes the propagation delays in a second step from the frequency correlation function (FCF) of the measured channel. This variant of the original INLSA algorithm will be called the INLSA-T-F method. The second alternative computes first the path gains jointly with the propagation delays by modeling the measured FCF, whereas the Doppler frequencies are obtained in a second step from the TACF of the measured channel. The second variant of the INLSA algorithm will be referred to as the INLSA-F-T method. These kinds of separate optimizations of the simulation model parameters may lead to erroneous parameter estimations when evaluating the resulting channel simulator with respect to the TFCF. Moreover, the INLSA-T-F and INLSA-F-T approaches result in different sets of estimated parameters for identical measured data.

In order to overcome the aforementioned drawbacks of the original INLSA algorithm, the proposed method computes the simulation model parameters jointly by fitting the TFCF of the simulation model to that of the measured channel. The proposed method is called INLSA-TF emphasizing the joint modeling of both the temporal and frequency correlation functions of real-world channels. The proposed

algorithm includes additional error compensation steps in the iterative estimation procedure to guarantee a perfect fitting at the origin of the measured TFCF. As a result, the proposed method provides a unique set of optimized model parameters while maintaining a perfect fitting at the origin. In order to demonstrate the performance of the proposed INLSA-TF method, we implemented the algorithm in MATLAB and compared the new approach with the two known variants of the original INLSA method. We focused on a number of issues which are of particular interest in channel modeling, such as the fitting accuracy with respect to the most important correlation functions and the scattering function of the measured channel. In addition to this, we studied the performance of the measurement-based simulation model as a function of the selected number of propagation paths.

This paper is structured as follows. In Section II, we introduce the wideband channel simulation model. In Section III, the parameter estimation problem is formulated. Section IV describes the proposed parameter computation method. The application to measurement data is presented in Section V. Finally, Section VI concludes this paper.

II. The Wideband Channel Simulation Model

In this section, we describe the simulation model on which we apply the parameter computation method presented in this work. We also derive the TFCF of the simulation model under the assumption that the autocorrelation ergodicity conditions are fulfilled.

An important objective for the design of channel simulation models is to guarantee that their statistical properties are as close as possible to real-world channels. When using a measurement-based approach, we have to consider that every measurement provides only propagation area specific information for a short period of time. This means we have to select a proper channel model the parameters of which can be estimated from given snapshot measurements. For this reason, we adopt the widely accepted model from [19], which represents the time-variant frequency response (TVFR) of multipath fading channel as a superposition of a finite number of N propagation paths in the form

$$H(f',t) = \sum_{n=1}^{N} c_n e^{j(2\pi f_n t - 2\pi f' \tau'_n + \theta_n)} \tag{B.1}$$

where t and f' are the time and frequency variables, respectively. Each propagation path is characterized by its path gain c_n, propagation delay τ'_n, Doppler frequency f_n,

and the phase shift θ_n. The number of propagation paths N determines the accuracy as well as the complexity of the simulation model. We assume that the elements of the set $\{\theta_n\}$ are independent and identically distributed (i.i.d.) random variables, each having a uniform distribution in the interval $[0, 2\pi)$. Our aim is to determine the remaining sets of parameters $\{c_n\}$, $\{f_n\}$, and $\{\tau'_n\}$ of the channel simulation model described in (B.1) such that the simulation model has almost the same statistical characteristics as a given measured channel. For our analysis, it will suffice to consider the TVFR $H(f',t)$ at discrete frequencies $f'_m = -B/2 + m\Delta f' \in [-B/2, B/2], m = 0, ..., M-1$, and at discrete time instances $t_k = k\Delta t \in [0, T], k = 0, ..., K-1$, where B and T denote the measured frequency bandwidth and the observation time interval, respectively. The time sampling interval Δt and the frequency sampling interval $\Delta f'$ are characteristic quantities of the channel sounder used to collect the measurement data. Consequently, the TVFR $H(f',t)$ can be represented as a discrete TVFR $H[f'_m, t_k]$. For simplicity's sake, it is assumed that the parameters of the simulation model described by (B.1) fulfill the following conditions

$$f_n \neq f_m, \tau'_n \neq \tau'_m, \quad \forall\, n \neq m \tag{B.2}$$

$$E\{e^{j(\theta_n - \theta_m)}\} = 0, \quad \forall\, n \neq m \tag{B.3}$$

where $E\{\cdot\}$ represents the statistical averaging operator. Condition (B.3) is always fulfilled as $\{\theta_n\}$ are i.i.d. random variables. As a result of the imposed constraints (B.2) and (B.3), the channel model in (B.1) is autocorrelation ergodic with respect to time and frequency [20]. In this case, the discrete TFCF $R[\nu'_p, \tau_q]$ of the simulation model can be deduced from a single realization of the discrete TVFR $H[f'_m, t_k]$ as follows

$$\begin{aligned} R[\nu'_p, \tau_q] &= \langle H[f'_m, t_k] H^*[f'_m + \nu'_p, t_k + \tau_q] \rangle \\ &= \sum_{n=1}^{N} c_n^2 e^{j2\pi(\tau'_n \nu'_p - f_n \tau_q)} \end{aligned} \tag{B.4}$$

where $\tau_q = 0, \Delta t, ..., (K-1)\Delta t$ and $\nu'_p = 0, \Delta f', ..., (M-1)\Delta f'$. The notation $\langle \cdot \rangle$ denotes averaging over time and frequency.

The preceding equation shows that $R[\nu'_p, \tau_q]$ depends on the number of paths N, path gains c_n, propagation delays τ'_n, and Doppler frequencies f_n, but not on the phase shifts θ_n. The TACF $r_{t_k}[\tau_q]$ is obtained from the TFCF $R[\nu'_p, \tau_q]$ by setting ν'_p to zero,

i.e.,

$$r_{t_k}[\tau_q] = R[0,\tau_q] = \sum_{n=1}^{N} c_n^2 e^{-j2\pi f_n \tau_q}. \tag{B.5}$$

The FCF $r_{f'_m}[\nu'_p]$ of the simulation model can be determined from the TFCF $R[\nu'_p,\tau_q]$ by setting τ_q to zero, i.e.,

$$r_{f'_m}[\nu'_p] = R[\nu'_p,0] = \sum_{n=1}^{N} c_n^2 e^{j2\pi\tau'_n\nu'_p}. \tag{B.6}$$

For mathematical convenience, the discrete TFCF $R[\nu'_p,\tau_q]$ will be represented by an $M \times K$ time-frequency correlation matrix (TFCM) $\mathbf{R}$. It is straightforward to show that the TFCM $\mathbf{R}$ can be formulated as

$$\mathbf{R} = \sum_{n=1}^{N} c_n^2 \mathbf{P}_n \tag{B.7}$$

where $\mathbf{P}_n$ is an $M \times K$ matrix and defined as follows

$$\mathbf{P}_n = \begin{pmatrix} \sum\limits_{n=1}^{N} e^{j2\pi(\tau'_n\nu'_0 - f_n\tau_0)} & \cdots & \sum\limits_{n=1}^{N} e^{j2\pi(\tau'_n\nu'_0 - f_n\tau_{K-1})} \\ \vdots & \ddots & \vdots \\ \sum\limits_{n=1}^{N} e^{j2\pi(\tau'_n\nu'_{M-1} - f_n\tau_0)} & \cdots & \sum\limits_{n=1}^{N} e^{j2\pi(\tau'_n\nu'_{M-1} - f_n\tau_{K-1})} \end{pmatrix}. \tag{B.8}$$

III. Problem Formulation

In this section, we describe the measured channel and discuss its correlation properties. We also formulate the problem of determining the simulation model parameters.

Let $\check{H}(f',t)$ denote the TVFR of a real-world channel measured at discrete frequencies f_m, and at discrete time instances t_k. In this case, the TVFR $\check{H}(f',t)$ can be represented in the form of a discrete function, which will be denoted by $\check{H}[f'_m,t_k]$. Further, we assume that the measured TVFR $\check{H}[f'_m,t_k]$ is wide-sense stationary [21] and autocorrelation ergodic with respect to time and frequency. This allows us to obtain the discrete TFCF $\check{R}[\nu'_p,\tau_q]$ of the measured channel from $\check{H}[f'_m,t_k]$ by averaging over time and frequency. Thus,

$$\check{R}[\nu'_p,\tau_q] = \frac{1}{KM} \sum_{k=0}^{K-1} \sum_{m=0}^{M-1} \check{H}[f'_m,t_k] \check{H}^*[f'_m+\nu'_p, t_k+\tau_q]. \tag{B.9}$$

The TACF $\check{r}_{t_k}[\tau_q]$ and the FCF $\check{r}_{f'_m}[\nu'_p]$ of the measured channel are obtained from $\check{R}[\nu'_p,\tau_q]$ in (B.9) by setting $\nu'_p = 0$ and $\tau_q = 0$, respectively, i.e., $\check{r}_{t_k}[\tau_q] = \check{R}[0,\tau_q]$ and $\check{r}_{f'_m}[\nu'_p] = \check{R}[\nu'_p,0]$. For mathematical convenience, we represent the discrete TFCF $\check{H}[f'_m,t_k]$ by an $M \times K$ TFCM $\check{\mathbf{R}}$.

With reference to the simulation model described by (B.1), the problem at hand is to determine the set of parameters $\mathbb{P} = \{N, c_n, f_n, \tau'_n\}$ in such a way that the statistical properties of the simulation model match those of the measured channel. Here, the desired statistical properties are described by the TFCM $\check{\mathbf{R}}$ of the measured channel. The problem of determining the set of parameters $\mathbb{P}$ can now be formulated as follows:

Given is the measured discrete TVFR $\check{H}[f'_m,t_k]$ of a real-world channel. Determine the set of parameters $\mathbb{P} = \{N, c_n, f_n, \tau'_n\}$ of the channel simulation model described by (1), such that the TFCM $\mathbf{R}$ of the simulation model is as close as possible (in the Frobenious norm sense) to the TFCM $\check{\mathbf{R}}$ of the measured channel, i.e.,

$$\mathbb{P} = \arg\min_{\mathbb{P}} \left\| \check{\mathbf{R}} - \mathbf{R} \right\|_F \tag{B.10}$$

where $\|\cdot\|_F$ denotes the Frobenius norm.

As it was pointed out in [17], the problem formulation in (B.10) is valid if the measured channel is autocorrelation ergodic.

IV. The Proposed Parameter Computation Method

This section focuses on the description of the INLSA-TF algorithm proposed for computing the parameters of the measurement-based channel simulator. By referring to the problem formulation discussed in Section III and assuming that the discrete TFCM $\check{\mathbf{R}}$ of the measured channel is known, we measure the model error between the measured channel and the simulation model by

$$E(\mathbb{P}) = \left\| \check{\mathbf{R}} - \sum_{n=1}^{N} c_n^2 \mathbf{P}_n \right\|_F. \tag{B.11}$$

The objective is to minimize the Frobenius norm in (B.11), such that the TFCM $\mathbf{R}$ of the simulation is fitted as close as possible to the given TFCM $\check{\mathbf{R}}$ of the measured channel. Owing to the complexity of this optimization problem, the implementation of the maximum-likelihood estimation of model parameters that minimizes the error in (B.11) is intractable. Therefore, the proposed method utilizes the iterative

approach to optimize the simulation model parameters. The iterative parameter computation method starts with $N = 1$ and arbitrarily chosen initial values for $f_1^{(0)}$ and $\tau_1'^{(0)}$. At every iteration i $(i = 0, 1, 2, ...)$, the algorithm computes the complete set of model parameters $\mathbb{P}$. The parameter computation procedure is carried out separately for each path l $(l = 1, 2, ..., N)$ by using the auxiliary error matrix as follows:

$$\mathbf{Y}_l^{(i)} = \check{\mathbf{R}} - \sum_{n=1, n\neq l}^{N} \left(c_n^{(i)}\right)^2 \mathbf{P}_n^{(i)} \tag{B.12}$$

$$c_l^{(i+1)} = \arg\min_{c_l} \left\| \mathbf{Y}_l^{(i)} - c_l^2 \mathbf{P}_l^{(i)} \right\|_F \tag{B.13}$$

$$f_l^{(i+1)} = \arg\min_{f_l} \left\| \mathbf{Y}_l^{(i)} - \left(c_l^{(i+1)}\right)^2 \mathbf{P}_l^{(i)} \right\|_F \tag{B.14}$$

$$\tau_l'^{(i+1)} = \arg\min_{\tau_l'} \left\| \mathbf{Y}_l^{(i)} - \left(c_l^{(i+1)}\right)^2 \mathbf{P}_l^{(i+1)} \right\|_F \tag{B.15}$$

where the $M \times K$ matrix $\mathbf{P}_l^{(i+1)}$ is recomputed by substituting the optimized values of $f_l^{(i+1)}$ in (B.8). In this algorithm, the iterative computation of the set of parameters $\mathbb{P}$ continues as long as the relative change in the model error $E(\mathbb{P})$ is larger than a predefined threshold level ε. When the threshold level ε is reached, the iteration stops, and the number of propagation paths N is increased by one, i.e., $N + 1 \rightarrow N$. The initial values of $c_N^{(0)}, f_N^{(0)}$, and $\tau_N'^{(0)}$ are set to zero. After this, the iterative parameter computation procedure is carried out again starting from (B.12). This process is repeated until no perceptible progress can be made by increasing N or the maximum number of paths $N_{\max}$ is reached.

It is straightforward to show that (B.13) results in a minimum if $c_l^{(i+1)}$ is computed as

$$c_l^{(i+1)} = \sqrt{\frac{\mathrm{Re}\left\{\mathbf{y}_l^{(i)}\right\}^T \mathrm{Re}\left\{\mathbf{p}_l^{(i)}\right\} + \mathrm{Im}\left\{\mathbf{y}_l^{(i)}\right\}^T \mathrm{Im}\left\{\mathbf{p}_l^{(i)}\right\}}{\left(\mathbf{p}_l^{(i)}\right)^H \mathbf{p}_l^{(i)}}} \tag{B.16}$$

where the operators $\{\cdot\}^T$ and $\{\cdot\}^H$ denote the transpose and complex-conjugate transpose, respectively. The symbol $\mathbf{y}_l^{(i)}$ refers to a column vector formed by mapping the elements in $\mathbf{Y}_l^{(i)}$ such that all columns in $\mathbf{Y}_l^{(i)}$ are stacked on top of each other. Analogously, the symbol $\mathbf{p}_l^{(i)}$ denotes a column vector, which is formed by applying the same mapping scheme to $\mathbf{P}_l^{(i)}$. However, in order to guarantee a perfect fitting at the origin $\nu_p' = 0$ and $\tau_q = 0$ of the TFCF $\check{R}[\nu_p', \tau_q]$, we replace the optimization step

in (B.13) by

$$c_l^{(i+1)} = \begin{cases} \sqrt{\dfrac{\mathrm{Re}\left\{\mathbf{y}_l^{(i)}\right\}^T \mathrm{Re}\left\{\mathbf{p}_l^{(i)}\right\} + \mathrm{Im}\left\{\mathbf{y}_l^{(i)}\right\}^T \mathrm{Im}\left\{\mathbf{p}_l^{(i)}\right\}}{\left(\mathbf{p}_l^{(i)}\right)^H \mathbf{p}_l^{(i)}}}, & l \neq N \\ \check{R}[0,0] - \sum\limits_{l=1}^{N-1} \left(c_l^{(i+1)}\right)^2, & l = N. \end{cases} \tag{B.17}$$

The preceding equation implies that the c_N is computed such that exact fitting of $\check{R}[\nu'_p, \tau_q]$ is always preserved if $\nu'_p = 0$ and $\tau_q = 0$.

The procedure above is coined INLSA-TF. It should be pointed out here that when using the INLSA-TF method, the path gains are optimized in combination with the corresponding Doppler frequencies and propagation delays, which result in an unambiguous and unique triple (c_n, f_n, τ'_n) for each propagation path $n = 1, 2, \ldots, N$. This is in contrast to the INLSA-T-F and INLSA-F-T methods for which we obtain only the unique tuples (c_n, f_n) and (c_n, τ'_n), respectively. Since the optimization process in the proposed method is carried out by modeling the TFCF of the measured channel, the INLSA-TF method provides an excellent performance when evaluating the channel simulator with respect to the TFCF. As we will see, the INLSA-T-F and INLSA-F-T methods cannot provide an accurate modeling of the TFCF of the measured channel, especially close to the origin. The results of a comparative study of these three approaches are demonstrated in the next section.

V. Application to Measurement Data

In this section, we demonstrate the usefulness and the performance of the proposed INLSA-TF algorithm. To accomplish these two objectives, we used measurement data collected in an urban area in the 2.1 GHz frequency band. In the measurement campaign, the transmitter antenna was mounted on a trolley and acted as a mobile part. The receiver antenna was stationary and mounted on the roof of a building at a height of 20 m. The performed measurements were double-directional multipath measurements conducted using a wideband channel sounder. The key parameters of the measurement equipment are:

- Time sampling interval: $\Delta t = 0.02$ s
- Frequency sampling interval: $\Delta f' = 195$ kHz
- Bandwidth: $B = 100$ MHz

- Observation time interval: $T = 0.5$ s

For comparative purposes, we first demonstrate the channel estimation capabilities of the proposed INLSA-TF algorithm and the two original variants of the INLSA method using the same measurement data. The threshold level ε of the proposed algorithm was empirically set to $\varepsilon = 0.01$ in all cases. Figure B.1 illustrates the normalized residual error norm $\|\check{R} - R\|_F / \|\check{R}\|_F$ versus the number of propagation paths N.

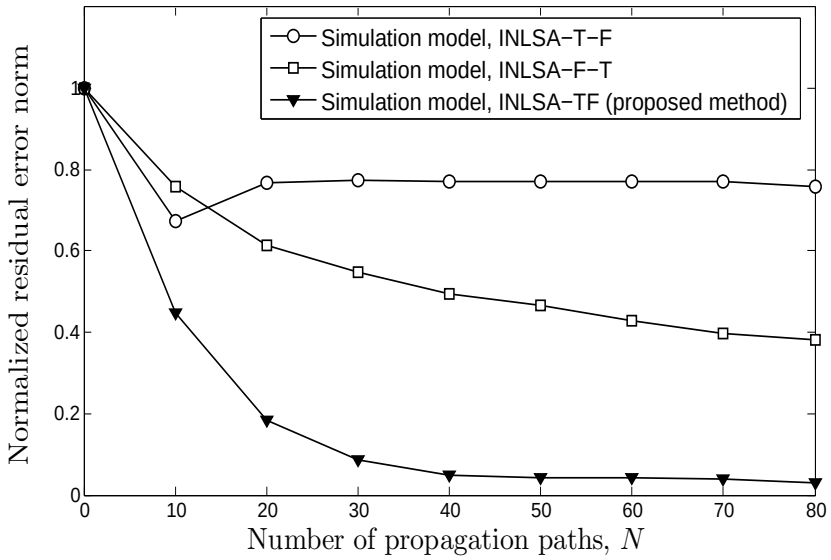

Figure B.1: Normalized residual error norm $\|\check{R} - R\|_F / \|\check{R}\|_F$ versus the number of propagation paths N.

As can be seen from the results shown in this figure, the proposed INLSA-TF method performs significantly better than the two original INLSA approaches. The different performances of the INLSA-T-F and INLSA-F-T originate from the fact that the estimated sets of model parameters are not identical when these methods are used. As an aside, we want to mention that the INLSA-TF algorithm as well as the two original versions (INLSA-T-F and INLSA-F-T) are initialization insensitive. This means that, for any chosen initial values of the Doppler frequencies and path delays, we always get the same graph for the normalized residual error norm. We also realize from the inspection of Fig. B.1 that the normalized residual error norm associated with the INLSA-TF method is approximately 10% if $N \geq 30$, whereas the error norm drops below 3% if $N \geq 80$. By referring to these results, the number of propagation paths $N_{\max} = 80$ is considered to be sufficient and adopted for further simulations as a stopping criterion in the iterative optimization procedure.

The important difference between the proposed and the original INLSA method is that the former one aims to model the TFCF of real-world channels, while the latter one focuses only on the behavior of the TFCF along the principal axes, meaning the TACF and the FCF. In order to demonstrate this difference, we have plotted the TFCFs of the measured channel and the simulation model by using the INLSA-TF and the INLSA-T-F in Figs. B.2, B.3, and B.4, respectively. From Figs. B.2–B.4, we can realize that the INLSA-TF method performs significantly better than the original INLSA-T-F. It is readily apparent from comparing the results in Fig. B.2 and Fig. B.4 that the main focus of the original INLSA algorithm falls only on the TACF and the FCF.

As mentioned in Section I, the separate parameter optimization approach implemented in the original INLSA algorithm may lead to incorrect estimations of the simulation model's parameters. To highlight this problem, we have illustrated the performance of the two variants of the original INLSA method in Figs. B.5 and B.6. As can be seen in those figures, if the INLSA-F-T approach is used, the difference between the TACF curves of the simulation model and the measured channel is significant, whereas the FCF of the simulation model closely matches the FCF of the measured channel. However, there is a significant gap between the FCFs close to the origin. The discrepancy between the FCFs of the simulation model and the measured channel is relatively small if the INLSA-T-F method is applied. This characteristic feature of the INLSA-F-T method close to the origin is a result of the used iterative approach for simplifying the maximum-likelihood optimization problem. We can also conclude from the inspection of Figs. B.5 and B.6 that the TACF and the FCF of the simulation model are well fitted to the corresponding correlation functions of the measured channel if the simulation model's parameters are computed by using the proposed INLSA-TF method. Impressively, the proposed method provides an exact correspondence between the correlation functions of the simulation model and the measured channel at the origin, as it was expected from (B.17).

In our performance analysis, we have also incorporated the study of the scattering function $S(\tau', f)$ of the simulation model, which is obtained by applying the two-dimensional discrete Fourier transform to the TFCF $R[\nu'_p, \tau_q]$. In Fig. B.7, we have depicted a comparison between the scattering function of the measured channel and that of the simulation model designed by using the proposed INLSA-TF algorithm. The corresponding results obtained by applying the original INLSA method are shown in Fig. B.8. An excellent agreement between the scattering functions of the measured channel and the simulation model is observed if the proposed INLSA-TF

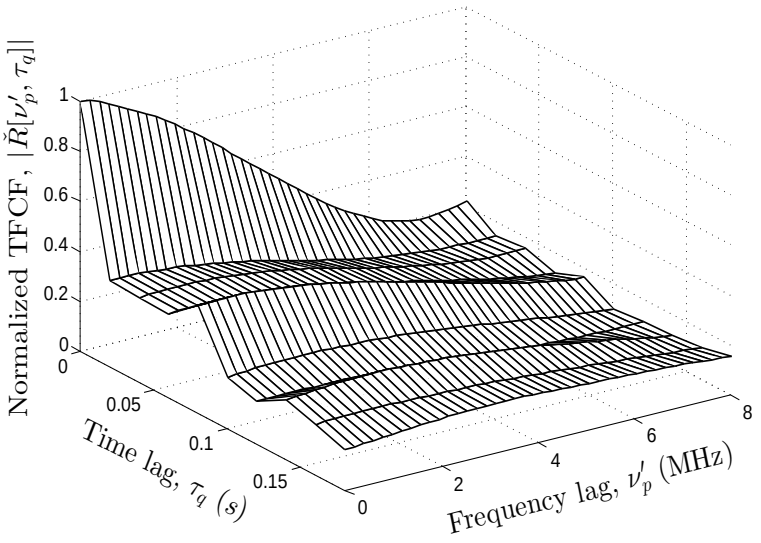

Figure B.2: Absolute value of the normalized TFCF $\left|\check{R}[\nu'_p, \tau_q]\right|$ of the measured channel.

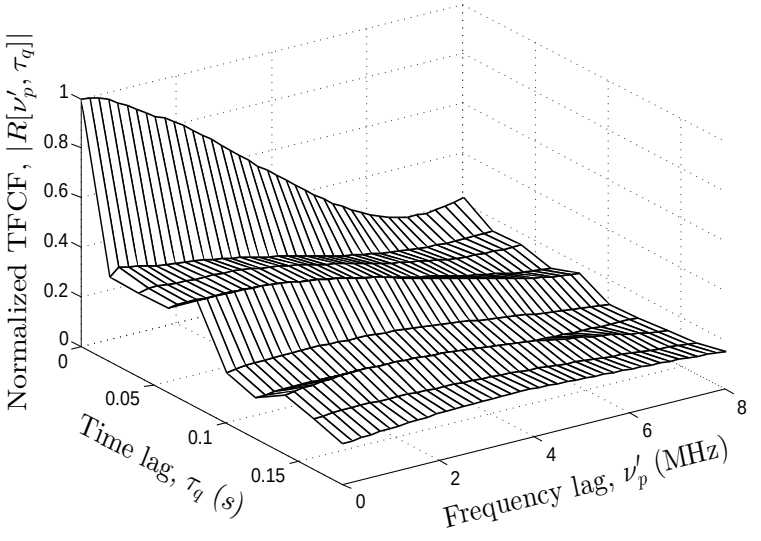

Figure B.3: Absolute value of the normalized TFCF $\left|R[\nu'_p, \tau_q]\right|$ of the simulation model with the parameters estimated by using the proposed INLSA-TF method.

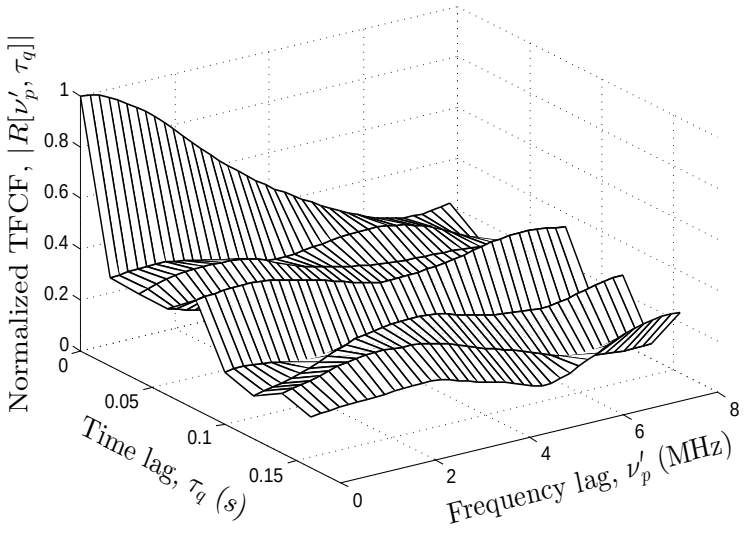

Figure B.4: Absolute value of the normalized TFCF $\left|R[\nu'_p, \tau_q]\right|$ of the simulation model with the parameters estimated by using the INLSA-T-F method.

method is used (see Fig. B.7). The results presented in Fig. B.8 demonstrate the poor performance of the INLSA-T-F and the INLSA-F-T methods in terms of modeling the scattering function of the measured channel.

VI. Summary and Conclusions

In this paper, we described the INLSA-TF method for designing the measurement-based stochastic channel simulation models. The proposed method is an extension of the INLSA method. The INLSA-TF method aims to iteratively estimate the optimal set of simulation model parameters by modeling the empirical TFCF of the given measurement data. The performance analysis of the proposed method has been made by applying the method to the measurement data collected in an urban environment to estimate the parameters of the simulation model. We have compared the correlation properties of the simulation model and the measured channel. A comparison has also been made with respect to the scattering function. The obtained results demonstrated that the proposed INLSA-TF algorithm precisely estimates the simulation model parameters and provides an excellent fitting to real-world channels. Finally, it has been shown that the proposed version of the INLSA method significantly outperforms the original version. Due to the low complexity and an excellent performance, the INLSA-TF method can be considered as a powerful tool for synthesizing the

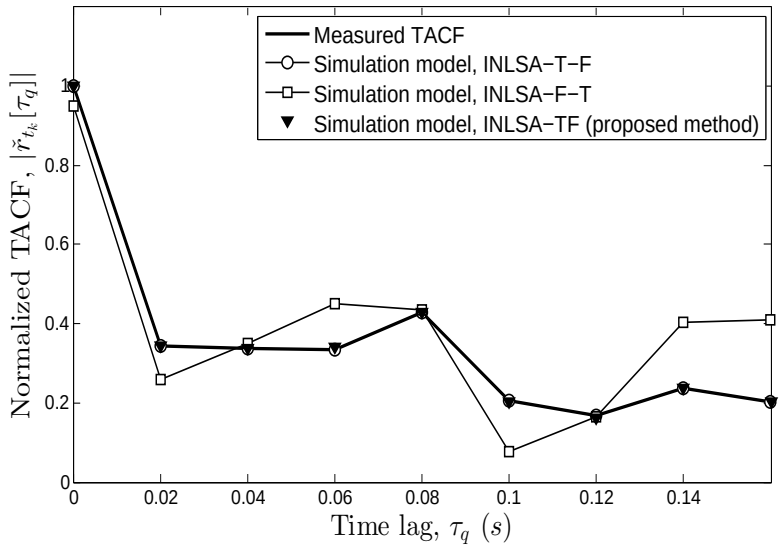

Figure B.5: Absolute value of the normalized TACFs $\left|\check{r}_{t_k}[\tau_q]\right|$ (measured channel) and $\left|r_{t_k}[\tau_q]\right|$ (simulation model) for different parameter computation methods.

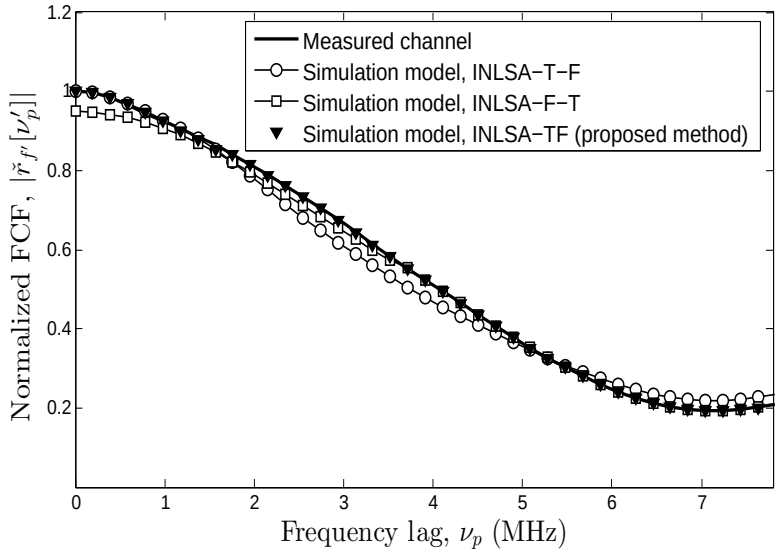

Figure B.6: Absolute value of the normalized FCFs $\left|\check{r}_{f'_m}[\nu'_p]\right|$ (measured channel) and $\left|r_{f'_m}[\nu'_p]\right|$ (simulation model) for different parameter computation methods.

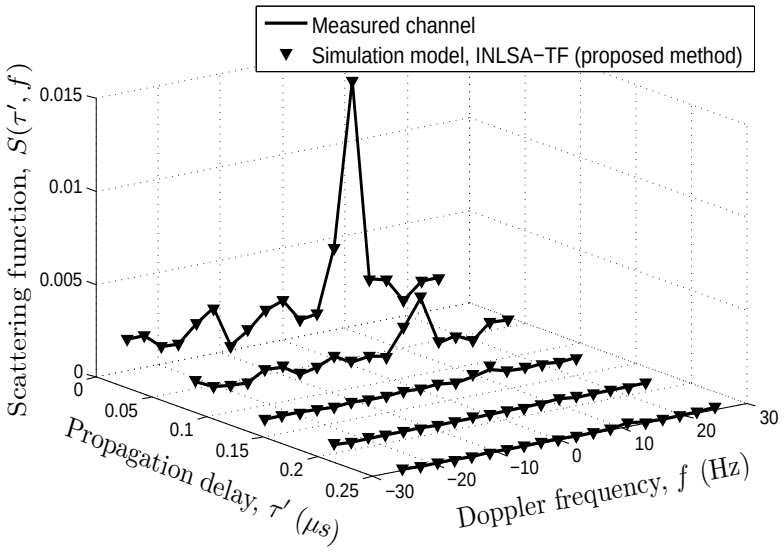

Figure B.7: Comparison between the scattering functions $\check{S}(\tau', f)$ (measured channel) and $S(\tau', f)$ (simulation model) designed by using the INLSA-TF method.

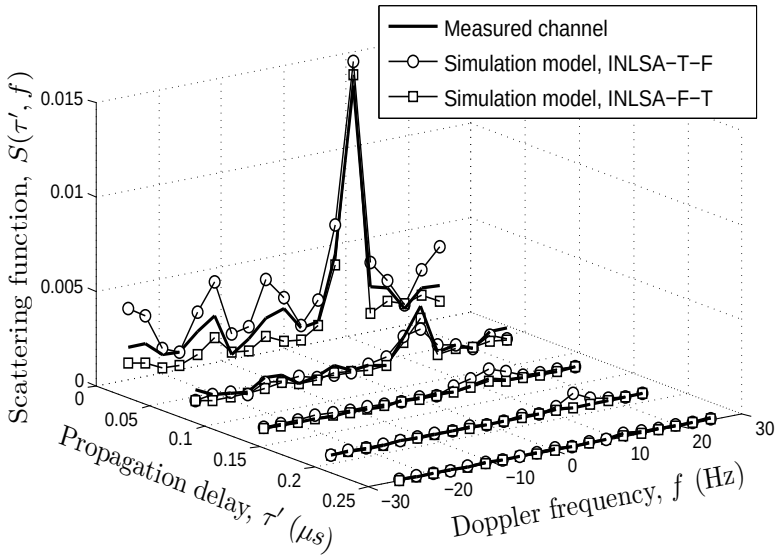

Figure B.8: Comparison between the scattering functions $\check{S}(\tau', f)$ (measured channel) and $S(\tau', f)$ (simulation model) designed by using the INLSA method.

real-world channels and can therefore be used for the performance analysis of communication systems.

REFERENCES

[1] H. Krim and M. Viberg, "Two decades of array signal processing research: The parametric approach," *IEEE Signal Processing Magazine*, vol. 13, pp. 67–94, July 1996.

[2] P. Almers, E. Bonek, A. Burr, N. Czink, M. Debbah, V. Degli-Esposti, H. Hofstetter, P. Kyösti, D. Laurenson, G. Matz, A. F. Molisch, C. Oestges, and H. Özcelik, "Survey of channel and radio propagation models for wireless MIMO systems," *EURASIP Journal on Wireless Communications and Networking*, vol. 2007, pp. Article ID: 19070, 19 pages, 2007.

[3] R. S. Thomä, D. Hampicke, M. Landmann, A. Richter, and G. Sommerkorn, "Measurement-based parametric channel modelling (MBPCM)," in *Int. Conf. on Electromagnetics in Advanced Applications, (ICEAA 2003)*, Torino, Italia, Sept. 2003.

[4] M. Pätzold, *Mobile Radio Channels*, 2nd ed. Chichester: John Wiley & Sons, 2011.

[5] R. Schmidt, "Multiple emitter location and signal parameter estimation," *IEEE Trans. Antennas Propag.*, vol. 34, no. 3, pp. 276–280, Mar. 1986.

[6] R. Roy and T. Kailath, "ESPRIT-estimation of signal parameters via rotational invariance techniques," *IEEE Trans. Acoust., Speech, and Signal Processing*, vol. 37, no. 7, pp. 984–995, Jul. 1989.

[7] M. Feder and E. Weinstein, "Parameter estimation of superimposed signals using the EM algorithm," *IEEE Trans. Acoust., Speech, and Signal Processing*, vol. 36, no. 4, pp. 477–489, Aug. 1988.

[8] B. H. Fleury, M. Tschudin, R. Heddergott, D. Dahlhaus, and K. I. Pedersen, "Channel parameter estimation in mobile radio environments using the SAGE algorithm," *IEEE J. Select. Areas Commun.*, vol. 17, no. 3, pp. 434–450, Mar. 1999.

[9] M. Vanderveen, A. Vanderveen, and A. Paulraj, "Estimation of multipath parameters in wireless communication," *IEEE Trans. Signal Processing*, vol. 46, no. 3, pp. 682–690, May 1998.

[10] M. Pätzold, *Mobile Fading Channels*. Chichester: John Wiley & Sons, 2002.

[11] A. van der Veen, M. Vanderveen, and A. Paulraj, "Joint angle and delay estimation using shift-invariance properties," *IEEE Signal Processing Lett.*, vol. 4, pp. 142–145, May 1997.

[12] M. Zoltowski, M. Haardt, and C. Mathews, "Closed-form 2-D angle estimation with rectangular arrays in element space or beamspace via unitary ESPRIT," *IEEE Trans. Signal Processing*, vol. 44, pp. 316–328, Feb. 1996.

[13] J. Fuhl, J.-P. Rossi, and E. Bonek, "High-resolution 3-D direction-of-arrival determination for urban mobile radio," *IEEE Trans. Antennas Propag.*, vol. 45, pp. 672–682, Apr. 1997.

[14] W. Li and Q. Ni, "Joint channel parameter estimation using evolutionary algorithm," in *Proc. 2010 IEEE International Conference on Communications, ICC 2010, Cape Town, South Africa*, May. 2010, pp. 1–6.

[15] W. Li, W. Yao, and P. J. Duffett-Smith, "Improving the SAGE algorithm with adaptive partial interference cancellation," in *Proc. IEEE 13th Digital Signal Processing Workshop and 5th IEEE Signal Processing Education Workshop DSP/SPE 2009*, 2009, pp. 404–409.

[16] C. B. Ribeiro, E. Ollila, and V. Koivunen, "Stochastic maximum likelihood method for propagation parameter estimation," in *Proc. 15th IEEE Int. Symp. Personal, Indoor and Mobile Radio Commun., PIMRC 2004*, vol. 3, Sept. 2004, pp. 1839–1843.

[17] D. Umansky and M. Pätzold, "Design of measurement-based wideband mobile radio channel simulators," in *Proc. 4th IEEE International Symposium on Wireless Communication Systems, ISWCS 2007, Trondheim, Norway*, Oct. 2007, pp. 229–235.

[18] A. Fayziyev and M. Pätzold, "An improved iterative nonlinear least square approximation method for the design of measurement-based wideband mobile

radio channel simulators," in *Proc. IEEE Advanced Technologies for Communications, ATC 2011*, Danang, Vietnam, Apr. 2011, pp. 106–111.

[19] G. D. Durgin, *Space-Time Wireless Channels*. NJ: Prentice Hall, 2003.

[20] C. A. Gutiérrez, A. Meléndez, A. Sandoval, and H. Rodriguez, "On the autocorrelation ergodic properties of sum-of-cisoids Rayleigh fading channel simulators," in *Proc. European Wireless, EW 2011*, Vienna, Austria, Apr. 2011, pp. 1–6.

[21] A. Papoulis and S. Pillai, *Probability, Random Variables and Stochastic Processes*. New York: McGraw-Hill, 2004.

Appendix C

Paper III

Title:	A Measurement-Based Channel Model for Vehicular Communications in Tunnels
Authors:	**Akmal Fayziyev**[1], Matthias Pätzold[1], Emilie Masson[2], Yann Cocheril[2] and Marion Berbineau[2]
Affiliations:	[1]University of Agder, Faculty of Engineering and Science, P. O. Box 509, NO-4898 Grimstad, Norway
	[2]Univ. Lille Nord de France, F-59000 Lille, France; IFSTTAR, LEOST, F-59650 Villeneuve dAscq, France
Conference:	*Wireless Communication and Network Conference, WCNC 2014*, Istanbul, Turkey, Apr. 2014.

A Measurement-Based Channel Model for Vehicular Communications in Tunnels

Akmal Fayziyev[1], Matthias Pätzold[1], Emilie Masson[2], Yann Cocheril[2] and Marion Berbineau[2]

[1]Faculty of Engineering and Science, University of Agder,
P.O. Box 509, NO-4898 Grimstad, Norway
E-mails: {akmal.fayziyev, matthias.paetzold}@uia.no

[2]Univ. Lille Nord de France, F-59000 Lille, France;
IFSTTAR, LEOST, F-59650 Villeneuve d'Ascq, France
E-mails: {emilie.masson, yann.cocheril, marion.berbineau}@ifsttar.fr

***Abstract* — In this paper, we present a new version of the iterative nonlinear least square approximation (INLSA) algorithm for the design of measurement-based channel simulators. The proposed method aims to match the time-variant impulse response (TVIR) of the simulation model to that of the measured channel. The propagation delays are discerned directly from the measurements, whereas the gains, the Doppler frequencies, and the phases are computed iteratively by minimizing a matching error norm. We evaluate the performance of the proposed method in terms of the approximation of the transfer function and correlation properties of the measured channel. We demonstrate how the resulting channel simulator can be deployed for a more reliable estimation of the channel statistics. The obtained results indicate that the proposed method allows a precise emulation of the measured channel impulse response. Its remarkable performance and simplicity makes the proposed method a powerful tool for designing realistic channel models.**

***Index Terms* — Wideband channel modelling, measurement data, parameter computation, time-variant impulse response, transfer function**

I. INTRODUCTION

The public transport domain relies more and more on wireless technologies to increase the quality, reliability, safety, and security of transportation systems while increasing simultaneously the accessibility and productivity. Owing to deployment and maintenance costs, wireless transmission systems are increasingly used in subways for communications-based train control (CBTC) [1] and closed-circuit television (CCTV) systems to perform signaling and train control (robustness needs), and video surveillance (high throughput needs), respectively. This trend is accentuated by the development of driverless subway systems, e.g., New York's Canarsie Line, and Lines 1 and 14 in Paris, etc. [2]. In this context, the requirements for reliability, availability, and robustness of wireless systems are higher and should be anticipated and integrated in the system architecture definition and deployment process. For the development of wireless communication systems for subway transportation systems, a sound knowledge of the channel characteristics in tunnels is of central importance. Gathering this knowledge requires to conduct channel measurement campaigns and to analyze the collected data. The problem at hand is then to extract all relevant parameters from the measurement data and to use the estimated parameters for the design of a real-world channel simulators. The aim of this paper is to present a solution to this problem.

The most widely used approach for the modelling of wideband channels is based on the multipath propagation phenomenon [3], which allows us to represent the TVIR by a finite sum of multipath components. However, the efficient deployment of this type of approach requires a careful determination of the model parameters, such as the propagation delays, path gains, Doppler frequencies, and phases. A number of parameter estimation methods have been discussed in the literature, e.g., [4–9]. The multiple signal classification (MUSIC) algorithm [6] and the estimation of signal parameters via rotational invariance techniques (ESPRIT) algorithms [7] were originally developed for the estimation of the angles of arrival. The MUSIC and the ESPRIT algorithms were later extended in [10] and [11], respectively, for the estimation of the propagation delays. However, the MUSIC and ESPRIT algorithms cannot be applied for the estimation of the path gains. Another well-known and more general approach is the so-called space-alternating generalized expectation-maximization (SAGE) algorithm [9], which is the extension of the expectation maximization approach presented in [12]. The SAGE algorithm has widely been used for the estimation of various channel parameters due to its superior performance in most

scenarios. However, the accurate emulation of the channel characteristics using the SAGE algorithm requires a relatively large number of specular components.

The main purpose of this paper is to design a model that not only allows a proper emulation of the statistics of the channel, but serves as well as a tool for enhancing the reliability of the channel statistics computed from the limited number of snapshot measurements. We introduce a new iterative method for the design of measurement-based channel models, which qualifies as an extension of the INLSA algorithm presented in [13]. In contrast to the original INLSA method that fits the time-frequency correlation function (TFCF) of the measured channel, the new version computes the model parameters iteratively by fitting the TVIR of the channel simulation model to that of the measured channel. The computed parameters are the gains, Doppler frequencies, and phases, whereas the propagation delays are obtained directly from the measurements. We evaluate the performance of the proposed method with respect to its fitting accuracy to the transfer function and the TFCF of the measured channel. The channel simulation model obtained by using the proposed method will then be used for the analysis of the channel beyond the measurement time limits, which favours a more reliable estimation of the channel statistics, in particular for measurement scenarios which are too short for computing the TFCF.

The paper is organized as follows. Section II describes the adopted deterministic channel simulation model. In Section III, we describe the proposed iterative parameter computation method. Section IV presents the measurement equipment and the propagation scenario. Section V is dedicated to the results obtained from the application of the proposed method to the tunnel measurement data. Section VI presents the conclusion and summarizes the main findings of this paper.

II. Measurement-Based Channel Model

In practice, the TVIR $h(\tau',t)$ of the measured channel is usually computed from a single snapshot measurement scenario, which is limited in both the time domain and the delay domain. Given a limited number of snapshot measurements of the TVIR $h(\tau',t)$ for $t \in [0, T_{\text{mes}}]$, our goal is to develop a channel simulation model that allows a proper emulation of the statistical properties of the measured channel for any value of t. The starting point will be a deterministic channel model represented in the following form [3, p. 397]

$$\tilde{h}(\tau',t) = \sum_{l=1}^{L} \tilde{\mu}_l(t)\,\delta(\tau' - \tau'_l) \tag{C.1}$$

where L denotes the number of paths with different propagation delays τ'_l. The time-variant channel gains $\tilde{\mu}_l(t)$ are defined as follows

$$\tilde{\mu}_l(t) = \sum_{n=1}^{N_l} c_{l,n} e^{j(2\pi f_{l,n} t + \theta_{l,n})} \tag{C.2}$$

where N_l is the number of paths having the same propagation delay. The parameters $c_{l,n}$, $f_{l,n}$, and $\theta_{l,n}$ are the path gains, Doppler frequencies, and phases, respectively, which are associated with the nth component of the lth propagation path.

III. The Proposed Parameter Computation Method

The principal task of a parameter computation method consists in finding the parameters of the simulation model to allow a proper emulation of the statistical properties of a given reference model or a measured channel. The parameters of the channel simulation model described by (C.1) are the propagation delays $\{\tau'_l\}$, path gains $\{c_{l,n}\}$, Doppler frequencies $\{f_{l,n}\}$, and phases $\{\theta_{l,n}\}$. The latter three sets of parameters can be computed by minimizing the following error norm

$$\varepsilon = |h(\tau', t) - \tilde{h}(\tau', t)| = \textbf{Min}! \tag{C.3}$$

The propagation delays τ'_l are not included in the parameter computation procedure, as they can directly be obtained from the measured TVIR. Unfortunately, the direct implementation of (C.3) is often intractable. Thus, one must find alternative ways to solve this problem. For finding a local minimum of the error norm ε in (C.3), we propose a new iterative method in the following. The derivation of the proposed iterative method is based on two basic assumptions. First, we assume that the propagation delays τ'_l are known. Second, we assume that each of the N_l components of the lth channel gain $\tilde{\mu}_l(t)$ is independent, i.e., all the parameters associated with $n' \neq n$ are irrelevant for the computation of the parameters $c_{l,n}$, $f_{l,n}$ and $\theta_{l,n}$. Based on these assumptions, we implement the parameter computation problem in (C.3) in L independent steps, each of which corresponds to estimating the parameters of the lth channel gain $\tilde{\mu}_l(t)$ by minimizing the error norm ε_l, i.e.,

$$\varepsilon_l = |\mu_l(t) - \tilde{\mu}_l(t)| = \textbf{Min}! \qquad l = 1, 2, \ldots, L \tag{C.4}$$

where $\mu_l(t)$ equals the measured TVIR $h(\tau', t)$ at $\tau' = \tau'_l$, i.e., $\mu_l(t) = h(\tau'_l, t)$. In order to solve each of the L minimization problems in (C.4), the proposed iterative

parameter computation method requires arbitrary initial values denoted as $c_{l,n}^{(0)}$, $f_{l,n}^{(0)}$, and $\theta_{l,n}^{(0)}$ for $l = 1,2,\ldots,L$ and $n = 1,2,\ldots,N_l$. The proposed method starts by setting the iteration index q to zero. The model parameters are then determined by using the auxiliary error function $y_{l,n}^{(q)}(t_k)$ $(k = 0,1,\ldots,K)$ as follows

$$y_{l,n}^{(q)}(t_k) = \mu_l(t_k) - \sum_{m=1,m\neq n}^{N_l} c_{l,m}^{(q)} e^{j(2\pi f_{l,m}^{(q)} t + \theta_{l,m}^{(q)})} \tag{C.5}$$

where $t_k = k\Delta t$ $(k = 0,1,\ldots,K)$ is the discrete time, and Δt denotes the measurement time sampling interval. We can determine the value of $c_{l,n}^{(q+1)}$ as follows

$$c_{l,n}^{(q+1)} = \arg\min_{c_{l,n}} \left\| \mathbf{y}_{l,n}^{(q)} - c_{l,n}\mathbf{s}_{l,n}^{(q)} \right\|_2^2 \tag{C.6}$$

where the symbol $\mathbf{y}_{l,n}^{(q)}$ refers to the column vector containing the stacked values of the auxiliary error function $y_{l,n}^{(q)}(t_k)$ in (C.5). The column vector $\mathbf{s}_{l,n}^{(q)}$ contains the stacked values of the exponential function $e^{j(2\pi f_{l,n}^{(q)} t + \theta_{l,n}^{(q)})}$. Fortunately, we can solve the minimization problem in (C.6) by the simple closed-form expression

$$c_{l,n}^{(q+1)} = \frac{\mathrm{Re}\left\{\mathbf{y}_{l,n}^{(q)}\right\}^T \mathrm{Re}\left\{\mathbf{s}_{l,n}^{(q)}\right\} + \mathrm{Im}\left\{\mathbf{y}_{l,n}^{(q)}\right\}^T \mathrm{Im}\left\{\mathbf{s}_{l,n}^{(q)}\right\}}{\left(\mathbf{s}_{l,n}^{(q)}\right)^H \mathbf{s}_{l,n}^{(q)}} \tag{C.7}$$

where the operators $\{\cdot\}^T$ and $\{\cdot\}^H$ denote the transpose and the complex-conjugate transpose, respectively. The result in (C.7) is obtained by finding the zeros of the first-order derivative from the norm in (C.6) with respect to $c_{l,n}$. The Doppler frequency $f_{l,n}^{(q+1)}$ is then obtained as follows

$$f_{l,n}^{(q+1)} = \arg\min_{f_{l,n}} \left\| \mathbf{y}_{l,n}^{(q)} - c_{l,n}^{(q+1)}\mathbf{s}_{l,n}^{(q)} \right\|_2^2. \tag{C.8}$$

Finally, the new value of the phase $\theta_{l,n}^{(q+1)}$ can be computed as follows

$$\theta_{l,n}^{(q+1)} = \arg\min_{\theta_{l,n}} \left\| \mathbf{y}_{l,n}^{(q)} - c_{l,n}^{(q+1)}\mathbf{s}_{l,n}^{(q)} \right\|_2^2. \tag{C.9}$$

The parameter computation procedure defined in (C.5), (C.7), (C.8), and (C.9) is applied to each of the N_l paths, which corresponds to one iteration. The error norm

ε_l should be re-evaluated at the end of each iteration. In case of a noticeable change in the error norm ε_l (C.4), the iteration index q is increased by one, i.e., $q+1 \rightarrow q$. After this, the parameter computation procedure is carried out again starting from (C.5). The iteration algorithm terminates if the relative change in the error norm ε_l is below a given threshold ε.

IV. Measurement Equipment and Scenario

A. Measurement Equipment

The channel sounder Propsound CS^{TM}described in [14] has been used for collecting the measurement data. This system provides all the single-input single-output (SISO) complex TVIRs in the time and spatial domain using the spread-spectrum sounding method in the delay domain. An advanced time-division multiplexed switching scheme [15] is used to determine the polarization parameters and the frequency division duplex frequencies. This rapid switching technique addresses also the spatial dimension needed for multiple-input multiple-output (MIMO) measurements in highly dynamic environments. MATLAB is used for post-processing and storing of the raw data. The results can be viewed in real time on a control laptop.

B. Measurement Scenario

The measurement campaign was performed in the Roux tunnel located in the Ardèche region in the south of France. The tunnel is arch shaped and straight over a length of 3325 m. Although it is a road tunnel, its geometry is also typical of railway tunnels, with a semicircular cross section (diameter of 8.52 m) and a maximum height of 6.25 m. Refer to Fig. C.1 for more details on the tunnel geometry and dimensions.

The 4×4 MIMO channel measurements were performed at 5.8 GHz over a 200 MHz band at a speed of 60 km/h. A laboratory van was used to carry the mobile reception unit. The four receiver antennas were fixed on a mast on the roof of the van (2.90 m height) and connected to the rapid switch unit that was placed as close as possible to the antennas. The four transmitter antennas were fixed on a mast in the cross section of the tunnel (4.10 m height, in the middle of the broadside of the tunnel) and connected to the switch unit placed as close as possible to the transmitter antennas to avoid signal losses. The measurement configuration in the tunnel is depicted in Fig. C.2.

Each antenna of the MIMO array at the transmitter and the receiver sides is a combination of four individual patches, which were adjusted such that the antenna

beam points in the direction of the tunnel's long side. The maximum antenna gain is about 14 dB at 5.8 GHz. Different propagation scenarios were measured in order to mimic operational scenarios in a two-lane road tunnel. For brevity, only one scenario is presented in this paper. It corresponds to an empty tunnel, where the receiver antennas on the vehicle are moving with a speed of 60 km/h away from the fixed transmitters. The velocity is constant over the first 1500 meters from the transmitter antennas. The antenna polarization and spacing are adjustable at the transmitter and the receiver. We focus in this paper on the configuration, where the transmitter and the receiver antennas are vertically polarized. The spacing between the antenna elements is equal to 2λ, where λ is the wavelength (10.3 cm at 5.8 GHz).

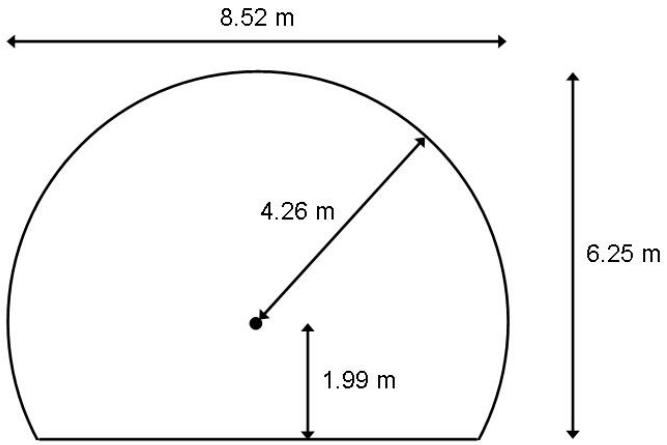

Figure C.1: Dimensions of the tunnel.

V. Numerical Results

In this section, we evaluate the performance of the proposed method with respect to its capability to approximate the transfer function $H(f',t)$ and the TFCF $R(\nu',\tau)$ obtained from the measurement data. For brevity, we focus here only on the SISO case. We start from the TVIR $h(\tau',t)$ that has been measured over a limited period of time, $T_{\text{mes}} = 40.88$ ms, during which $K = 100$ samples were collected. Hence, the sampling interval in the time domain equals $\Delta t = T_{\text{mes}}/K = 0.4088$ ms. In the delay domain, the measurement equipment allows a resolution of paths with a minimum delay difference of $\Delta\tau' = 5$ ns. The absolute value of the measured TVIR $|h(\tau',t)|$ is shown in Fig. C.3. Computing the Fourier transform of the measured TVIR $h(\tau',t)$

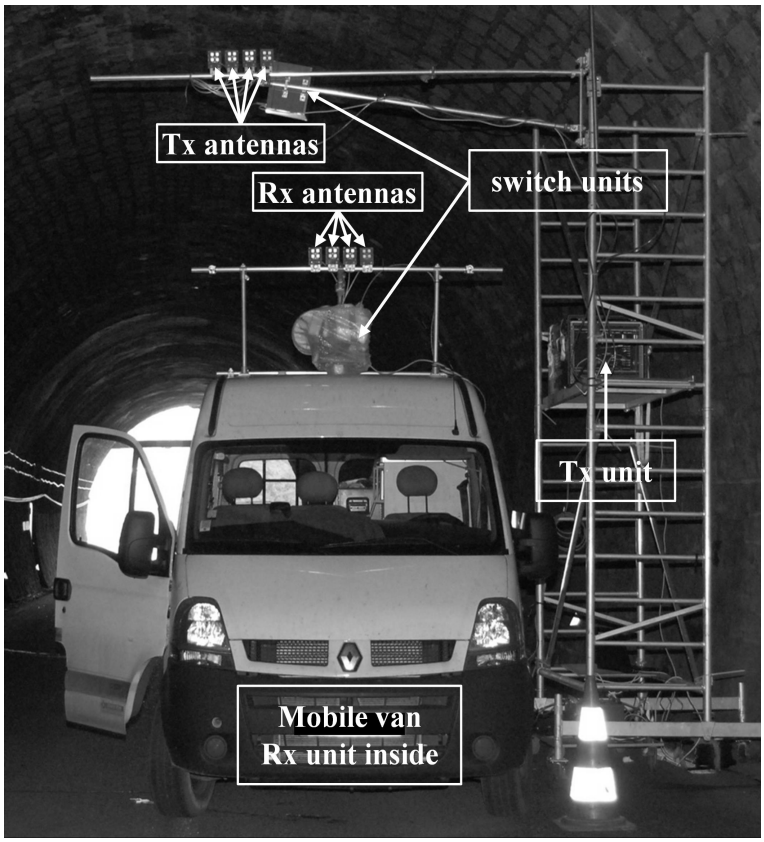

Figure C.2: Measurement configuration in the tunnel.

with respect to τ' gives the time-variant transfer function $H(f',t)$ of the measured channel. The absolute value of the channel transfer function $|H(f',t)|$ is presented in Fig. C.4. From the measured time-variant transfer function $H(f',t)$, the TFCF $R(\nu',\tau)$ has been obtained. The absolute value of the normalized TFCF $|R(\nu',\tau)|$ is presented in Fig. C.5. It is important to note that the TFCF $R(\nu',\tau)$ is strongly affected by the short measurement period T_{mes}. This effect explains the triangular shape of $|R(\nu',\tau)|$ in the direction of τ.

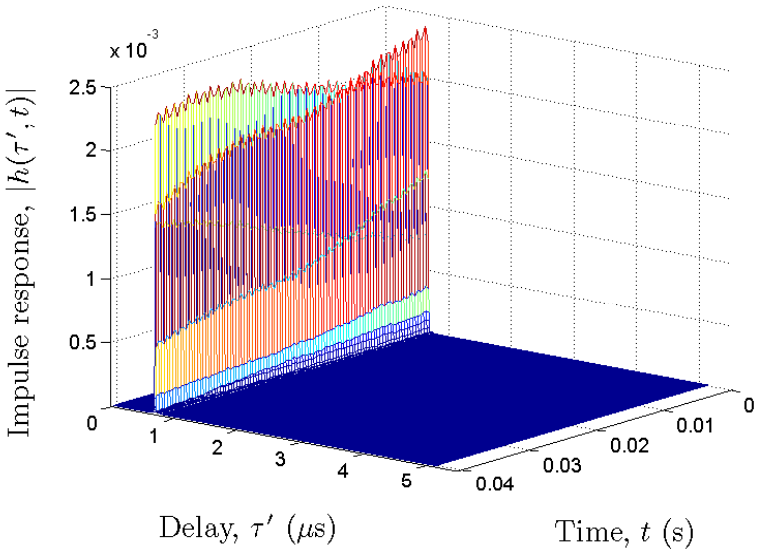

Figure C.3: Absolute value of the TVIR $|h(\tau',t)|$ of the measured channel.

In Section III, we stated that the propagation delays can directly be extracted from the measurement data. This process is illustrated in Fig. C.6. By plotting and observing the sample TVIR $|h(\tau',t_0)|$ at a fixed point in time $t = t_0$, we can identify only $L = 6$ relevant paths which contribute significantly to the total path power and the values of the propagation delays τ'_l. The channel gains $\mu_l(t)$ corresponding to those propagation delays were then used as a target function for the parameter computation method described in Section III. The complete set of parameters that we found using the new version of the INLSA is presented in Table C.1. Those results can easily be used for computing the TVIR $\tilde{h}(\tau',t)$ of the simulation model by simply substituting the listed values of the channel model parameters in (C.1). Computing the Fourier transform of the TVIR $\tilde{h}(\tau',t)$ with respect to τ' gives the time-variant transfer function $\tilde{H}(f',t)$ of the simulation model.

The absolute values of the obtained transfer function $|\tilde{H}(f',t)|$ and the resulting normalized TFCF $|\tilde{R}(\nu',\tau)|$ of the simulation model are illustrated in Figs. C.7

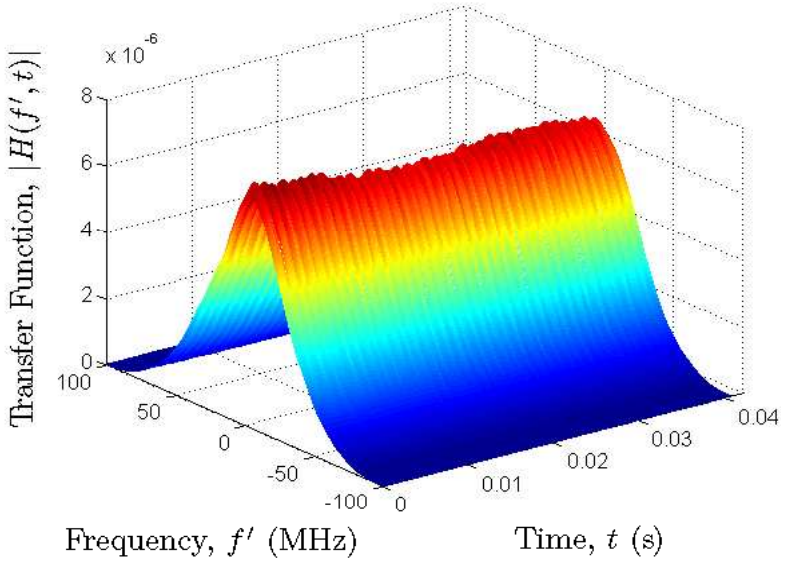

Figure C.4: Absolute value of the transfer function $|H(f',t)|$ of the measured channel.

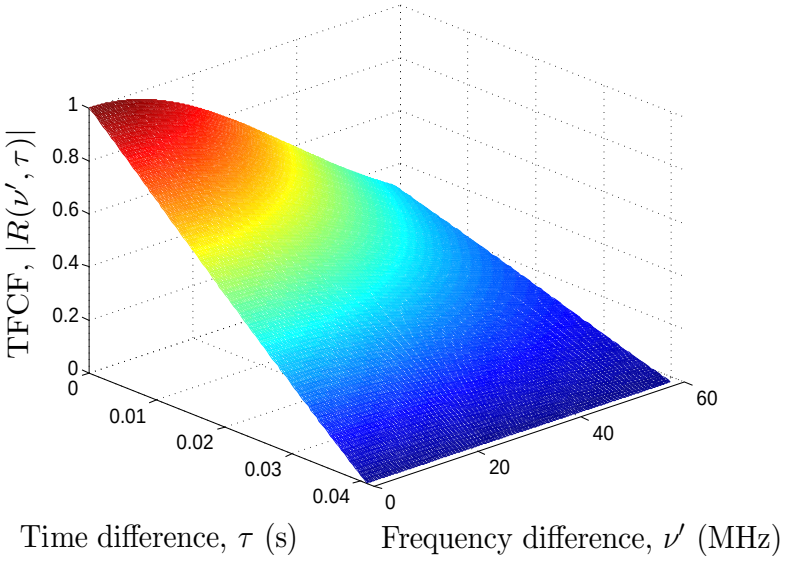

Figure C.5: Absolute value of the TFCF $|R(\nu',\tau)|$ of the measured channel.

and C.8, respectively. The results clearly show that the proposed method achieves an exceptional accuracy in approximating the transfer function and the TFCF of the measured channel. Figure C.7 shows the transfer function $\tilde{H}(f',t)$ that has been obtained for the same measurement period T_{mes} as the measured channel. Hence, the TFCF $\tilde{R}(\nu',\tau)$ is also affected by the limited measurement period. However, this problem can easily be avoided by simulating the transfer function $\tilde{H}(f',t)$ for a longer simulation time $T_{\text{sim}} \gg T_{\text{mes}}$. An example of the absolute value of the transfer function $|\tilde{H}(f',t)|$ of the simulation model is shown in Fig. C.9 for $T_{\text{sim}} = 4 \cdot T_{\text{mes}}$. The corresponding normalized TFCF $|\tilde{R}(\nu',\tau)|$ is illustrated in Fig. C.10. When comparing Figs. C.10 and C.8, we can notice that the triangular shape of the TFCF $|\tilde{R}(\nu',\tau)|$ vanishes if T_{sim} increases. As a result, the TFCF $|\tilde{R}(0,\tau)|$ becomes flatter in τ-direction, which indicates that the received signal envelope remains correlated over a longer period of time. An important result is also that the tunnel channel can be modelled as a flat fading channel for dedicated short range communication (DSRC) systems, where a system bandwidth is 10 MHz. This result is reasonable when considering that the scatterers inside the tunnel are located very close to each other.

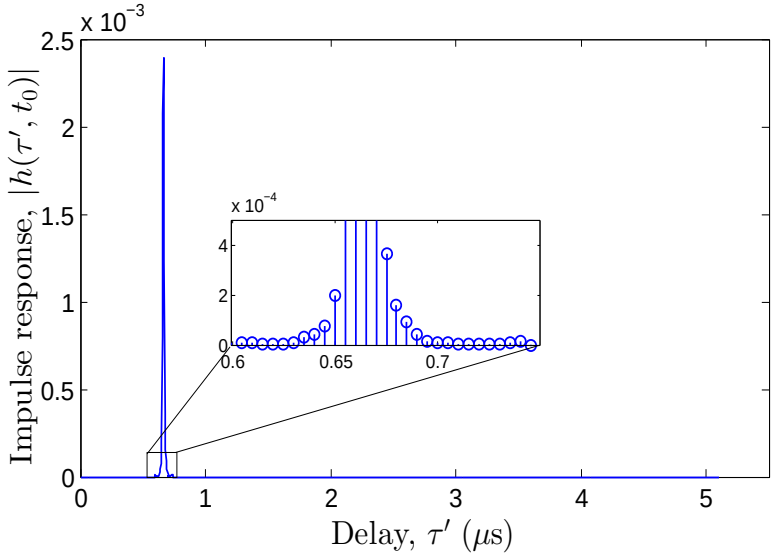

Figure C.6: Absolute value of the TVIR $|h(\tau',t_0)|$ of the measured channel at a fixed point in time $t = t_0$.

Table C.1: Parameters of the real-world channel simulator for tunnels.

L	N_l	τ'_l (μs)	$c_{l,n} \times 10^3$	$f_{l,n}$ (kHz)	$\theta_{l,n}$
1	1		0.2208	2.91	34.4°
	2	0.65	0.0436	2.92	126°
	3		0.1596	0.45	88.8°
2	1		1.1077	−1.99	42.9°
	2	0.655	0.1607	−2.00	137.5°
	3		0.1516	2.91	134.6°
3	1		2.0837	−1.99	42.9°
	2	0.66	0.2649	2.91	163.3°
	3		0.0913	2.89	171.9°
4	1		2.0168	0.46	40.1°
	2	0.665	0.1792	2.92	8.59°
	3		0.2071	2.89	11.46°
5	1		0.8555	0.45	34.37°
	2	0.67	0.1604	2.91	28.65°
	3		0.1150	−2.00	28.65°
6	1		0.2365	−1.99	25.78°
	2	0.675	0.0544	2.91	28.64°
	3		0.0436	0.44	25.78°

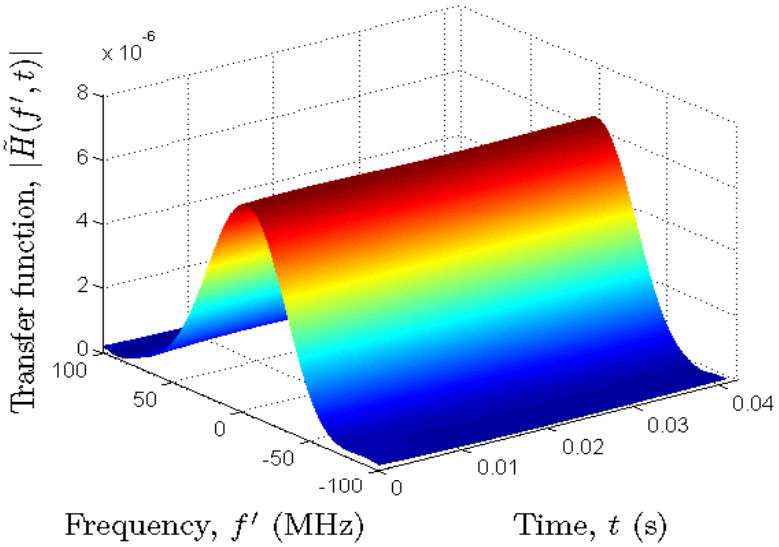

Figure C.7: Absolute value of the transfer function $|\tilde{H}(f',t)|$ of the channel model (simulator).

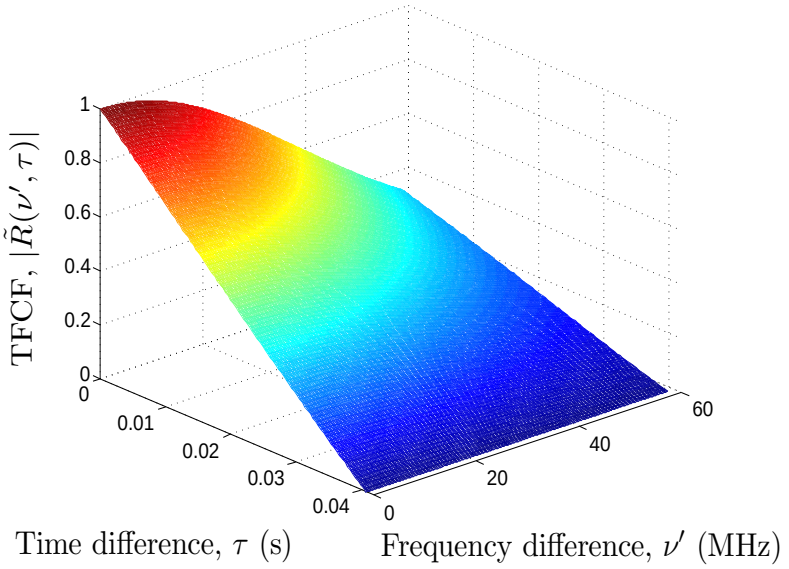

Figure C.8: Absolute value of the TFCF $|\tilde{R}(\nu',\tau)|$ of the channel model (simulator).

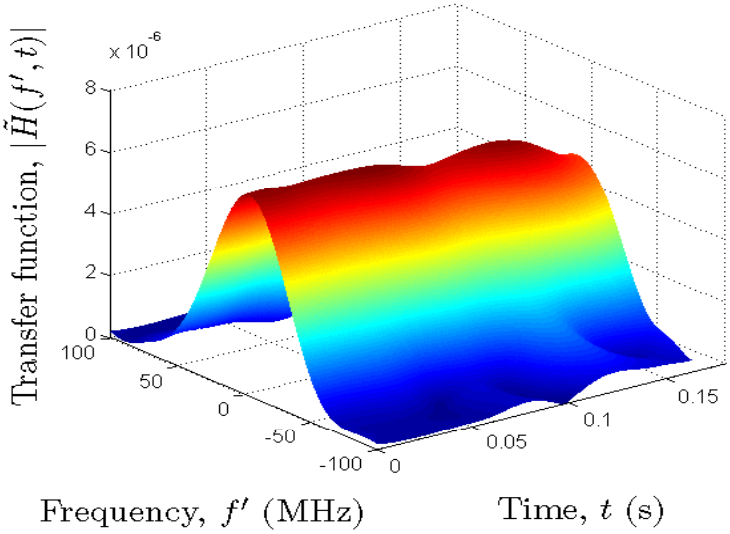

Figure C.9: Absolute value of the transfer function $|\tilde{H}(f',t)|$ of the channel model (simulator).

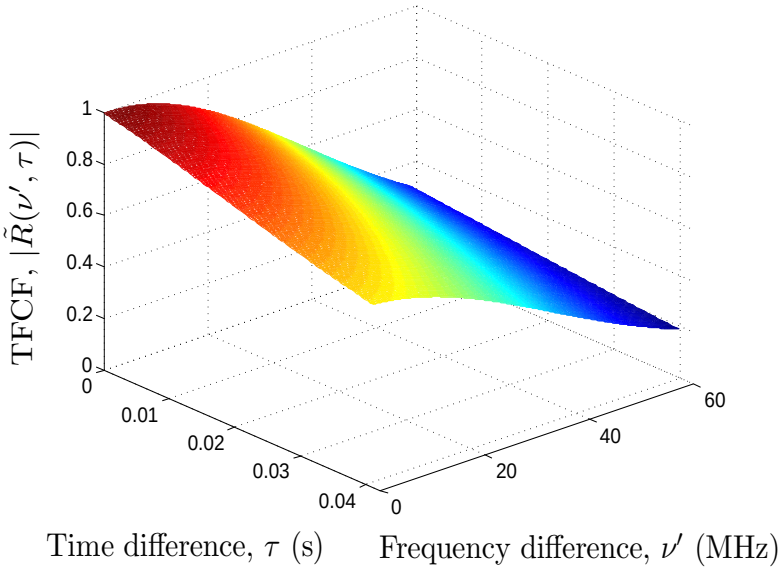

Figure C.10: Absolute value of the TFCF $|\tilde{R}(\nu', \tau)|$ of the channel model (simulator).

VI. Summary and Conclusions

In this paper, we presented a new version of the INLSA method for designing measurement-based channel models. The proposed method has been applied to road tunnel measurement data to estimate the parameters of the channel (simulation) model. The transfer function of the channel model has been compared to that of the measured channel. A comparison has also been made with respect to the goodness of fit between the TFCF of the channel (simulation) model and that of a measured channel. The obtained results show that the proposed method precisely estimates the channel model parameters and provides an excellent fitting to real-world channels. Additionally, we demonstrated that the designed simulation model can increase the reliability of the correlation properties estimated from the limited available data. From the analysis of the obtained TFCF, we conclude that the tunnel channel can be modelled as a flat fading channel for DSRC systems with the system bandwidth of 10 MHz. Owing to its excellent performance and the implementation simplicity, we also conclude that the proposed design approach can be used for the development of realistic channel models based on measurements, which are essential in the design phase of mobile communication systems.

ACKNOWLEDGEMENT

The measurements were performed within the national research project MOCAMIMODYN (Modéles de Canaux MIMO DYNamiques) and in the framework of the regional cluster of research CISIT (Campus International sur la Sécurité et Intermodalité des Transports). The authors would like to thank the French research agency, the NPDC Region and the European commission (FEDER) for their financial supports.

REFERENCES

[1] "IEEE standard method for CBTC performance and functional requirements," IEEE, Tech. Rep. IEEE Std 1474, Dec. 2004.

[2] M. Fitzmaurice, "Use of 2.4 GHz frequency band for CBTC data communication systems," in *Proc. of the 2006 IEEE/ASME Joint*. Atlanta, USA, Apr. 2006, pp. 263–267.

[3] M. Pätzold, *Mobile Radio Channels*, 2nd ed. Chichester: John Wiley & Sons, 2011, 583 pages.

[4] H. Krim and M. Viberg, "Two decades of array signal processing," *IEEE Signal Processing Magazine*, vol. 13, no. 4, pp. 67–94, Jul. 1996.

[5] A. Paulraj, R. Roy, and T. Kailath, "A subspace rotation approach to signal parameter estimation," in *Proceedings of the IEEE*, Jul. 1986, pp. 1044–1046.

[6] R. Schmidt, "Multiple emitter location and signal parameter estimation," *IEEE Trans. Antennas Propag.*, vol. 34, no. 3, pp. 276–280, Mar. 1986.

[7] R. Roy and T. Kailath, "ESPRIT-estimation of signal parameters via rotational invariance techniques," *IEEE Trans. Acoust., Speech, Signal Processing*, vol. 37, no. 7, pp. 984–995, Jul. 1989.

[8] M. Haardt and J. A. Nossek, "Unitary ESPRIT: how to obtain increased estimation accuracy with a reduced computational burden," *IEEE Trans. Signal Process.*, vol. 43, no. 5, pp. 1232–1242, May 1995.

[9] B. H. Fleury, M. Tschudin, R. Heddergott, D. Dahlhaus, and K. I. Pedersen, "Channel parameter estimation in mobile radio environments using the SAGE

algorithm," *IEEE J. Select. Areas Commun.*, vol. 17, no. 3, pp. 434–450, Mar. 1999.

[10] T. Lo, J. Litva, and H. Leung, "A new approach for estimating indoor radio propagation characteristics," *IEEE Trans. Antennas Propag.*, vol. SP-43, no. 10, pp. 1369–1376, 1994.

[11] A. J. van der Veen, M. C. van der Veen, and A. J. Paulraj, "Joint angle and delay estimation using shift-invariance properties," *IEEE Signal Processing Lett.*, vol. 4, pp. 142–145, May 1997.

[12] M. Feder and E. Weinstein, "Parameter estimation of superimposed signals using the EM algorithm," *IEEE Trans. Acoust., Speech, and Signal Processing*, vol. 36, no. 4, pp. 477–489, Aug. 1988.

[13] A. Fayziyev and M. Pätzold, "An improved iterative nonlinear least square approximation method of the design of measurement-based wideband mobile radio channel simulators," in *Proc. International Conference on Advanced Technologies for Communications, ATC 2011*. Da Nang City, Vietnam, Aug. 2011, pp. 106–111.

[14] Propsound CS, "Propsound CS - Multi-dimensional Channel Sounder," [online], http://www.anite.com/propsim (Accessed: 30 September 2013).

[15] L. Hentilä, P. Kyösti, J. Ylitalo, X. Zhao, J. Meinilä, and J.-P. Nuutinen, "Experimental characterization of multi-dimensional parameters at 2.45 and 5.25 GHz indoor channels," in *Proc. 8th International Symposium on Wireless Personal Multimedia Communications, WPMC 2005*. Aalborg, Denmark, Sep. 2005.

Appendix D

Paper IV

Title:	The Design of Sum-of-Sinusoids Channel Simulators Using the Iterative Nonlinear Least Square Approximation Method
Authors:	**Akmal Fayziyev** and Matthias Pätzold
Affiliation:	University of Agder, Faculty of Engineering and Science, P. O. Box 509, NO-4898 Grimstad, Norway
Conference:	*IEEE International Conference on Software, Telecommunications and Computer Networks, SoftCOM 2012*, Split, Croatia, Sep. 2012.

The Design of Sum-of-Sinusoids Channel Simulators Using the Iterative Nonlinear Least Square Approximation Method

Akmal Fayziyev and Matthias Pätzold
Faculty of Engineering and Science, University of Agder,
P.O. Box 509, NO-4898 Grimstad, Norway
E-mails: {akmal.fayziyev, matthias.paetzold}@uia.no

***Abstract* — In this paper, we introduce an iterative nonlinear least square approximation (INLSA) as an effective method for the design of sum-of-sinusoids (SOS) channel simulators. The proposed method determines the parameters of the simulation model iteratively by minimizing the Frobenius norm, which serves as a metric for measuring the fitting error. We compare the performance of the INLSA method with that of the method of exact Doppler spread (MEDS) and the L_p-norm method (LPNM). The performance comparisons will be carried out in terms of the goodness of fit to the autocorrelation functions (ACFs) corresponding to the Jakes and the Gaussian power spectral densities (PSDs). The obtained results indicate that the INLSA method is very precise in both cases. The results also show that the proposed method is better suited than the MEDS and the LPNM method to emulate the desired statistical properties of Gaussian shaped PSDs. Owing to its simplicity and excellent performance, the INLSA method is a powerful tool for designing channel simulation platforms required for the performance analysis of mobile communication systems.**

***Index Terms* — Channel modelling, sum-of-sinusoids, parameter computation, autocorrelation function, Doppler power spectral density**

I. INTRODUCTION

The achievable data rates of wireless communication systems are heavily dependent on the propagation environment in which the system operates. Thus, a thorough investigation of mobile radio channels is of crucial importance for the optimization and performance evaluation of wireless systems. The interest of researchers was therefore devoted to the design of channel simulators enabling an accurate emulation of wireless propagation channels. The Rice's sum-of-sinusoids (SOS) principle [1, 2] for the modeling of coloured Gaussian processes has been widely employed for designing simulation models for fading channels [3–9]. The main idea behind the SOS principle is to approximate coloured Gaussian processes by a finite sum of sinusoidal waveforms controlled by the model parameters, namely the gains, the Doppler frequencies, and the phases. By making use of the deterministic channel modeling approach [10] and by appropriately computing the SOS model parameters, one can efficiently design channel simulators having the desired statistical properties.

Several methods for computing the SOS model parameters can be found in the literature [11–14]. In [11] and [12], the authors presented the method of equal distances and the mean-square-error method, respectively. The common characteristic of both methods is that the distances between the two adjacent Doppler frequencies are equal. These two methods merely differ in the way of computing the Doppler coefficients. Due to the equidistance property of the Doppler frequencies, both methods have one major disadvantage, namely that the designed SOS process is periodical. Another well-known method is the method of equal areas presented in [11, 12]. The decisive disadvantage of this method is that it requires a relatively large number of sinusoids to approximate accurately the desired statistics in case of Gaussian shaped PSDs. The method of exact Doppler spread (MEDS), which was first introduced in [13], provides an excellent approximation of the autocorrelation function (ACF) corresponding to the Jakes PSD. The L_p-norm method (LPNM) [13, 14] is one of the widely used methods for computing the SOS channel model parameters. The LPNM utilizes optimization techniques and demonstrates an excellent performance with respect to the approximation of the ACF corresponding to both the Jakes and the Gaussian PSDs. However, the determination of the model parameters using the LPNM is relatively time consuming. The development of new accurate and computationally efficient methods is therefore desirable for the performance analysis of wireless communication systems.

In this paper, we propose a simple and efficient iterative method for the design of SOS channel simulators. The proposed iterative nonlinear least square approximation (INLSA) method is based on the expectation maximization approach [15] and computes the model parameters by iteratively fitting the ACF of the simulation model to that of the reference model. The proposed method involves optimization techniques to determine the model parameters. In contrast to the LPNM method, however, the optimization procedure used in the INLSA method is carried out iteratively such that a multidimensional search in determining the model parameters is avoided. This kind of iterative procedure reduces significantly the computational cost, while maintaining the same high level of fitting accuracy as that of the LPNM. In order to demonstrate the performance of the INLSA method, we implemented the algorithm in MATLAB and compared the new method with two well-known methods, namely the MEDS and the LPNM. We focused on an isotropic scattering scenario and considered the ACFs corresponding to the Jakes and the Gaussian PSDs as reference ACFs. The comparisons of all three methods are made with respect to the fitting accuracy and parameter computation time.

This paper has the following structure. In Section II, we discuss the reference model. In Section III, we present the deterministic simulation model. Section IV describes the proposed parameter computation method. Numerical examples and results are presented in Section V. Finally, Section VI concludes this paper.

II. The Reference Model

In this section, we discuss the reference model, which serves as a target for the parameter computation method. We consider a small-scale frequency-nonselective Rayleigh fading channel as the reference model. In this case, we can model the complex channel gain in the equivalent complex baseband as a zero-mean complex Gaussian process, denoted by

$$\mu(t) = \mu_1(t) + j\mu_2(t) \tag{D.1}$$

where $\mu_1(t)$ and $\mu_2(t)$ are the real-valued Gaussian processes, each having a variance of σ_0^2. A typical and often assumed shape for the Doppler PSD $S_{\mu\mu}(f)$ of $\mu(t)$ is known as the Jakes PSD, which is defined as

$$S_{\mu\mu}(f) = \begin{cases} \frac{2\sigma_0^2}{\pi f_{\max}\sqrt{1-(f/f_{\max})^2}}, & |f| \leq f_{\max}, \\ 0, & |f| > f_{\max}, \end{cases} \tag{D.2}$$

where $f_{\max}$ denotes the maximum Doppler frequency. From (D.2), it follows that the corresponding ACF $r_{\mu\mu}(\tau)$ of $\mu(t)$ is given by

$$r_{\mu\mu}(\tau) = 2r_{\mu_i\mu_i}(\tau) = 2\sigma_0^2 J_0(2\pi f_{\max}\tau),\ i = 1,2 \tag{D.3}$$

where $J_0(\cdot)$ denotes the zeroth order Bessel function of the first kind. Another widely used Doppler PSD $S_{\mu\mu}(f)$ is the Gaussian PSD

$$S_{\mu\mu}(f) = \frac{2\sigma_0}{f_c}\sqrt{\frac{\ln 2}{\pi}}e^{-\ln 2\left(\frac{f}{f_c}\right)^2} \tag{D.4}$$

where f_c is the 3-dB-cut-off frequency. The inverse Fourier transform of the Gaussian PSD results in the ACF

$$r_{\mu\mu}(\tau) = 2r_{\mu_i\mu_i}(\tau) = 2\sigma_0^2 e^{-\left(\pi\frac{f_c}{\sqrt{\ln 2}}\tau\right)^2},\ i = 1,2. \tag{D.5}$$

III. The Deterministic Simulation Model

In this section, we first introduce the deterministic SOS simulation model, and subsequently, we review briefly the MEDS and the LPNM. Let us start by presenting two SOS processes $\tilde{\mu}_1(t)$ and $\tilde{\mu}_2(t)$ in the following form

$$\tilde{\mu}_i(t) = \sum_{n=1}^{N_i} c_{i,n}\cos(2\pi f_{i,n}t + \theta_{i,n}),\quad i = 1,2 \tag{D.6}$$

where N_i denotes the number of sinusoids. The quantities $c_{i,n}$, $f_{i,n}$, and $\theta_{i,n}$ are the model parameters called the gains, the Doppler frequencies, and the phases, respectively. The parameters $c_{i,n}$, $f_{i,n}$, and $\theta_{i,n}$ have to be determined in the simulation set-up phase and then they are kept constant during the whole simulation. From the fact that all the parameters of the SOS process $\tilde{\mu}_i(t)$ are constant, it follows that $\tilde{\mu}_i(t)$ is a deterministic process. The probability density function (PDF) of the deterministic process $\tilde{\mu}_i(t)$ is given as [14]

$$\tilde{p}_{\mu_i}(x) = 2\int_0^\infty \prod_{n=1}^{N_i} J_0(2\pi c_{i,n}\nu)\cos(2\pi\nu x)d\nu. \tag{D.7}$$

The ACF of the deterministic process $\tilde{\mu}_i(t)$ can be computed as

$$\tilde{r}_{\mu_i\mu_i}(\tau) = \lim_{T\to\infty} \frac{1}{2T} \int_{-T}^{T} \tilde{\mu}_i(t)\tilde{\mu}_i(t+\tau)dt. \tag{D.8}$$

Substituting (D.6) in (D.8) results in the following expression for the ACF $\tilde{r}_{\mu_i\mu_i}(\tau)$ [14]

$$\tilde{r}_{\mu_i\mu_i}(\tau) = \sum_{n=1}^{N_i} \frac{c_{i,n}^2}{2} \cos(2\pi f_{i,n}\tau). \tag{D.9}$$

It should be noted that the deterministic processes $\tilde{\mu}_1(t)$ and $\tilde{\mu}_2(t)$ are uncorrelated iff $f_{1,n} \neq \pm f_{2,m}$ for all $n = 1,2,\ldots,N_1$ and $m = 1,2,\ldots,N_2$. For the purpose of comparison, we review in the next two subsections two methods (MEDS and LPNM) for computing the model parameters.

A. MEDS

The MEDS [13] has been especially developed for the Jakes PSD, for which it results in an excellent approximation of the corresponding ACF in (D.3). According to this method, the gains $c_{i,n}$ and Doppler frequencies $f_{i,n}$ are defined as

$$c_{i,n} = \sigma_0 \sqrt{\frac{2}{N_i}} \tag{D.10}$$

and

$$f_{i,n} = f_{\max} \sin\left[\frac{\pi}{2N_i}\left(n - \frac{1}{2}\right)\right] \tag{D.11}$$

respectively, for all $n = 1,2,\ldots,N_i$ $(i = 1,2)$. If we apply the MEDS in connection with the Gaussian PSD, then the Doppler frequencies $f_{i,n}$ are computed by finding the zeros of

$$\frac{2n-1}{2N_i} - \operatorname{erf}\left(\frac{f_{i,n}}{f_c}\sqrt{\ln 2}\right) = 0 \tag{D.12}$$

for all $n = 1,2,\ldots,N_i$ $(i = 1,2)$, where $\operatorname{erf}(\cdot)$ is the error function. The gains $c_{i,n}$ remain unchanged, i.e., they are computed according to (D.10).

B. LPNM

The LPNM [13, 14] is based on the idea that the sets of model parameters $\{c_{i,n}\}$ and $\{f_{i,n}\}$ are obtained by minimizing the following L_p-norm

$$E^{(p)}_{r_{\mu_i\mu_i}} := \left\{ \frac{1}{\tau_{\max}} \int_0^{\tau_{\max}} |r_{\mu_i\mu_i}(\tau) - \tilde{r}_{\mu_i\mu_i}(\tau)|^p d\tau \right\}^{1/p} \tag{D.13}$$

where $\tau_{\max}$ defines the time-lag interval [0, $\tau_{\max}$] over which the approximation is carried out. In the LPNM, we do not impose any boundary conditions on the model parameters $c_{i,n}$ and $f_{i,n}$. With reference to the L_p-norm in (D.13), the ACF $\tilde{r}_{\mu_i\mu_i}(\tau)$ of the deterministic SOS process $\tilde{\mu}_i(t)$ needs to be fitted as close as possible to a desired ACF $r_{\mu_i\mu_i}(\tau)$ of the reference model $\mu_i(t)$. It should be noted that the determination of the sets of model parameters constitutes a multidimensional optimization problem.

IV. The Proposed Parameter Computation Method

This section focuses on the description of the proposed INLSA algorithm for computing the parameters of the SOS simulation model. In the following, we consider the ACF $r_{\mu_i\mu_i}(\tau)$ of the reference model at the discrete time-lags τ_k, where $\tau_k = k\Delta\tau,\ k = 0,1,\ldots,K$, and $\Delta\tau$ is the time-lag sampling interval. In this case, the ACF $r_{\mu_i\mu_i}(\tau)$ can be represented in the form of a discrete ACF $r_i[\tau_k]$. Also, by using (D.9), we can compute the discrete ACF $\tilde{r}_i[\tau_k]$ of the simulation model at the discrete time-lags τ_k. In order to determine the set of model parameters $\mathbb{P} = \{c_{i,n}, f_{i,n}\}$ such that the discrete ACF $\tilde{r}_i[\tau_k]$ of the simulation model approximates the discrete ACF $r_i[\tau_k]$ of the reference model, we need to minimize the following squared Frobenius norm

$$E(\mathbb{P}) = \left\| r_i[\tau_k] - \tilde{r}_i[\tau_k] \right\|_2^2. \tag{D.14}$$

Owing to the computational complexity, the direct minimization of the model error $E(\mathbb{P})$ in (D.14) is intractable. Therefore, the proposed method utilizes an iterative approach to determine the model parameters. The proposed INLSA method starts with $N_i = 1$ and an arbitrarily chosen initial value for $f^{(0)}_{i,1}$. At every iteration q $(q = 0,1,2,\ldots)$, the algorithm computes the complete set of model parameters $\mathbb{P}$. The parameter computation procedure is carried out separately for each sinusoid

l ($l = 1,2,\ldots,N_i$) by using the auxiliary error function $y_l^{(q)}[\tau_k]$ as follows:

$$y_l^{(q)}[\tau_k] = r_i[\tau_k] - \frac{1}{2}\sum_{n=1,n\neq l}^{N_i}\left(c_{i,n}^{(q)}\right)^2\cos(2\pi f_{i,n}^{(q)}\tau_k) \tag{D.15}$$

$$c_{i,l}^{(q+1)} = \arg\min_{c_{i,l}}\left\|y_l^{(q)}[\tau_k] - \frac{1}{2}c_{i,l}^2\cos(2\pi f_{i,l}^{(q)}\tau_k)\right\|_2^2 \tag{D.16}$$

$$f_{i,l}^{(q+1)} = \arg\min_{f_{i,l}}\left\|y_l^{(q)}[\tau_k] - \frac{1}{2}\left(c_{i,l}^{(q+1)}\right)^2\cos(2\pi f_{i,l}\tau_k)\right\|_2^2. \tag{D.17}$$

In this algorithm, the iterative computation of the set of parameters $\mathbb{P}$ continues as long as the relative change in the model error $E(\mathbb{P})$ is larger than a predefined threshold level ε. When the threshold level ε is reached, the iteration stops, and the number of propagation paths N_i is increased by one, i.e., $N_i + 1 \rightarrow N_i$. The initial values for $c_{i,N}^{(0)}$ and $f_{i,N}^{(0)}$ are set to zero. After this, the iterative parameter computation procedure is carried out again starting from (D.15). This process is repeated until no perceptible progress can be observed by increasing N_i or a given maximum number of paths is reached. Further simplifications can be made by using the closed-form solution for the minimization problem in (D.16) as

$$c_{i,l}^{(q+1)} = \sqrt{\frac{\left\{\mathbf{y}_{i,l}^{(q)}\right\}^T\mathbf{p}_{i,l}^{(q)}}{\left\{\mathbf{p}_{i,l}^{(q)}\right\}^T\mathbf{p}_{i,l}^{(q)}}} \tag{D.18}$$

where the operator $\{\cdot\}^T$ designates the transpose. The symbol $\mathbf{y}_{i,l}^{(q)}$ refers to the column vector containing the stacked values of the auxiliary error function $y_l^{(q)}[\tau_k]$. The column vector $\mathbf{p}_{i,l}^{(q)}$ contains the stacked values of the samples $\cos(2\pi f_{i,l}^{(q)}\tau_k)$. The result in (D.18) is obtained by setting the first-order derivative of the squared Frobenius norm in (D.16) with respect to $c_{i,l}$ equal to zero. The important characteristics of the proposed method is the iterative optimization approach used to determine the model parameters. The comparison of the proposed method to the MEDS and LPNM is demonstrated in the next section.

V. Numerical Results

This section discusses the performance of the proposed INLSA method. We compare the proposed method to the methods discussed in Section III. The comparisons

are made with respect to their capabilities to approximate the Jakes and Gaussian ACFs. The numerical simulation results presented in this section have been obtained by choosing $f_{\max}$ = 91 Hz and σ_0^2 = 1. In the LPNM, we restricted ourselves to the case p = 2. In Fig. D.1, we have depicted the curves for the ACFs $\tilde{r}_{\mu_i\mu_i}(\tau)$ and $r_{\mu_i\mu_i}(\tau)$ corresponding to the Jakes PSD, where the value 10 has been chosen for the number of sinusoids N_i. From Fig. D.1, it can be observed that the proposed method, as well as the MEDS and LPNM provide an excellent fitting accuracy within the interval [0, $\tau_{\max}$], where $\tau_{\max} = N_i/(2f_{\max})$. For a better performance assessment of the proposed INLSA method, we have also plotted in Fig. D.2 the curves for the following mean-square error

$$E_{r_{\mu_i\mu_i}} = \frac{1}{\tau_{\max}} \int_0^{\tau_{\max}} |r_{\mu_i\mu_i}(\tau) - \tilde{r}_{\mu_i\mu_i}(\tau)|^2 d\tau. \tag{D.19}$$

In Fig. D.2, we can observe which influence the number of sinusoids N_i has on the performance of the various methods. We conclude from the inspection of Fig. D.2 that the proposed method results in a significantly lower mean-square error $E_{r_{\mu_i\mu_i}}$ compared to the MEDS. In the following, we present the performance evaluations concerning the Gaussian PSD for N_i = 10 and $\tau_{\max} = N_i/(2\kappa_c f_c)$, where $f_c = \sqrt{\ln 2} f_{\max}$ and $\kappa_c = 2\sqrt{2/\ln 2}$. The corresponding ACFs $\tilde{r}_{\mu_i\mu_i}(\tau)$ and $r_{\mu_i\mu_i}(\tau)$ are il-

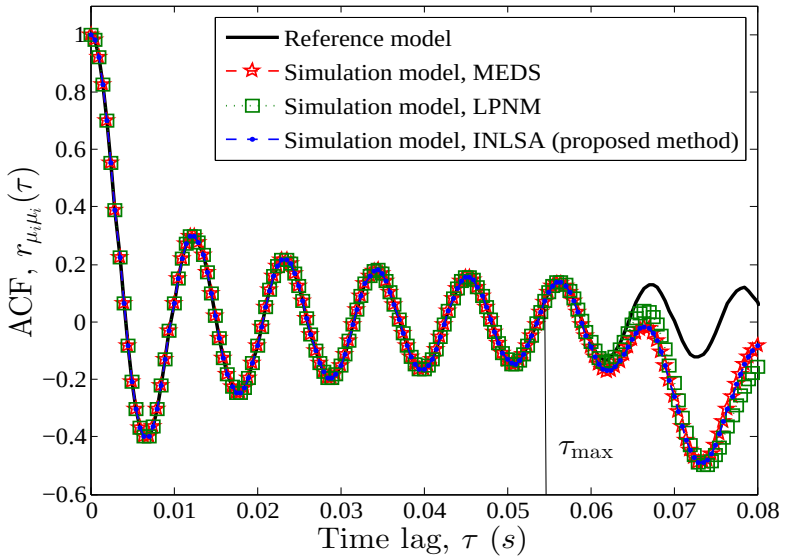

Figure D.1: The ACFs $r_{\mu_i\mu_i}(\tau)$ (reference model) and $\tilde{r}_{\mu_i\mu_i}(\tau)$ (simulation model) for different parameter computation methods (Jakes PSD).

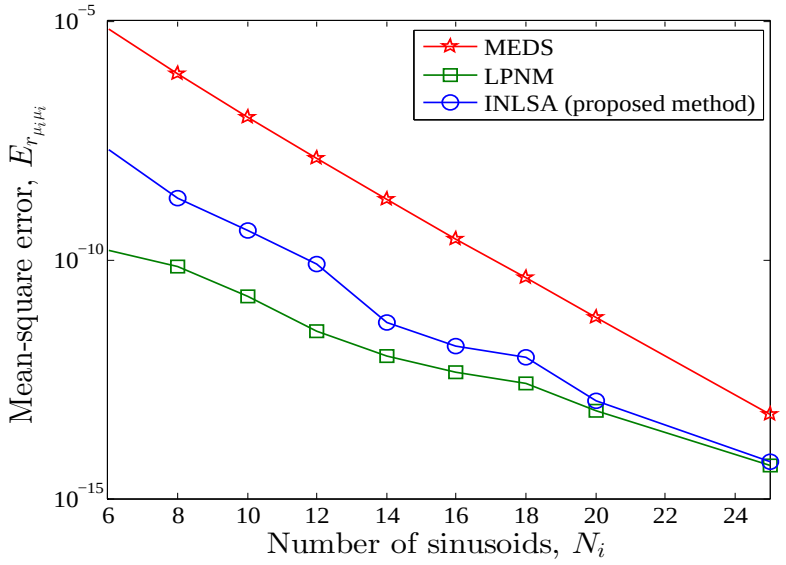

Figure D.2: Mean-square error $E_{r_{\mu_i\mu_i}}$ (Jakes PSD).

lustrated in Fig. D.3. From Fig. D.3, we observe an excellent agreement between the ACFs of the simulation model and the reference model when the proposed method is used. In Fig. D.3, one can also see that the ACF $\tilde{r}_{\mu_i\mu_i}(\tau)$ of the deterministic SOS process is considerably different from the reference ACF $r_{\mu_i\mu_i}(\tau)$ in case of the Gaussian PSD when the MEDS is used. Studying Fig. D.4, it becomes obvious that the MEDS leads clearly to higher values of $E_{r_{\mu_i\mu_i}}$ in comparison with the proposed method and the LPNM. The obtained results so far, clearly state that the proposed method along with the LPNM demonstrates an exceptional performance in approximating the ACFs corresponding to both the Jakes and the Gaussian PSDs. This performance is achieved by including the gains $c_{i,n}$ and the Doppler frequencies $f_{i,n}$ into optimization procedure. However, aforementioned procedure leads to degradations with respect to the PDF of the SOS process. In order to demonstrate this problem, we have plotted in Fig. D.5 the graphs for the mean-square error of the PDF

$$E_{p_{\mu_i}} = \int_{-\infty}^{\infty} |p_{\mu_i}(x) - \tilde{p}_{\mu_i}(x)|^2 dx \tag{D.20}$$

where $p_{\mu_i}(x)$ is the Gaussian distribution of the stochastic process $\mu_i(t)$. When studying Fig. D.5, it becomes obvious that the LPNM has the largest mean-square error $E_{p_{\mu_i}}$. From Fig. D.5, we also notice that the MEDS allows the lowest values of $E_{p_{\mu_i}}$ among the three methods. In contrast to the LPNM, the mean-square error $E_{p_{\mu_i}}$ of

Table D.1: Parameter computation time (Gaussian PSD).

Methods	N_i =10	N_i =20	N_i =30	N_i =40
LPNM	8.67 s	44.21 s	105.39 s	149.21 s
INLSA (proposed method)	0.73 s	3.43 s	5.91 s	11.2 s
MEDS	0.62 s	0.84 s	1.91 s	2.25 s

the INLSA method is still very good and close to that of the MEDS.

In Fig. D.6, the mean-square error $E_{r_{\mu_i\mu_i}}$ curves are presented for the case that $c_{i,n} = \sigma_0\sqrt{2/N_i}$ is chosen for all three methods, i.e., only the Doppler frequencies $f_{i,n}$ are optimized using the INLSA method and the LPNM. By comparing Figs. D.4 and D.6, we can observe that fixing the gains reduces significantly the approximation quality of both the INLSA method and the LPNM. Finally, we have illustrated the influence of the number of sinusoids N_i on the amount of time consumed by the various methods in Table D.1. Obviously, among the three considered methods, the MEDS requires the shortest time for computing the model parameters. The results presented in Table D.1 also show that the proposed method has a significantly lower computational complexity than the LPNM. Thus, among the methods discussed, the INLSA method is the best choice for modeling the desired statistical properties of the Gaussian Doppler PSDs.

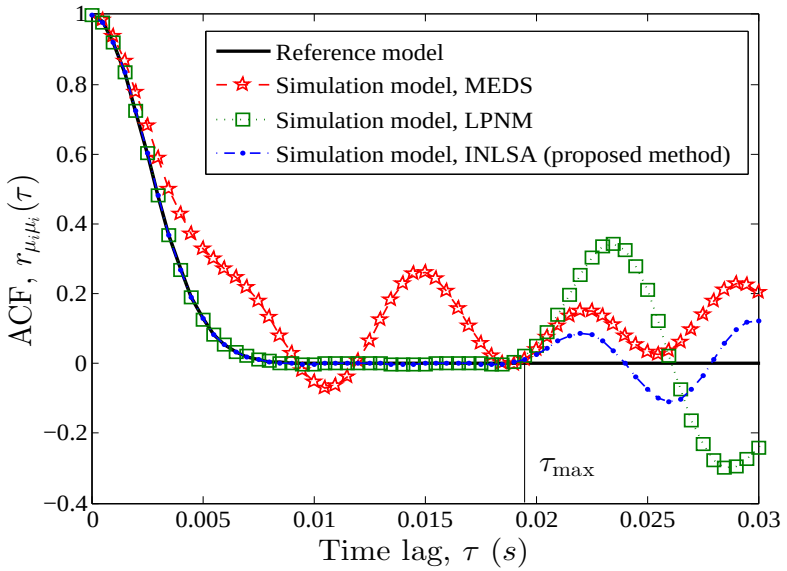

Figure D.3: The ACFs $r_{\mu_i\mu_i}(\tau)$ (reference model) and $\tilde{r}_{\mu_i\mu_i}(\tau)$ (simulation model) for different parameter computation methods (Gaussian PSD).

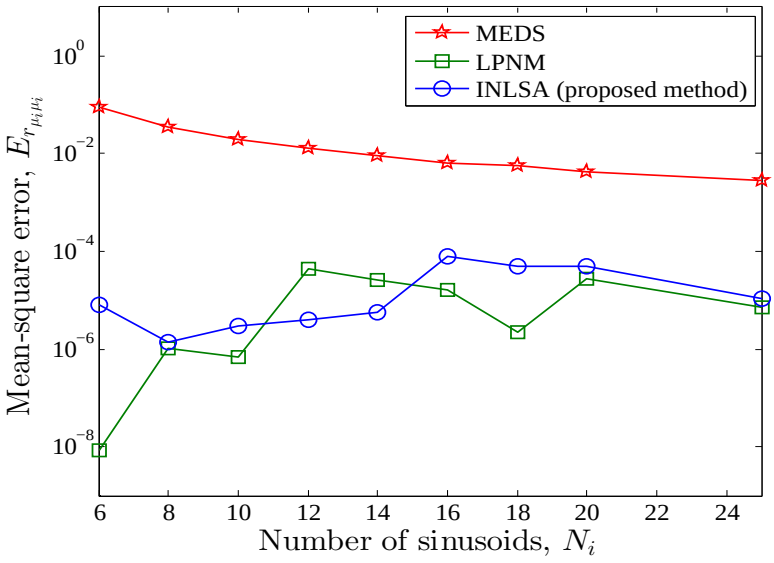

Figure D.4: Mean-square error $E_{r_{\mu_i\mu_i}}$ (Gaussian PSD).

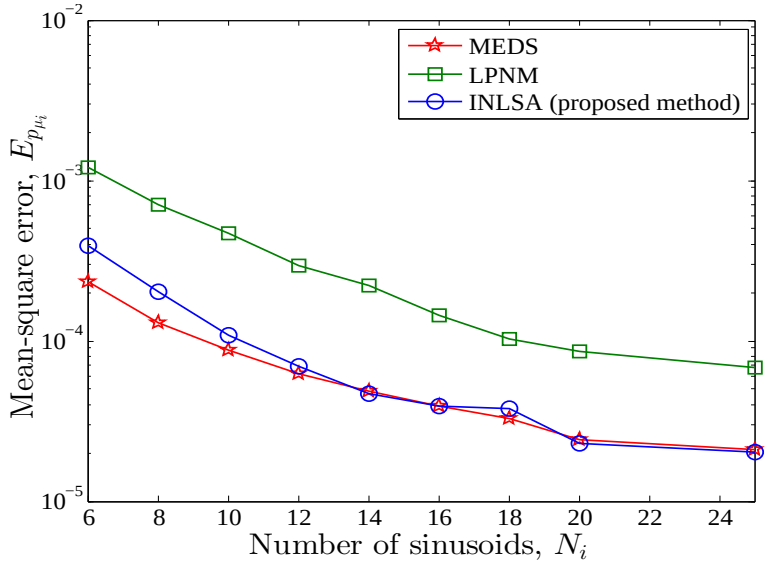

Figure D.5: Mean-square error $E_{p_{\mu_i}}$ (Gaussian PSD).

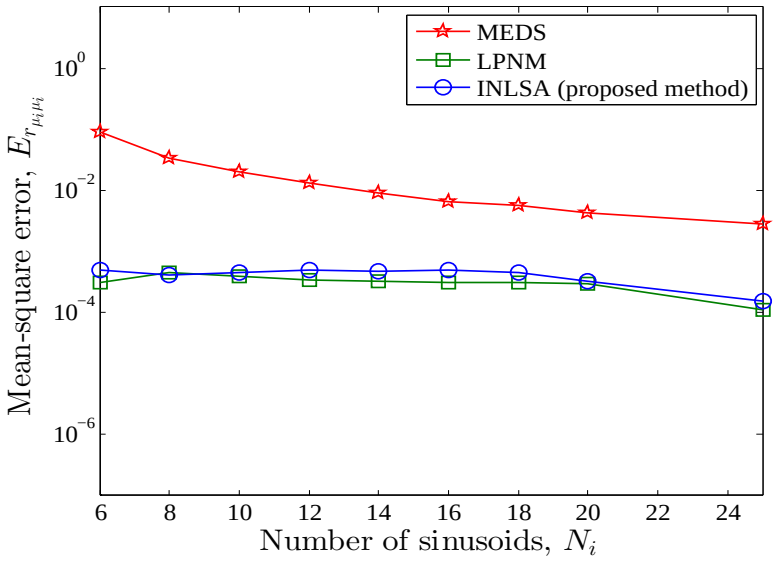

Figure D.6: Mean-square error $E_{r_{\mu_i\mu_i}}$, $c_{i,n} = \sigma_0\sqrt{2/N_i}$ with $\sigma_0 = 1$ (Gaussian PSD).

VI. Summary and Conclusions

In this paper, we described the INLSA method for designing SOS channel simulators. The INLSA method aims to determine the optimal set of model parameters by approximating iteratively a given reference ACF. The performance analysis of the proposed method has been made by evaluating the fitting error for the Jakes and the Gaussian ACFs. We have demonstrated that the INLSA method delivers an excellent performance in both cases. A performance comparison between the well-known LPNM and the proposed INLSA method with respect to the parameter computation time has shown that the proposed method is superior to the LPNM. Owing to the low complexity and the excellent performance, we conclude that the INLSA method is an excellent choice for designing SOS channel simulators, which are important for the design, optimization, and test of mobile communication systems.

References

[1] S. O. Rice, "Mathematical analysis of random noise," *Bell Syst. Tech. J.*, vol. 23, pp. 282–332, Jul. 1944.

[2] ——, "Mathematical analysis of random noise," *Bell Syst. Tech. J.*, vol. 24, pp. 46–156, Jan. 1945.

[3] W. C. Jakes, Ed., *Microwave Mobile Communications*. Piscataway, NJ: IEEE Press, 1994.

[4] C. S. Patel, G. L. Stüber, and T. G. Pratt, "Comparative analysis of statistical models for the simulation of Rayleigh faded cellular channels," *IEEE Trans. Commun.*, vol. 53, no. 6, pp. 1017–1026, Jun. 2005.

[5] T.-M. Wu and S.-Y. Tzeng, "Sum-of-sinusoids-based simulator for Nakagami-*m* fading channels," in *Proc. 58th IEEE Semiannual Veh. Techn. Conf., VTC'03-Fall*, vol. 1. Orlando, Florida, USA, Oct. 2003, pp. 158–162.

[6] C. Xiao, Y. R. Zheng, and N. C. Beaulieu, "Novel sum-of-sinusoids simulation models for Rayleigh and Ricean fading channels," *IEEE Trans. Wireless Commun.*, vol. 5, no. 12, pp. 3667–3679, Dec. 2006.

[7] C. A. Gutiérrez and M. Pätzold, "Efficient sum-of-sinusoids-based simulation of mobile fading channels with asymmetric Doppler power spectra," in *Proc. 4th IEEE International Symposium on Wireless Communication Systems, ISWCS 2007*. Trondheim, Norway, Oct. 2007, pp. 246–251.

[8] M. Pätzold and K. Yang, "An exact solution for the level-crossing rate of shadow fading processes modelled by using the sum-of-sinusoids principle," *Wireless Personal Communications (WPC)*, vol. 52, no. 1, pp. 57–68, Jan. 2010.

[9] M. Pätzold, C.-X. Wang, and B. Hogstad, "Two new sum-of-sinusoids-based methods for the efficient generation of multiple uncorrelated Rayleigh fading waveforms," *IEEE Trans. Wireless Commun.*, vol. 8, no. 6, pp. 3122–3131, Jun. 2009.

[10] M. Pätzold, *Mobile Radio Channels*, 2nd ed. Chichester: John Wiley & Sons, 2011, 583 pages.

[11] M. Pätzold, U. Killat, and F. Laue, "A deterministic model for a shadowed Rayleigh land mobile radio channel," in *Proc. 5th IEEE Int. Symp. Personal, Indoor and Mobile Radio Commun., PIMRC'94*. The Hague, The Netherlands, Sep. 1994, pp. 1202–1210.

[12] ——, "A deterministic digital simulation model for Suzuki processes with application to a shadowed Rayleigh land mobile radio channel," *IEEE Trans. Veh. Technol.*, vol. 45, no. 2, pp. 318–331, May 1996.

[13] M. Pätzold, U. Killat, F. Laue, and Y. Li, "A new and optimal method for the derivation of deterministic simulation models for mobile radio channels," in *Proc. IEEE 46th Veh. Technol. Conf., VTC'96*, vol. 3. Atlanta, Georgia, USA, Apr./May 1996, pp. 1423–1427.

[14] ——, "On the statistical properties of deterministic simulation models for mobile fading channels," *IEEE Trans. Veh. Technol.*, vol. 47, no. 1, pp. 254–269, Feb. 1998.

[15] M. Feder and E. Weinstein, "Parameter estimation of superimposed signals using the EM algorithm," *IEEE Trans. Acoust., Speech, and Signal Processing*, vol. 36, no. 4, pp. 477–489, Aug. 1988.

Appendix E

Paper V

Title:	The Design of Sum-of-Cisoids Channel Simulators Using the Iterative Nonlinear Least Square Approximation Method
Authors:	**Akmal Fayziyev** and Matthias Pätzold
Affiliation:	University of Agder, Faculty of Engineering and Science, P. O. Box 509, NO-4898 Grimstad, Norway
Conference:	*IEEE International Conference on Advanced Technologies for Communications, ATC 2013*, Ho Chi Minh City, Vietnam, Oct. 2013.

The Design of Sum-of-Cisoids Channel Simulators Using the Iterative Nonlinear Least Square Approximation Method

Akmal Fayziyev and Matthias Pätzold
Faculty of Engineering and Science, University of Agder,
P.O. Box 509, NO-4898 Grimstad, Norway
E-mails: {akmal.fayziyev, matthias.paetzold}@uia.no

***Abstract* — In this paper, we propose the iterative nonlinear least square approximation (INLSA) algorithm as an effective method for the design of sum-of-cisoids (SOC) channel simulators assuming non-isotropic scattering conditions. For the characterization of non-isotropic scattering scenarios, we use the von Mises distribution for describing the distribution of the angles-of-arrival (AOAs). The INLSA method relies partially on numerical optimization techniques. This method determines the SOC model parameters iteratively by minimizing the Frobenius error norm. We evaluate the performance of the INLSA method and compare the results with those obtained for the Riemann sum method (RSM) and the L_p-norm method (LPNM). The performance comparisons will be carried out with respect to the autocorrelation function (ACF) and the distribution of the envelope. The obtained results indicate that the proposed method is more preferable than the RSM and the LPNM when emulating the statistical properties of the channel under non-isotropic scattering conditions. In addition to its efficiency and excellent performance, the simplicity of the INLSA makes the method a powerful tool for designing channel simulators required for the test and evaluation of mobile communication systems.**

***Index Terms* — Channel modelling, sum-of-cisoids, parameter computation, autocorrelation function, angles-of-arrival, non-isotropic scattering**

I. INTRODUCTION

Increasing demands for higher data rates and more reliable communication links strain the capabilities of the most modern wireless communication systems, this gives rise to new challenges for future development. In order to meet these demands faced in the design and performance assessment phase of new wireless systems, the precise knowledge of the statistics of the underlying multipath fading channel is of crucial importance. Therefore, the development of accurate and efficient channel simulators reproducing the statistical properties of wireless propagation channels has become an attractive topic for many studies [1–6].

The sum-of-sinusoids (SOS) principle introduced by Rice in [7] and [8], has found its application in the development of simulation models for a large variety of mobile fading channels [9–12]. The investigations in [13] have demonstrated that SOS processes are better choice if isotropic scattering conditions are assumed, while SOC processes are better suited for the modelling of mobile radio channels under realistic non-isotropic scattering conditions. However, to fully exploit the advantages of SOC models, one must carefully determine the model parameters, namely the gains, the Doppler frequencies, and the phases. The literature offers only some few solutions to the parametrization problem of SOC models. These include the extended method of exact Doppler spread (EMEDS) [14], the generalized method of equal areas (GMEA) [15], the Riemann sum method (RSM) [16], and the L_p-norm method [17, 18]. The decisive disadvantage of the EMEDS is that its application is restricted to computing the model parameters of SOC channel simulators only under the assumption of isotropic scattering. The LPNM and the GMEA perform remarkably well with respect to the approximation of the correlation properties of the channel [19, 20]. However, the LPNM method relies on numerical optimization techniques that make the parameter computation a time-consuming process, whereas the GMEA requires a comparatively large number of cisoids to approximate accurately the channel statistics. In [20], the authors demonstrated that the RSM is well suited for the emulation of the channel's correlation properties. Nevertheless, the RSM performs poorly regarding the approximation of the envelope probability density function (PDF). Further research on the development of simple and efficient methods is, therefore, highly desirable for the development and performance analysis of future wireless communication systems.

In this paper, we extend the iterative nonlinear least square approximation (INLSA) method presented in [21] to the design of SOC channel simulators. The INLSA

method is based on the expectation maximization approach presented in [22] and computes the model parameters iteratively by fitting the ACF of the SOC simulation model to that of the reference model. To determine the SOC model parameters, the INLSA method relies partially on numerical optimization techniques. However, the optimization procedure is carried out iteratively such that a multidimensional search in the model parameter computation process is evaded. An iterative procedure utilized in the INLSA method reduces significantly the computational cost, while maintaining the same high approximation accuracy level as that of the LPNM. We evaluate the performance of the INLSA method with respect to its fitting accuracy to the ACF and the envelope distribution of the reference channel model. In addition, we compare its performance to that of the RSM and the LPNM. We carry out our investigations by focusing on non-isotropic scattering scenarios, where the AOA characteristics are determined by the von Mises distribution.

The remainder of this paper is set up as follows. In Section II, we discuss the statistical characteristics of the reference model. Section III presents the deterministic simulation model. Section IV introduces the proposed parameter computation method. The performance evaluation of the INLSA method is presented in Section V. Finally, Section VI summarizes the main points of this paper.

II. The Reference Model

In this section, we present the reference model against which the designed SOC simulation model will be compared. We consider a small-scale frequency-nonselective Rayleigh fading environment. This consideration allows the representation of the complex channel gain in the equivalent baseband by a stationary zero-mean complex Gaussian process $\boldsymbol{\mu}(t)$ with variance $\sigma_{\boldsymbol{\mu}}^2$. An important fact about the Gaussian process $\boldsymbol{\mu}(t)$ is that it can be completely characterized by means of its ACF $r_{\boldsymbol{\mu}\boldsymbol{\mu}}(\tau)$, which is defined as $r_{\boldsymbol{\mu}\boldsymbol{\mu}}(\tau) = E\{\boldsymbol{\mu}^*(t)\boldsymbol{\mu}(t+\tau)\}$, where $E\{\cdot\}$ denotes statistical averaging and the superscripted asterisk * is the complex conjugation operator. The ACF $r_{\boldsymbol{\mu}\boldsymbol{\mu}}(\tau)$ depends on the distribution of the AOAs of the scattered waves on the receiver antenna. The von Mises distribution is often considered as a proper model for the distribution of the AOAs in non-isotropic scattering environments [23]. The von Mises distribution $p_{\boldsymbol{\alpha}}(\alpha)$ of the AOA α and its even part $g_{\boldsymbol{\alpha}}(\alpha)$ are given by

$$p_{\boldsymbol{\alpha}}(\alpha) = \frac{e^{\kappa\cos(\alpha - m_\alpha)}}{2\pi I_0(\kappa)} \tag{E.1}$$

and

$$g_{\boldsymbol{\alpha}}(\alpha) = \frac{e^{\kappa\cos(\alpha - m_\alpha)}}{2\pi I_0(\kappa)} \cdot \cosh(\kappa \sin(\alpha)\sin(m_\alpha)) \tag{E.2}$$

respectively, where $\alpha \in [-\pi, \pi)$. The parameter $m_\alpha \in [-\pi, \pi)$ designates the mean AOA, $\kappa > 0$ is the parameter that controls the angular spread, and $I_0(\cdot)$ is the zeroth order modified Bessel function of the first kind. For $\kappa = 0$, the von Mises distribution reduces to the uniform distribution characterizing isotropic scattering, i.e., $p_{\boldsymbol{\alpha}}(\alpha) = 1/2\pi$ if $\kappa = 0$.

On the basis of Clark's two-dimensional scattering model [24], we can represent the reference ACF $r_{\boldsymbol{\mu}\boldsymbol{\mu}}(\tau)$ of $\boldsymbol{\mu}(t)$ for the von Mises distribution of the AOAs as follows [23]

$$\begin{aligned} r_{\boldsymbol{\mu}\boldsymbol{\mu}}(\tau) &= \frac{\sigma_{\boldsymbol{\mu}}^2}{I_0(\kappa)} I_0\big(\{\kappa^2 - (2\pi f_{\max}\tau)^2 \\ &+ j4\pi\kappa f_{\max}\cos(m_\alpha)\tau\}^{1/2}\big) \end{aligned} \tag{E.3}$$

where $f_{\max}$ designates the maximum Doppler frequency. It is worth noticing that, the ACF in (E.3) simplifies to $r_{\boldsymbol{\mu}\boldsymbol{\mu}}(\tau) = \sigma_{\boldsymbol{\mu}}^2 J_0(2\pi f_{\max}\tau)$ if $\kappa = 0$. Concerning the distribution of the reference model's envelope $\boldsymbol{\zeta}(t) = |\boldsymbol{\mu}(t)|$, one can show that the PDF $p_{\boldsymbol{\zeta}}(z)$ of $\boldsymbol{\zeta}(t)$ follows the Rayleigh distribution regardless of the correlation properties of the channel [9].

III. The Deterministic Simulation Model

In this section, we will introduce the deterministic SOC simulation model, which will serve as a target for the development of the proposed parameter computation method. We also present a brief review of the conventional methods, namely the RSM and the LPNM. The starting point will be the SOC process presented in the following form

$$\hat{\boldsymbol{\mu}}(t) = \sum_{n=1}^{N} c_n e^{j(2\pi f_n t + \theta_n)} \tag{E.4}$$

where N denotes the number of complex sinusoids (cisoids). The parameters c_n and θ_n are called the gains and the phases, respectively. The Doppler frequencies f_n are defined as $f_n = f_{\max}\cos(\alpha_n)$, where $\alpha_n \in [-\pi, \pi)$ denotes the AOA of the nth path ($n = 1, 2, \ldots, N$). Since the model parameters are constant quantities, the SOC process $\hat{\boldsymbol{\mu}}(t)$ is a deterministic process. It can be easily verified that the ACF $r_{\hat{\boldsymbol{\mu}}\hat{\boldsymbol{\mu}}}(\tau)$

of $\hat{\boldsymbol{\mu}}(t)$ can be represented in the following form [13]

$$r_{\hat{\boldsymbol{\mu}}\hat{\boldsymbol{\mu}}}(\tau) = \sum_{n=1}^{N} c_n^2 e^{j2\pi f_n \tau}. \tag{E.5}$$

The distribution of the envelope $\hat{\boldsymbol{\zeta}}(t) = |\hat{\boldsymbol{\mu}}(t)|$ of the SOC model is given by [13]

$$\hat{p}_{\boldsymbol{\zeta}}(z) = (2\pi)^2 z \int_0^{\infty} \left[\prod_{n=1}^{N} J_0(2\pi |c_n| x) \right] J_0(2\pi z x) x dx \tag{E.6}$$

for $z > 0$. The results presented in [9] indicate that the PDF $\hat{p}_{\boldsymbol{\zeta}}(z)$ in (E.6) approaches the Rayleigh density if $c_n = \sigma_{\boldsymbol{\mu}}/\sqrt{N}$ and $N \to \infty$. From (E.5) and (E.6), we can deduce that the phases θ_n have no influence on the ACF and the PDF of the simulation model. Therefore, we may focus only on the computation of the principal parameters, namely the gains c_n and the AOAs α_n.

A. RSM

The RSM [16] suggests that the ACF $r_{\hat{\boldsymbol{\mu}}\hat{\boldsymbol{\mu}}}(\tau)$ of the simulation model will provide a good approximation to the ACF $r_{\boldsymbol{\mu}\boldsymbol{\mu}}(\tau)$ of the reference model in (E.3) if the gains c_n and AOAs α_n are computed as

$$c_n = \sigma_{\boldsymbol{\mu}} \sqrt{\frac{g_{\boldsymbol{\alpha}}(\alpha_m)}{\sum_{m=1}^{N} g_{\boldsymbol{\alpha}}(\alpha_m)}} \tag{E.7}$$

and

$$\alpha_n = \frac{\pi}{N}\left(n - \frac{1}{2}\right) \tag{E.8}$$

respectively, for all $n = 1, 2, \ldots, N$.

B. LPNM

In the following, we consider two versions of the LPNM [17, 18]. In the first version, the path gains c_n are computed according to the equation $c_n = \sigma_{\boldsymbol{\mu}}\sqrt{1/N}$ for all $n = 1, 2, \ldots, N$, whereas the AOAs α_n are computed in such a way that the L_p-norm

$$E_{r_{\boldsymbol{\mu}\boldsymbol{\mu}}}^{(p)} := \left\{ \frac{1}{\tau_{\max}} \int_0^{\tau_{\max}} |r_{\boldsymbol{\mu}\boldsymbol{\mu}}(\tau) - r_{\hat{\boldsymbol{\mu}}\hat{\boldsymbol{\mu}}}(\tau)|^p d\tau \right\}^{1/p} \tag{E.9}$$

results in a minimum, where p is a positive integer, and $\tau_{\max} > 0$ defines the interval $[0, \tau_{\max}]$ inside of which the approximation of the ACF $r_{\hat{\boldsymbol{\mu}}\hat{\boldsymbol{\mu}}}(\tau)$ is of interest. In the second version, both the gains c_n and AOAs α_n are computed by minimizing the L_p-norm in (E.9). We will refer to the first and the second versions of the LPNM as the LPNM I and the LPNM II, respectively. In the LPNM I and LPNM II, we do not impose any boundary conditions on the optimized model parameters. It should be noted that the LPNM's inherent optimization technique makes the determination of the model parameters a time-consuming task.

IV. The INLSA Method

The principal task of a parameter computation method consists in finding the parameters of the simulation model to allow a proper emulation of the statistical properties of the reference model. In the present case, the parameters are the gains c_n and AOAs α_n (or equivalently Doppler frequencies f_n), the statistical property to be emulated is the ACF $r_{\boldsymbol{\mu}\boldsymbol{\mu}}(\tau)$ in (E.3). One idea to accomplish this task is to determine the set of parameters $\mathbb{P} = \{c_n, \alpha_n\}$ of the simulation model in such a way that the squared Frobenius norm $E(\mathbb{P})$ becomes minimal, i.e.,

$$E(\mathbb{P}) = \left\| \boldsymbol{r} - \hat{\boldsymbol{r}} \right\|_2^2 = \textbf{Min}! \tag{E.10}$$

In (E.10), $\boldsymbol{r}$ is the vector $\boldsymbol{r} = \big(r_{\boldsymbol{\mu}\boldsymbol{\mu}}(\tau_0), r_{\boldsymbol{\mu}\boldsymbol{\mu}}(\tau_1), \ldots, r_{\boldsymbol{\mu}\boldsymbol{\mu}}(\tau_K)\big)$ that contains the values of $r_{\boldsymbol{\mu}\boldsymbol{\mu}}(\tau)$ at the discrete time-lags $\tau_k = k\Delta\tau$, where $k = 0, 1, \ldots, K$ and $\Delta\tau$ denotes the sampling interval. Analogously, the vector $\hat{\boldsymbol{r}}$ combines the values of $r_{\hat{\boldsymbol{\mu}}\hat{\boldsymbol{\mu}}}(\tau)$ at the time-lags τ_k, i.e., $\hat{\boldsymbol{r}} = \big(r_{\hat{\boldsymbol{\mu}}\hat{\boldsymbol{\mu}}}(\tau_0), r_{\hat{\boldsymbol{\mu}}\hat{\boldsymbol{\mu}}}(\tau_1), \ldots, r_{\hat{\boldsymbol{\mu}}\hat{\boldsymbol{\mu}}}(\tau_K)\big)$. To solve the minimization problem in (E.10), the INLSA method requires initial values of the gains $c_n^{(0)}$ and AOAs $\alpha_n^{(0)}$ for $n = 1, 2, \ldots, N$. Those values can be chosen arbitrarily or inherited from other parameter computation methods, e.g., the RSM or LPNM. The proper selection of the initial values leads to a faster convergence and reduces the computation time for the model parameters. The proposed method starts with setting the iteration index q equal to zero. The model parameters c_n and α_n are then determined separately for each of the N terms in (E.5) by using the auxiliary error function $y_n^{(q)}(\tau_k)$ $(k = 0, 1, \ldots, K)$ as follows

$$y_n^{(q)}(\tau_k) = r_{\boldsymbol{\mu}\boldsymbol{\mu}}(\tau_k) - \sum_{l=1, l\neq n}^{N} \left(c_l^{(q)}\right)^2 e^{j2\pi f_{max} \cos(\alpha_l^{(q)})\tau_k} \tag{E.11}$$

$$c_n^{(q+1)} = \arg\min_{c_n} \left\| \mathbf{y}_n^{(q)} - c_n^2 \mathbf{s}_n^{(q)} \right\|_2^2. \tag{E.12}$$

where the symbol $\mathbf{y}_n^{(q)}$ refers to the column vector containing the stacked values of the auxiliary error function $y_n^{(q)}(\tau_k)$. The column vector $\mathbf{s}_n^{(q)}$ contains the stacked values of the exponential function $e^{j2\pi f_{max}\cos(\alpha_n^{(q)})\tau_k}$. Fortunately, we can solve the minimization problem in (E.12) by the simple closed-form expression

$$c_n^{(q+1)} = \sqrt{\frac{\mathrm{Re}\left\{\mathbf{y}_n^{(q)}\right\}^T \mathrm{Re}\left\{\mathbf{s}_n^{(q)}\right\} + \mathrm{Im}\left\{\mathbf{y}_n^{(q)}\right\}^T \mathrm{Im}\left\{\mathbf{s}_n^{(q)}\right\}}{\left(\mathbf{s}_n^{(q)}\right)^H \mathbf{s}_n^{(q)}}} \tag{E.13}$$

The result in (E.13) is obtained by finding the zeros of the first order derivative of the Frobenius norm in (E.12) with respect to c_n. The new estimates for the AOAs $\alpha_n^{(q+1)}, n = 1,2,\ldots,N$, are then obtained as follows

$$\alpha_n^{(q+1)} = \arg\min_{\alpha_n} \left\| \mathbf{y}_n^{(q)} - \left(c_n^{(q+1)}\right)^2 \mathbf{s}_n^{(q)} \right\|_2^2. \tag{E.14}$$

The squared Frobenius norm $E(\mathbb{P})$ is re-evaluated at the end of each iteration. In case of a noticeable change in the error norm $E(\mathbb{P})$, the iteration index q is increased by one, i.e., $q+1 \rightarrow q$. After that, the parameter computation procedure is carried out again starting from (E.12). If the relative change in the error norm $E(\mathbb{P})$ reaches a threshold ε, the iteration algorithm terminates.

The important feature of the INLSA method is the relatively simple iterative optimization approach used to determine the model parameters. The performance comparison of the INLSA method against the RSM and LPNM is demonstrated in the next section.

V. Numerical Results

In this section, we evaluate the performance of the INLSA method with respect to its capabilities to approximate the reference model's ACF $r_{\mu\mu}(\tau)$ and the envelope PDF $p_{\zeta}(z)$ under non-isotropic scattering conditions. In addition, we compare the performance of the INLSA method to that of the RSM and two versions of the LPNM reviewed in Subsection III-B. We have carried out the simulations by choosing $f_{\max}$ = 91 Hz and σ_{μ}^2 = 1. Regarding the configuration of the LPNM I and the LPNM II, we have set p = 2 and $\tau_{\max} = N/(4f_{\max})$. The threshold $\varepsilon = 10^{-6}$ has been used as a stopping criterion for the INLSA method. In Figs. E.1 and E.2, we

have plotted the curves of the absolute values of $r_{\boldsymbol{\mu}\boldsymbol{\mu}}(\tau)$ and $r_{\hat{\boldsymbol{\mu}}\hat{\boldsymbol{\mu}}}(\tau)$ by applying the different parameter computation methods using $N = 10$. To enable a fair comparison with the LPNM I and LPNM II, we have set $\tau_{\max}$ equal to $N/(4f_{\max})$ for all methods. For comparative purposes, the curves have been plotted for three different values of κ and m_α, namely $\kappa \in \{0, 5, 10\}$ and $m_\alpha \in \{0, \pi/4, \pi/3\}$. It can be seen in Fig. E.1 that the graphs of $|r_{\boldsymbol{\mu}\boldsymbol{\mu}}(\tau)|$ match perfectly the ones of $|r_{\hat{\boldsymbol{\mu}}\hat{\boldsymbol{\mu}}}(\tau)|$ obtained by applying the INLSA method, as well as the RSM and LPNM II. However, it is evident from the visual inspection of Fig. E.2 that the INLSA method and LPNM II perform significantly better than the RSM for higher values of m_α. For the sake of clarity, we have illustrated the curves of the mean-square error

$$E_{r_{\boldsymbol{\mu}\boldsymbol{\mu}}} = \frac{1}{\tau_{\max}} \int_0^{\tau_{\max}} (r_{\boldsymbol{\mu}\boldsymbol{\mu}}(\tau) - r_{\hat{\boldsymbol{\mu}}\hat{\boldsymbol{\mu}}}(\tau))^2 d\tau \tag{E.15}$$

of the ACF $r_{\hat{\boldsymbol{\mu}}\hat{\boldsymbol{\mu}}}(\tau)$ in Fig. E.3. The obtained results confirm that the INLSA method is better suited than the RSM and the LPNM I to approximate the ACF $r_{\boldsymbol{\mu}\boldsymbol{\mu}}(\tau)$. The results also show that the LPNM II produces in general the smallest mean-square error among the compared methods.

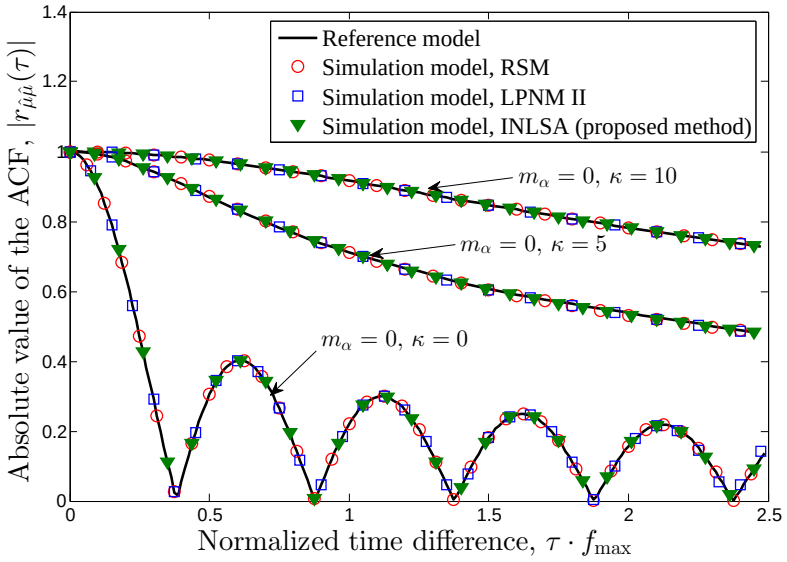

Figure E.1: The ACFs $r_{\boldsymbol{\mu}\boldsymbol{\mu}}(\tau)$ (reference model) and $r_{\hat{\boldsymbol{\mu}}\hat{\boldsymbol{\mu}}}(\tau)$ (simulation model) for different different values of κ with $m_\alpha = 0$ and $N = 10$.

In the following, we present the performance evaluations with respect to the Rayleigh distribution $p_{\boldsymbol{\zeta}}(z)$ of the envelope $\zeta(t)$. The corresponding PDFs $p_{\boldsymbol{\zeta}}(z)$

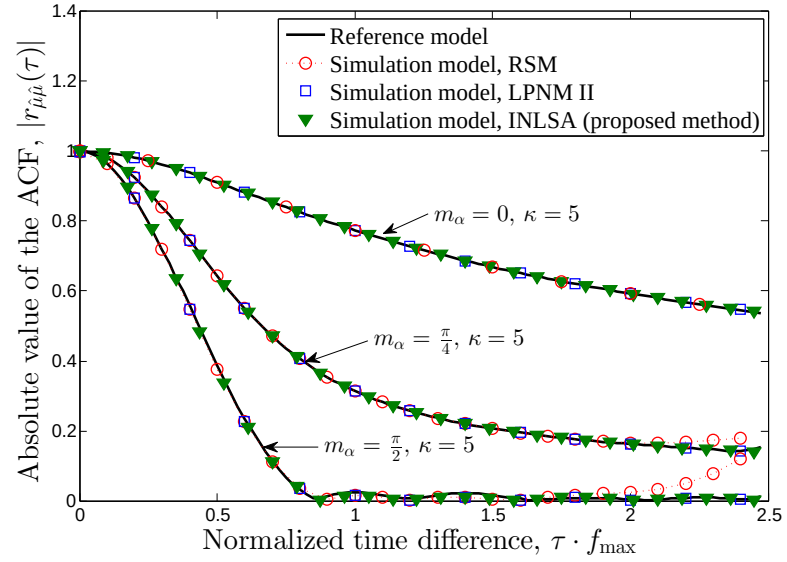

Figure E.2: The ACFs $r_{\boldsymbol{\mu}\boldsymbol{\mu}}(\tau)$ (reference model) and $r_{\hat{\boldsymbol{\mu}}\hat{\boldsymbol{\mu}}}(\tau)$ (simulation model) for different different values of m_α with $\kappa = 5$ and $N = 10$.

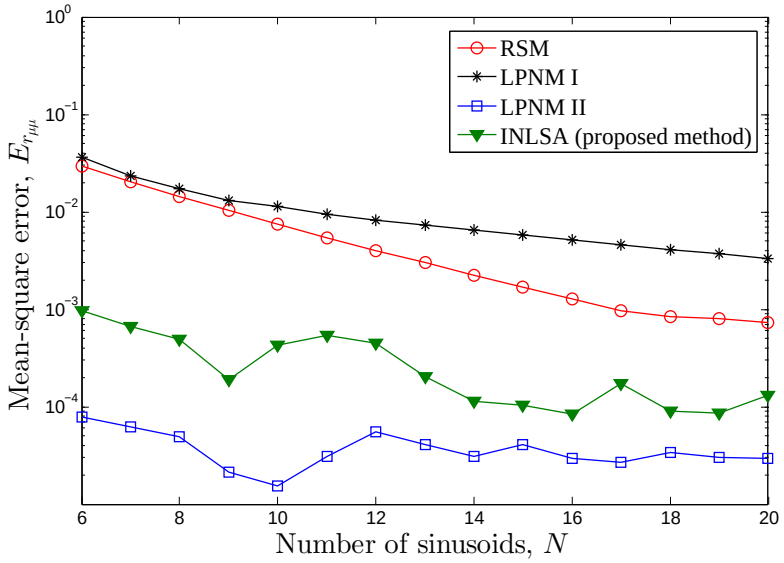

Figure E.3: Mean-square error $E_{r_{\boldsymbol{\mu}\boldsymbol{\mu}}}$ of $r_{\hat{\boldsymbol{\mu}}\hat{\boldsymbol{\mu}}}(\tau)$ for different parameter computation methods with $\kappa = 5$ and $m_\alpha = \pi/2$.

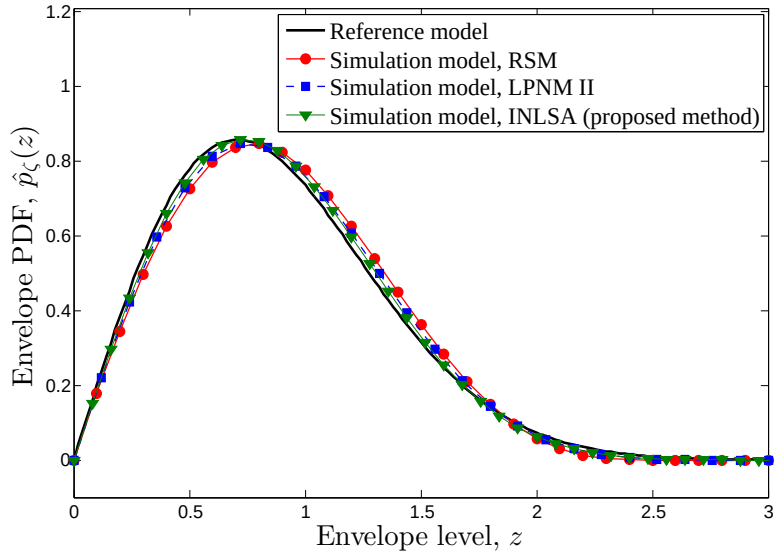

Figure E.4: The envelope PDF $p_{\boldsymbol{\zeta}}(z)$ (reference model) and $\hat{p}_{\boldsymbol{\zeta}}(z)$ (simulation model) for different parameter computation methods with $\kappa = 5$, $m_\alpha = \pi/2$ and $N = 10$.

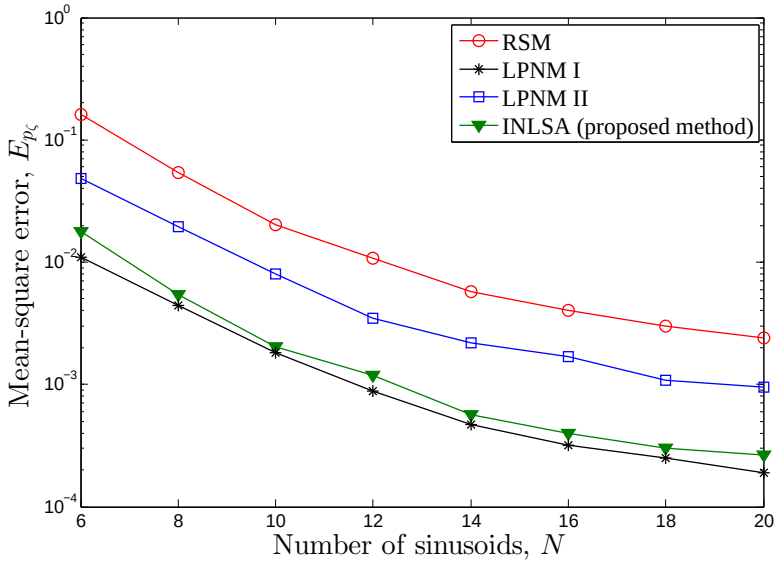

Figure E.5: Mean-square error E_{p_ζ} of $\hat{p}_{\boldsymbol{\zeta}}(z)$ for different parameter computation methods with $\kappa = 5$ and $m_\alpha = \pi/2$.

and $\hat{p}_{\boldsymbol{\zeta}}(z)$ are illustrated in Fig. E.4 by considering $N = 10$. From Fig. E.4, we observe a good agreement between the envelope distributions of the reference model and the simulation model if the INLSA method is applied. The results presented in Fig. E.4 also indicate that the RSM and the LPNM II are less accurate than the INLSA method regarding the approximation of the Rayleigh distribution. In order to better assess the methods' performance, we present in Fig. E.5 the graphs of the mean-square error E_{p_ζ} of the envelope PDF $\hat{p}_{\boldsymbol{\zeta}}(z)$, i.e.,

$$E_{p_\zeta} = \int_0^\infty \Big(p_{\boldsymbol{\zeta}}(z) - \hat{p}_{\boldsymbol{\zeta}}(z) \Big)^2 dz. \tag{E.16}$$

The results, presented in Fig. E.5, provide evidence that the INLSA method and the LPNM I are better suited than the other two methods to approximate the envelope PDF $p_{\boldsymbol{\zeta}}(z)$ when the scattering conditions are non-isotropic. Figure E.5 also shows that the highest mean-square error is produced by the RSM. We notice from inspection of Fig. E.5 that the LPNM II produces worse results than the INLSA method. This is due to the fact that the LPNM II sacrifices significant accuracy in the approximation of $p_{\boldsymbol{\zeta}}(z)$ by involving the gains c_n into the optimization procedure without maintaining any boundary conditions. As was to be expected, the LPNM I produces the smallest mean-square error among the analyzed methods.

VI. Summary and Conclusions

In this paper, we presented the INLSA method as an effective method for designing SOC channel simulators assuming non-isotropic scattering conditions. We evaluated the performance of the INLSA method with respect to its capability to approximate the ACF and the envelope PDF of the reference model. The performance of the INLSA method has also been compared with the RSM and two versions of the LPNM. The obtained results indicate that the INLSA method is more precise than the LPNM II and the RSM regarding the approximation of the envelope PDF. Moreover, performance of the INLSA method with respect to the approximation $r_{\hat{\boldsymbol{\mu}}\hat{\boldsymbol{\mu}}}(\tau) \approx r_{\boldsymbol{\mu}\boldsymbol{\mu}}(\tau)$ approaches to that of the LPNM II with increasing N, which in fact does not increase the parameter computation complexity exponentially as in case of the LPNM II. In conclusion, we can say that the proposed INLSA method provides the best compromise (among the analyzed methods) between matching the ACF and the envelope PDF of the reference model.

REFERENCES

[1] H. Suzuki, "A statistical model for urban radio propagation," *IEEE Trans. Commun.*, vol. 25, no. 7, pp. 673–680, Jul. 1977.

[2] M. Pätzold, U. Killat, and F. Laue, "An extended Suzuki model for land mobile satellite channels and its statistical properties," *IEEE Trans. Veh. Technol.*, vol. 47, no. 2, pp. 617–630, May 1998.

[3] C. Loo, "A statistical model for a land mobile satellite link," *IEEE Trans. Veh. Technol.*, vol. 34, no. 3, pp. 122–127, Aug. 1985.

[4] A. S. Akki and F. Haber, "A statistical model of mobile-to-mobile land communication channel," *IEEE Trans. Veh. Technol.*, vol. 35, no. 1, pp. 2–7, Feb. 1986.

[5] A. S. Akki, "Statistical properties of mobile-to-mobile land communication channels," *IEEE Trans. Veh. Technol.*, vol. 43, no. 4, pp. 826–831, Nov. 1994.

[6] M. Pätzold, B. O. Hogstad, and N. Youssef, "Modeling, analysis, and simulation of MIMO mobile-to-mobile fading channels," *IEEE Trans. Wireless Commun.*, vol. 7, no. 2, pp. 510–520, Feb. 2008.

[7] S. O. Rice, "Mathematical analysis of random noise," *Bell Syst. Tech. J.*, vol. 23, pp. 282–332, Jul. 1944.

[8] ——, "Mathematical analysis of random noise," *Bell Syst. Tech. J.*, vol. 24, pp. 46–156, Jan. 1945.

[9] M. Pätzold, *Mobile Radio Channels*, 2nd ed. Chichester: John Wiley & Sons, 2011, 583 pages.

[10] C. A. Gutiérrez and M. Pätzold, "Sum-of-sinusoids-based simulation of flat fading wireless propagation channels under non-isotropic scattering conditions," in *Proc. 50th IEEE Global Communications Conference, IEEE GLOBECOM 2007*. Washington DC, USA, Nov. 2007, pp. 3842–3846.

[11] K.-W. Yip and T.-S. Ng, "Efficient simulation of digital transmission over WSSUS channels," *IEEE Trans. Commun.*, vol. 43, no. 12, pp. 2907–2913, Dec. 1995.

[12] C.-X. Wang, M. Pätzold, and Q. Yao, "Stochastic modeling and simulation of frequency-correlated wideband fading channels," *IEEE Trans. Veh. Technol.*, vol. 56, no. 3, pp. 1050–1063, May 2007.

[13] M. Pätzold and B. Talha, "On the statistical properties of sum-of-cisoids-based mobile radio channel simulators," in *Proc. 10th International Symposium on Wireless Personal Multimedia Communications, WPMC 2007*. Jaipur, India, Dec. 2007, pp. 394–400.

[14] B. O. Hogstad, M. Pätzold, N. Youssef, and D. Kim, "A MIMO mobile-to-mobile channel model: Part II – The simulation model," in *Proc. 16th IEEE Int. Symp. on Personal, Indoor and Mobile Radio Communications, PIMRC 2005*, vol. 1. Berlin, Germany, Sep. 2005, pp. 562–567.

[15] C. A. Gutiérrez and M. Pätzold, "The generalized method of equal areas for the design of sum-of-cisoids simulators for mobile Rayleigh fading channels with arbitrary Doppler spectra," *Wireless Communications and Mobile Computing*, 2011, published online, DOI 10.1002/wcm.1154.

[16] ——, "A generalized method for the design of ergodic sum-of-cisoids simulators for multiple uncorrelated Rayleigh fading channels," in *Proc. 4th International Conference on Signal Processing and Communication Systems, ICSPCS 2010*. Gold Coast, Australia, Dec. 2010, DOI 10.1109/ICSPCS.2010.5709688.

[17] M. Pätzold, U. Killat, F. Laue, and Y. Li, "On the statistical properties of deterministic simulation models for mobile fading channels," *IEEE Trans. Veh. Technol.*, vol. 47, no. 1, pp. 254–269, Feb. 1998.

[18] ——, "A new and optimal method for the derivation of deterministic simulation models for mobile radio channels," in *Proc. IEEE 46th Veh. Technol. Conf., VTC'96*, vol. 3. Atlanta, Georgia, USA, Apr./May 1996, pp. 1423–1427.

[19] C. A. Gutiérrez, "Channel simulation models for mobile broadband communication systems," Ph.D. dissertation, University of Agder, Norway, 2009.

[20] C. A. Gutiérrez and M. Pätzold, "The design of sum-of-cisoids Rayleigh fading channel simulators assuming non-isotropic scattering conditions," *IEEE Trans. Wireless Commun.*, vol. 9, no. 4, pp. 1308–1314, Apr. 2010.

[21] A. Fayziyev and M. Pätzold, "The design of sum-of-sinusoids channel simulators using the iterative nonlinear least square approximation method," in *Proc. 20th International Conference on Software, Telecommunications and Computer Networks - SoftCOM 2012*. Split, Croatia, Sep. 2012.

[22] M. Feder and E. Weinstein, "Parameter estimation of superimposed signals using the EM algorithm," *IEEE Trans. Acoust., Speech, and Signal Processing*, vol. 36, no. 4, pp. 477–489, Aug. 1988.

[23] A. Abdi, J. A. Barger, and M. Kaveh, "A parametric model for the distribution of the angle of arrival and the associated correlation function and power spectrum at the mobile station," *IEEE Trans. Veh. Technol.*, vol. 51, no. 3, pp. 425–434, May 2002.

[24] R. H. Clarke, "A statistical theory of mobile-radio reception," *Bell Syst. Tech. Journal*, vol. 47, pp. 957–1000, Jul./Aug. 1968.

Appendix F

Paper VI

Title:	The Performance of the INLSA in Comparison with the SAGE and ESPRIT Algorithms
Authors:	**Akmal Fayziyev** and Matthias Pätzold
Affiliation:	University of Agder, Faculty of Engineering and Science, P. O. Box 509, NO-4898 Grimstad, Norway
Conference:	*IEEE International Conference on Advanced Technologies for Communications, ATC 2014*, Ho Chi Minh City, Vietnam, Oct. 2014.

The Performance of the INLSA in Comparison with the SAGE and ESPRIT Algorithms

Akmal Fayziyev and Matthias Pätzold
Faculty of Engineering and Science, University of Agder,
P.O. Box 509, NO-4898 Grimstad, Norway
E-mails: {akmal.fayziyev, matthias.paetzold}@uia.no

***Abstract* — In this paper we investigate the application potential of three known algorithms, namely the ESPRIT, SAGE and INLSA, to properly emulate the statistical properties of the mobile fading channel. The performance comparisons of those methods will be carried out with respect to their fitting accuracy to the autocorrelation function (ACF) of the reference model. The methods' accuracy will be assessed in the synthetic reference channel model, which is based on the sum-of-cisoids (SOC) principle. In our reference model, we consider the scenarios with equal gains and Rayleigh distributed gains. The obtained results indicate that in both scenarios the INLSA method is more preferable than the ESPRIT and the SAGE algorithms when emulating the correlation properties of the mobile fading channel. An excellent performance and the simplicity of the INLSA make the method a powerful tool for designing realistic channel simulators.**

***Index Terms* — channel modelling, measurement data, sum-of-cisoids, parameter computation, autocorrelation function, time complexity analysis**

I. INTRODUCTION

A channel model that provides an accurate emulation of the real-world fading channel characteristics is essential for the understanding of radio propagation phenomena and for the successful deployment of future mobile communication systems. The modelling and analysis of mobile fading channels have therefore been a topic of research for many years. As a result, a large variety of modelling approaches have been developed [1, 2].

In general, the fading channel is described as a multipath propagation channel where the received signal is represented as a sum of multiple waves arriving from different directions with different amplitudes and phases [1, 3]. The intuitive approach for modelling these types of channels is the sum-of-cisoids (SOC) principle, which has proven to be well suited for modelling various channels under realistic scattering conditions. However, to fully exploit the advantages of the SOC approach, one must carefully determine the simulation model parameters, such as the path gains, the angles-of-arrival (AOAs), and the phases.

When considering wideband scenarios, the measurement data is often given in the form of the channel impulse response (or the transfer function). Owing to the complex nature of propagation phenomena, extensive propagation measurements can play an important role in the characterization of the mobile fading channel. The SOC model's parameters can be extracted from the measurement data for a more reliable emulation of the fading channel characteristics. However, the measurement data is often distorted by noise and therefore the robust parameter computation methods are required to accurately estimate these model parameters.

In the last few decades, various parameter computation methods have been developed for deducing the parameters of interest from the measurements [4–8]. Owing to its relative simplicity, the estimation of signal parameters via rotational invariance techniques (ESPRIT) [6] has become one of the most popular AOA estimation methods. However, the application of the ESPRIT scheme is restricted to the multiple element antenna arrays. In [9], the authors proposed the unitary ESPRIT, which is the real-valued implementation of the standard ESPRIT method presented in [6]. Compared to the standard ESPRIT algorithm, the unitary implementation of the ESPRIT provides a significant reduction in computational complexity. The extensions of the standard and unitary ESPRIT methods for the joint delay and azimuth estimation are discussed in [10] and [11], respectively. In our analysis, the application of those methods is restricted only to the estimation of the AOAs. Owing to this drawback,

maximum-likelihood-based algorithms are more preferable for the parametrization of the SOC-based channel models. These include the expectation maximization [7] and the space alternating generalized expectation maximization (SAGE) [8] algorithms. The tremendous interest in maximum-likelihood-based algorithms is mainly due to the SAGE algorithm. The SAGE algorithm is widely used for channel parameter estimation due to its excellent performance in most scenarios. However, the main drawback of the SAGE algorithm is that it requires a large amount of specular components for proper emulation of the channel characteristics. Moreover, in [12], the authors reported on the initialization sensitivity problem of the SAGE algorithm. Several approaches have been proposed in [12–15] to mitigate the drawbacks of the SAGE algorithm. In [15], the authors proposed the iterative nonlinear least square approximation (INLSA) method for the design of wideband channel simulators. In that paper, the authors also demonstrated that the INLSA algorithm provides a good match to empirical data by keeping the complexity lower than that of the SAGE algorithm. The INLSA algorithm has further been refined in [16].

In this paper, we compare the performance of the INLSA method with those of the SAGE and the standard ESPRIT approaches. We evaluate the performance of those methods with respect to their fitting accuracy to the autocorrelation function (ACF) of the reference channel model, which is the complex channel gain modelled as an SOC process. Two different scenarios will be considered for the performance comparisons. In the first scenario, the path gains are assumed to be equal, whereas the second scenario considers more severe conditions with Rayleigh distributed path gains. In order to make the reference model realistic, we assume that the reference SOC process is noise-corrupted, which is the case when dealing with measurement data. The SOC-based simulation model parameters are extracted from the noise-corrupted reference model by using one of the three methods. The performance of the methods is then evaluated with respect to their capabilities to reproduce the statistical properties of the reference model. The comparisons are also made with respect to the time consumed by the methods to determine the simulation model parameters.

The remainder of this paper is set up as follows. In Section II, we discuss the reference model and its statistical properties. Section III provides the detailed discussion of the ESPRIT and the SAGE algorithms. Section IV introduces the INLSA parameter computation method. The performance evaluations of the methods are presented in Section V. Finally, Section VI summarizes the results of this paper.

II. The Reference and Simulation Models

In this section, we will introduce the synthetic SOC-based reference and simulation models. We also present the analytical expression for the ACF of the reference model. This expression will be used for the parameter computation and comparison purposes in the following sections. We consider an SOC-based reference process $\mu(t)$ for modelling the scattered component of the received signal in a fading channel in the complex baseband. The reference model $\mu(t)$ can be expressed as follows

$$\mu(t) = \sum_{n=1}^{N} \mu_n(t) = \sum_{n=1}^{N} c_n e^{j(2\pi f_{\max}\cos(\alpha_n)t+\theta_n)} \tag{F.1}$$

where N denotes the number of complex sinusoids (cisoids) $\mu_n(t)$. The parameters c_n and θ_n are called the gains and the phases, respectively. The parameter α_n denotes the AOA of the nth path ($n = 1,2,\ldots,N$), whereas $f_{\max}$ denotes the maximum Doppler frequency. It can be easily verified that the ACF $r_{\mu\mu}(\tau)$ of $\mu(t)$ can be represented in the following form [17]

$$r_{\mu\mu}(\tau) = \sum_{n=1}^{N} c_n^2 e^{j2\pi f_{\max}\cos(\alpha_n)\tau}. \tag{F.2}$$

In real-world conditions, parameter computation methods often have to deal with imperfect data. Therefore, we consider a case where the complex channel gain is affected by noise, which has an additive behavior. We first combine the N complex cisoids $\mu_n(t)$, $n = 1,2,\ldots,N$ into an $N \times 1$ column vector, i.e., $\boldsymbol{\mu}(t) = [\mu_1(t), \mu_2(t), \ldots, \mu_N(t)]^T$. Then the noise-corrupted $M \times 1$ vector $\boldsymbol{x}(t)$ of the complex channel gains, taken at the M receiving sensors, is represented as

$$\boldsymbol{x}(t) = \boldsymbol{A}\boldsymbol{\mu}(t) + \boldsymbol{n}(t) \tag{F.3}$$

where $\boldsymbol{A}$ is an $M \times N$ complex array steering matrix, i.e., $\boldsymbol{A} \in \mathbb{C}^{M\times N}$. The additive noise vector $\boldsymbol{n}(t) \in \mathbb{C}^{M\times 1}$ is taken from a complex-valued Gaussian random process with zero mean and covariance matrix $\sigma_N^2 \boldsymbol{I}_M$, where $\boldsymbol{I}_M$ is the identity matrix of size M.

By applying one of the parameter computation methods to the noise-corrupted process $\boldsymbol{x}(t)$, we obtain the computed values of the parameters $\tilde{c}_n$, $\tilde{\alpha}_n$ and $\tilde{\theta}_n$ for $n = 1,2,\ldots,N_s$, where N_s refers to the number of cisoids in the simulation model. The simulation model $\tilde{\mu}(t)$ and its ACF $\tilde{r}_{\mu\mu}(\tau)$ can be derived by inserting those

computed parameters into (F.1) and (F.2), respectively. In the next two sections, we will discuss the parameter computation methods we used to compute the simulation model parameters.

III. The Parameter Computation Methods

In this section, we present a brief review of the two well-known approaches, namely the ESPRIT and SAGE, for determining the SOC model parameters. For the purpose of comparison, we will only consider the original versions of both ESPRIT [6] and SAGE [8] algorithms.

A. ESPRIT

Let us first consider the standard ESPRIT scenario, i.e., an M-element uniform linear array composed of two overlapping subarrays with m identical sensors (see Fig. F.1).

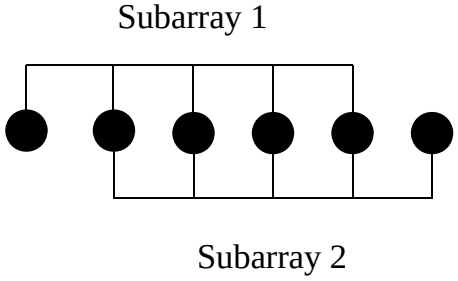

Figure F.1: Uniform linear array of $M = 6$ identical sensors and subarrays with $m = 5$ required for ESPRIT algorithm.

Let the nth spatial frequency be computed as $\nu_n = -\pi \sin\theta_n$. In this case, the complex array steering vector corresponding to ν_n can be written as

$$\boldsymbol{a}(\nu_n) = [1 \;\; e^{j\nu_n} \;\; e^{j2\nu_n} \;\; \cdots \;\; e^{j(M-1)\nu_n}]^T, \; n = 1,2,\ldots,N. \tag{F.4}$$

The $M \times N$ complex array steering matrix $\boldsymbol{A}$ can now be formed by combining N steering vectors as

$$\boldsymbol{A} = \Big[\boldsymbol{a}(\nu_1) \;\; \boldsymbol{a}(\nu_2) \;\; \cdots \;\; \boldsymbol{a}(\nu_N)\Big]. \tag{F.5}$$

In this case, the covariance matrix corresponding to the noise-corrupted process $\boldsymbol{x}(t)$ is given by

$$\boldsymbol{R}_{\boldsymbol{xx}} = E\{\boldsymbol{x}(t)\boldsymbol{x}^H(t)\} = \boldsymbol{A}\boldsymbol{R}_{\mu\mu}\boldsymbol{A}^H + \sigma_n^2\boldsymbol{I}_M. \tag{F.6}$$

The eigenvalue decomposition of the covariance matrix $\boldsymbol{R_{xx}}$ can be expressed as

$$\boldsymbol{R_{xx}} = \boldsymbol{U}\Lambda\boldsymbol{U}^H \tag{F.7}$$

where the diagonal matrix $\Lambda = \mathbf{diag}\{\lambda_m\}_{m=1}^{M}$ contains the nonzero eigenvalues in descending order, i.e., $\lambda_1 \geq \lambda_2 \geq \ldots \geq \lambda_M$. The unitary columns of the $M \times M$ matrix $\boldsymbol{U}$ are the eigenvectors $\boldsymbol{u}_i$ corresponding to λ_i, where $i = 1,2,\ldots,M$, i.e., $\boldsymbol{U} = [\boldsymbol{u}_1\ \boldsymbol{u}_2\ \cdots\ \boldsymbol{u}_M]$. By using the first N vectors $\boldsymbol{U}_S = [\boldsymbol{u}_1\ \boldsymbol{u}_2\ \cdots\ \boldsymbol{u}_N]$ in $\boldsymbol{U}$, we can now represent the so-called invariance equation as

$$\boldsymbol{J}_1\boldsymbol{U}_S\boldsymbol{\Psi} \approx \boldsymbol{J}_2\boldsymbol{U}_S \tag{F.8}$$

where the selection matrices $\boldsymbol{J}_1 = [\boldsymbol{I}_N\ \ 0]$ and $\boldsymbol{J}_2 = [0\ \ \boldsymbol{I}_N]$ are centrosymmetric with respect to each other. Here, $\boldsymbol{I}_N$ is the identity matrix of size N. The eigenvalues of the resulting solution $\boldsymbol{\Psi} \in \mathbb{C}^{N\times N}$ in (F.8) represent the estimates of $e^{j\nu_n}$, $n = 1,2,\ldots,N$. The corresponding AOAs can be estimated from the following relationship

$$\tilde{\alpha}_n = -\arcsin\left(\frac{e^{j\nu_n}}{\pi}\right),\ n = 1,2,\ldots,N. \tag{F.9}$$

By using the ESPRIT algorithm, we can only compute the AOAs. Therefore, the parameters $\tilde{c}_n$, are assumed to be known during the simulations, i.e., $\tilde{c}_n = c_n$.

B. SAGE

The SAGE algorithm does not require multiple antenna elements to resolve the parameters corresponding to different cisoids. Hence, we consider a single antenna sensor at the receiver side. In this case, we can represent the $1 \times N$ steering vector $\boldsymbol{A}$ as $\boldsymbol{A} = [1\ 1\ \ldots\ 1]$. The noise-corrupted channel gain will then have the following form

$$x(t) = \boldsymbol{A}\boldsymbol{\mu}(t) + n(t) = \sum_{n=1}^{N} c_n e^{j(2\pi f_{\max}\cos(\alpha_n)t + \theta_n)} + n(t) \tag{F.10}$$

where $n(t)$ is a complex Gaussian noise process with zero mean and variance σ_N^2. Let us now consider a set of model parameters $\mathbb{P}_n = \{\tilde{c}_n, \tilde{\alpha}_n, \tilde{\theta}_n\}$ corresponding to the nth cisoid. The SAGE algorithm starts with the initial setting $\mathbb{P}'_n = \{0,0,0\}$ for $n = 1,2,\ldots,N_s$, where N_s is the number of cisoids in the simulation model, which can be different from N. Given the process $x(t)$ and the initial set of parameters $\mathbb{P}'_n$,

the SAGE estimates each cisoid as follows

$$\tilde{\mu}_n(t) = x(t) - \sum_{l=1, l\neq n}^{N_s} \tilde{c}_l e^{j(2\pi f_{\max}\cos(\tilde{\alpha}_l)t + \tilde{\theta}_l)}. \tag{F.11}$$

The update procedure is then required to compute the new values of the parameters $\mathbb{P}_n''$ corresponding to the nth wave. The update procedure can be described as follows

$$\tilde{\alpha}_l'' = \arg\max_{\tilde{\alpha}_l} \left\{ |z(\tilde{\alpha}_l, \tilde{\theta}_l')| \right\} \tag{F.12}$$

$$\tilde{\theta}_l'' = \arg\max_{\tilde{\theta}_l} \left\{ |z(\tilde{\alpha}_l'', \tilde{\theta}_l)| \right\} \tag{F.13}$$

$$\tilde{c}_l'' = \frac{1}{T} |z(\tilde{\alpha}_l'', \tilde{\theta}_l'')| \tag{F.14}$$

where T is the maximum time for which $x(t)$ has been evaluated and

$$z(\tilde{\alpha}_l, \tilde{\theta}_l) = \int_0^T \tilde{\mu}_n(t) e^{-j(2\pi f_{\max}\cos(\tilde{\alpha}_l)t + \tilde{\theta}_l)} dt. \tag{F.15}$$

The SAGE iteration stage corresponds to finding the set of parameters $\mathbb{P}_n''$ for $n = 1, 2, \ldots, N_s$. After each iteration the process $\tilde{\mu}(t)$ is formed by inserting those parameters into (F.1). The log-likelihood function L is then evaluated as

$$L = \frac{1}{\sigma_N} \left[2 \int_0^T Re\{\tilde{\mu}^H(t) x(t)\} dt - \int_0^T ||\tilde{\mu}(t)||^2 dt \right] \tag{F.16}$$

where $Re\{\cdot\}$ and $||\cdot||$ denote the real part and the norm of the argument, respectively. The SAGE algorithm is carried out until L reaches its maximum.

IV. INLSA Method

The principal task in the INLSA method consists in finding the parameters of the simulation model to allow a proper emulation of the ACF of the reference model. Considering (F.2), we notice that the phases θ_n have no impact on the ACF $r_{\mu\mu}(\tau)$. Therefore, only the gains $\tilde{c}_n$ and AOAs $\tilde{\alpha}_n$ are computed in the INLSA method. The parameters of the simulation model $\tilde{\mu}(t)$ are determined by implementing the approximation $\tilde{r}_{\mu\mu}(\tau) \approx r_{\mu\mu}(\tau)$. However, considering the fact that $x(t)$ is the only available process, we will need to estimate the ACF $r_{\mu\mu}(\tau)$ from $x(t)$. The estimated

ACF of $\mu(t)$ will be denoted as $\hat{r}_{\mu\mu}(\tau)$. First, we have to derive the ACF $r_{xx}(\tau)$ of $x(t)$ as

$$r_{xx}(\tau) = E\{x^*(t)x(t+\tau)\} \tag{F.17}$$

where $E\{\cdot\}$ represents the statistical averaging. From $r_{xx}(\tau)$, we can now obtain the ACF $\hat{r}_{\mu\mu}(\tau)$ as

$$\hat{r}_{\mu\mu}(\tau) = \begin{cases} r_{xx}(\tau) - \sigma_N^2, & \tau = 0, \\ r_{xx}(\tau), & \text{otherwise.} \end{cases} \tag{F.18}$$

In order to achieve a good approximation of $r_{\mu\mu}(\tau)$, we compute the set of parameters $\mathbb{P} = \{\tilde{c}_n, \tilde{\alpha}_n\}$ of the simulation model in such a way that the squared Frobenius norm $E(\mathbb{P})$ becomes minimal, i.e.,

$$E(\mathbb{P}) = \left\| \hat{\boldsymbol{r}} - \tilde{\boldsymbol{r}} \right\|_2^2 = \textbf{Min}! \tag{F.19}$$

where $\hat{\boldsymbol{r}}$ is the vector $\hat{\boldsymbol{r}} = \left[\hat{r}_{\mu\mu}(\tau_0), \hat{r}_{\mu\mu}(\tau_1), \ldots, \hat{r}_{\mu\mu}(\tau_K)\right]$ that contains the values of $\hat{r}_{\mu\mu}(\tau)$ at the discrete time-lags $\tau_k = k\Delta\tau$, where $k = 0, 1, \ldots, K$ and $\Delta\tau$ denotes the sampling interval. Similarly, the vector $\tilde{\boldsymbol{r}}$ combines the values of $\tilde{r}_{\mu\mu}(\tau)$ at the time-lags τ_k, i.e., $\tilde{\boldsymbol{r}} = \left[\tilde{r}_{\mu\mu}(\tau_0), \tilde{r}_{\mu\mu}(\tau_1), \ldots, \tilde{r}_{\mu\mu}(\tau_K)\right]$. In order to solve the minimization problem presented in (F.19), the INLSA method requires the initial values of the simulation model parameters. As an example we consider $\mathbb{P}_n^0 = \{0, 0\}$ for $n = 1, 2, \ldots, N_s$. It is worth to mention that the proper selection of the initial values leads to a faster convergence and reduces the time required for computing the model parameters. The INLSA method starts with setting the iteration index q equal to zero. The simulation model parameters $\tilde{c}_n$ and $\tilde{\alpha}_n$ are then determined separately for each of the N_s cisoids by using the auxiliary error function $y_n^{(q)}(\tau_k)$ $(k = 0, 1, \ldots, K)$ as follows

$$y_n^{(q)}(\tau_k) = \hat{r}_{\mu\mu}(\tau_k) - \sum_{l=1, l\neq n}^{N_s} \left(\tilde{c}_l^{(q)}\right)^2 e^{j2\pi f_{\max} \cos(\tilde{\alpha}_l^{(q)})\tau_k} \tag{F.20}$$

$$\tilde{c}_n^{(q+1)} = \arg\min_{\tilde{c}_n} \left\| \mathbf{y}_n^{(q)} - \tilde{c}_n^2 \mathbf{s}_n^{(q)} \right\|_2^2 \tag{F.21}$$

where the symbol $\mathbf{y}_n^{(q)}$ refers to the column vector containing the stacked values of the auxiliary error function $y_n^{(q)}(\tau_k)$. The column vector $\mathbf{s}_n^{(q)}$ contains the stacked values of the exponential function $e^{j2\pi f_{\max} \cos(\alpha_n^{(q)})\tau_k}$. Fortunately, we can solve the

minimization problem in (F.21) by the simple closed-form expression

$$\tilde{c}_n^{(q+1)} = \sqrt{\frac{\mathrm{Re}\left\{\mathbf{y}_n^{(q)}\right\}^T \mathrm{Re}\left\{\mathbf{s}_n^{(q)}\right\} + \mathrm{Im}\left\{\mathbf{y}_n^{(q)}\right\}^T \mathrm{Im}\left\{\mathbf{s}_n^{(q)}\right\}}{\left(\mathbf{s}_n^{(q)}\right)^H \mathbf{s}_n^{(q)}}}. \tag{F.22}$$

The result in (F.22) is obtained by finding the zeros of the first-order derivative of the Frobenius norm in (F.21) with respect to $\tilde{c}_n$. The new estimates for the AOAs $\tilde{\alpha}_n^{(q+1)}, n = 1, 2, \ldots, N_s$, are then obtained as follows

$$\tilde{\alpha}_n^{(q+1)} = \arg\min_{\tilde{\alpha}_n} \left\| \mathbf{y}_n^{(q)} - \left(\tilde{c}_n^{(q+1)}\right)^2 \mathbf{s}_n^{(q)} \right\|_2^2. \tag{F.23}$$

The squared Frobenius norm $E(\mathbb{P})$ is re-evaluated at the end of each iteration. In case of a noticeable change in the error norm $E(\mathbb{P})$, the iteration index q is increased by one, i.e., $q+1 \rightarrow q$. The parameter computation procedure is then carried out again starting from (F.21). This process is repeated until no perceptible change can be observed in the error norm $E(\mathbb{P})$.

The important feature of the INLSA method is the relatively simple iterative optimization approach used to determine the model parameters. Unlike the ESPRIT algorithm, the application of the INLSA method is not restricted to the computation of AOAs only. Moreover, in contrast to the SAGE algorithm, the proposed method does not require the optimization of the phases $\tilde{\theta}_n$ for implementing the approximation $\tilde{r}_{\mu\mu}(\tau) \approx r_{\mu\mu}(\tau)$. The performance comparisons of the INLSA method against the ESPRIT and SAGE algorithms are discussed in the next section.

V. Numerical Results

In this section, we evaluate the performance of the methods discussed in Sections II and III. We compare those methods with respect to their capabilities to approximate the reference model's ACF $r_{\mu\mu}(\tau)$ for two different scenarios.

In the following, we have carried out the simulations by choosing $f_{\max} = 91$ Hz, $\sigma_N^2 = 1$ and $\tau_{\max} = N/(4f_{\max})$. In Figs. F.2 and F.3, we have plotted the curves of the absolute values of $\tilde{r}_{\mu\mu}(\tau)$ and $r_{\mu\mu}(\tau)$ by applying the different parameter computation methods using $N = 14$. For comparative purposes, the curves have been plotted for two different scenarios, referred to as Scenario I and Scenario II. In both scenarios, we assumed that the gains $\tilde{c}_n$ are known, i.e., $\tilde{c}_n = c_n$, and applied the parameter computation methods to obtain only the AOAs $\tilde{\alpha}_n$. Although, in case of the

SAGE algorithm the computation of the phases $\tilde{\theta}_n$ is also required. In Fig. F.2, we considered Scenario I where $c_n = 1/\sqrt{N}$ $(n = 1, 2, \ldots, N)$. It can be seen in Fig. F.2 that the graphs of $|r_{\mu\mu}(\tau)|$ match perfectly the ones of $|\tilde{r}_{\mu\mu}(\tau)|$ obtained by applying the INLSA method. From Fig. F.2, it is also evident that the INLSA and SAGE methods perform significantly better than the ESPRIT method. The same is true for Scenario II where the gains c_n are assumed to have a Rayleigh distribution. In this scenario, the $\tilde{r}_{\mu\mu}(\tau) \approx r_{\mu\mu}(\tau)$ approximation accuracy of the ESPRIT method is even worse than it was in Scenario I. The comparison of the results in Figs. F.2 and F.3 demonstrates that the Rayleigh distributed gains cause more severe problems for the parameter computation methods than the identical gains. For the sake of clarity, we have illustrated the curves of the mean-square error

$$E_{r_{\mu\mu}} = \frac{1}{\tau_{\max}} \int_0^{\tau_{\max}} (r_{\mu\mu}(\tau) - \tilde{r}_{\mu\mu}(\tau))^2 d\tau \tag{F.24}$$

for the Scenario II in Fig. F.4. In that figure, the mean-square error $E_{r_{\mu\mu}}$ is presented as a function of N_s. The obtained results confirm that the INLSA method is significantly better suited than the SAGE and the ESPRIT methods to approximate the ACF $r_{\mu\mu}(\tau)$. The results also show that the INLSA method produces the smallest mean-square error among the compared methods.

In Fig. F.5, we have illustrated the parameter computation time in seconds that was consumed by the various methods to obtain the results presented in Fig. F.4. It is obvious that among the three methods compared, the ESPRIT approach requires the shortest time for computing the channel model parameters. The reason is that the ESPRIT approach computes the AOAs $\tilde{\alpha}_n$ numerically. However, as we have noticed from Fig. F.4, it also demonstrates the worst mean-square error $E_{r_{\mu\mu}}$ among the three investigated methods. The results in Figs. F.4 and F.5 clearly indicate that in addition to achieving a better approximation of the ACF $r_{\mu\mu}(\tau)$ than the SAGE approach, the proposed method also provides significant savings in parameter computation time T_c. It is important to mention that, computing the gains $\tilde{c}_n$ jointly with the AOAs $\tilde{\alpha}_n$ will not have significant impact on the gap between the curves corresponding to the SAGE and INLSA methods observed in Fig F.5. The reason for this fact is the numerical computation of the gains $\tilde{c}_n$, which provides in both methods a negligible contribution to the overall parameter computation time.

As it was mentioned in Section III, the ESPRIT method is designed to estimate only the AOAs. Hence, it cannot be involved into further investigations, where the

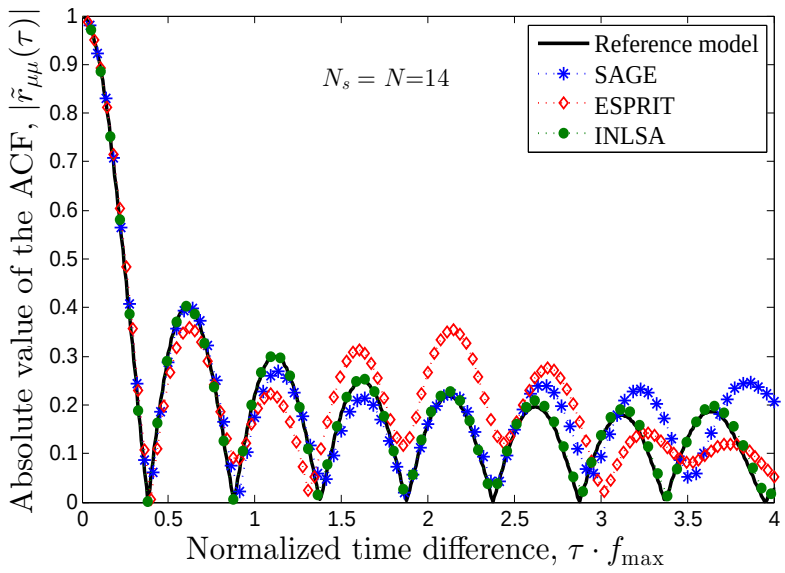

Figure F.2: The ACFs $r_{\mu\mu}(\tau)$ (reference model) and $\tilde{r}_{\mu\mu}(\tau)$ (simulation model) for Scenario I.

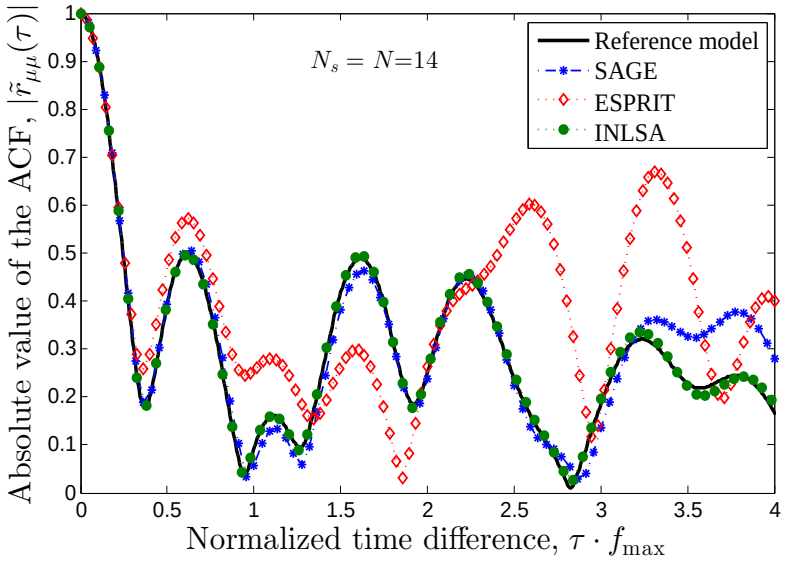

Figure F.3: The ACFs $r_{\mu\mu}(\tau)$ (reference model) and $\tilde{r}_{\mu\mu}(\tau)$ (simulation model) for Scenario II.

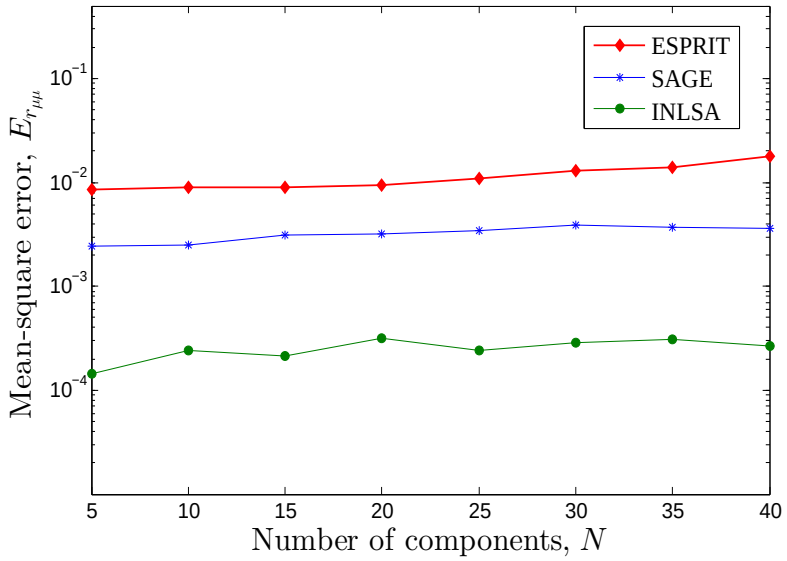

Figure F.4: Mean-square error $E_{r_{\mu\mu}}$ of $\tilde{r}_{\mu\mu}(\tau)$ for Scenario II.

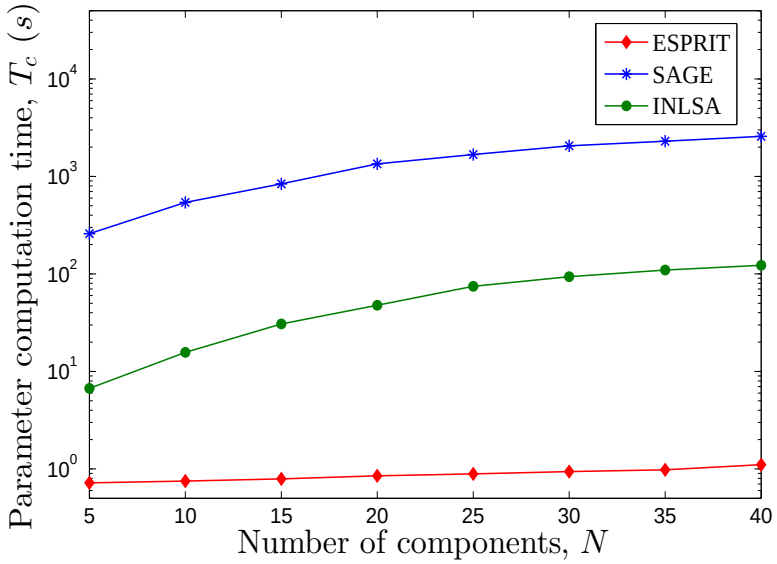

Figure F.5: Parameter computation time T_c for Scenario II.

parameter computation methods have been applied to obtain the gains $\tilde{c}_n$ as well as the AOAs $\tilde{\alpha}_n$. In the following, we focus on the reference model $\mu(t)$ with Rayleigh distributed gains c_n. The ACFs $|r_{\mu\mu}(\tau)|$ and $|\tilde{r}_{\mu\mu}(\tau)|$ are plotted in Figs. F.6 and F.7 for $N_s = N$ and $N_s < N$, respectively. From those figures we notice that the approximation $\tilde{r}_{\mu\mu}(\tau) \approx r_{\mu\mu}(\tau)$ is very good in both cases if the INLSA method is used. A significant degradation of the ACF $\tilde{r}_{\mu\mu}(\tau)$ can be observed in Fig. F.7 if the SAGE method is used. In order to better assess the methods' performance, we present in Fig. F.8 the graphs of the mean-square error $E_{r_{\mu\mu}}$ as a function of N_s. Again, Fig. F.8 shows that the mean-square error produced by the SAGE method is significantly worse than that of the INLSA method. Hence, the INLSA algorithm is without doubt the best choice for implementing the approximation $\tilde{r}_{\mu\mu}(\tau) \approx r_{\mu\mu}(\tau)$.

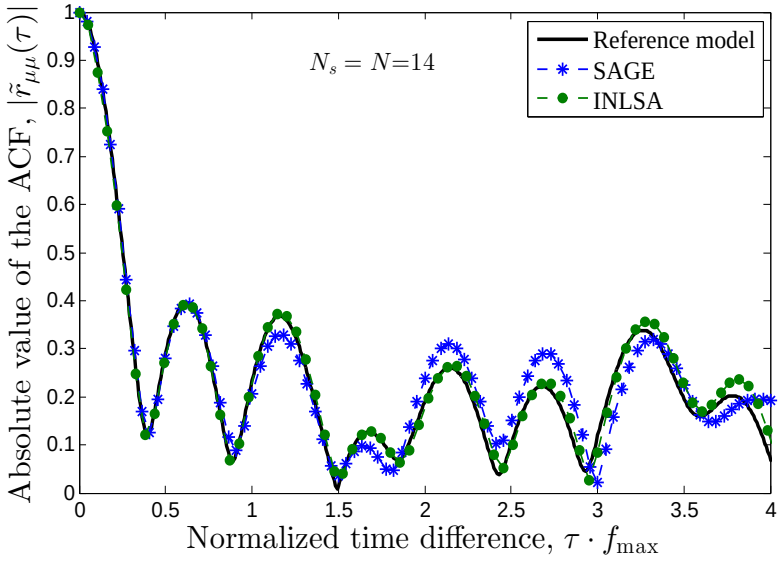

Figure F.6: The ACFs $r_{\mu\mu}(\tau)$ (reference model) and $\tilde{r}_{\mu\mu}(\tau)$ (simulation model) for Rayleigh distributed and optimized c_n, $N_s = N$.

VI. Summary and Conclusions

In this paper, we compared the performance of the INLSA, SAGE, and ESPRIT algorithms. The performance comparisons of those methods were performed with respect to their fitting accuracy to the ACF of a synthetic (reference) model as well as to the parameter computation time. The SOC reference model was generated by considering two scenarios, one with equal gains and another one with Rayleigh distributed gains. The obtained simulation results demonstrate that in both scenarios, the INLSA method is more precise than the ESPRIT and the SAGE algorithms regarding

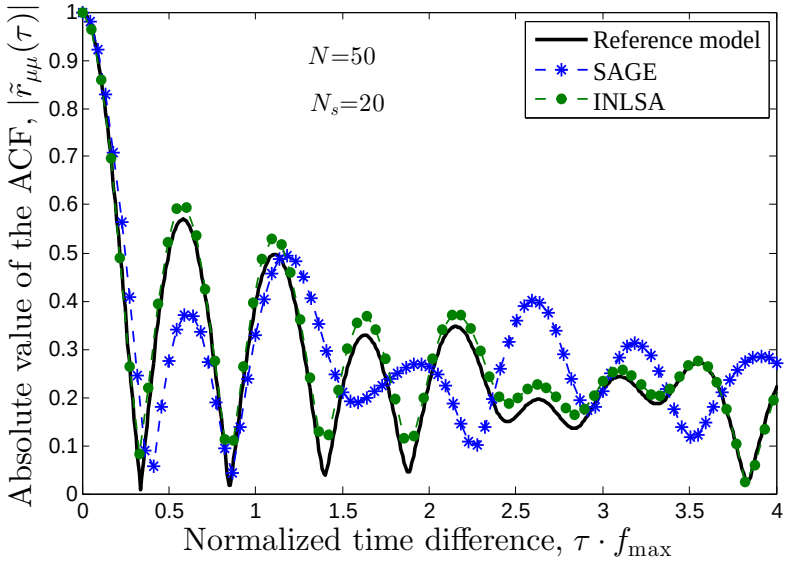

Figure F.7: The ACFs $r_{\mu\mu}(\tau)$ (reference model) and $\tilde{r}_{\mu\mu}(\tau)$ (simulation model) for Rayleigh distributed and optimized c_n, $N_s < N$.

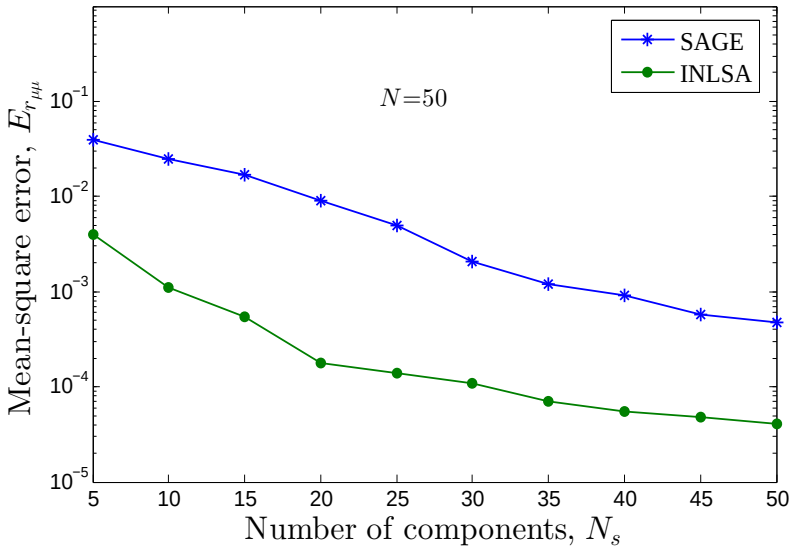

Figure F.8: Mean-square error $E_{r_{\mu\mu}}$ of $\tilde{r}_{\mu\mu}(\tau)$ for Rayleigh distributed and optimized c_n.

the approximation of the reference models ACF. Additionally, a computational complexity comparison in terms of the parameter computation time demonstrated that the INLSA approach is even more efficient than the SAGE method. In conclusion, we can say that the INLSA method is the best choice (among the analyzed methods) for the parameter estimation and modelling of measurement-based fading channel simulators, where the proper emulation of the ACF is of crucial importance.

REFERENCES

[1] M. Pätzold, *Mobile Radio Channels*, 2nd ed. Chichester: John Wiley & Sons, 2011, 583 pages.

[2] P. Almers, E. Bonek, A. Burr, N. Czink, M. Debbah, V. Degli-Esposti, H. Hofstetter, P. Kyösti, D. Laurenson, G. Matz, A. F. Molisch, C. Oestges, and H. Özcelik, "Survey of channel and radio propagation models for wireless MIMO systems," *EURASIP Journal on Wireless Communications and Networking*, vol. 2007, pp. Article ID: 19070, 19 pages, 2007.

[3] R. S. Thomä, D. Hampicke, M. Landmann, A. Richter, and G. Sommerkorn, "Measurement-based parametric channel modelling (MBPCM)," in *Int. Conf. on Electromagnetics in Advanced Applications, (ICEAA 2003)*, Torino, Italia, Sept. 2003.

[4] H. Krim and M. Viberg, "Two decades of array signal processing," *IEEE Signal Processing Magazine*, vol. 13, no. 4, pp. 67–94, Jul. 1996.

[5] R. Schmidt, "Multiple emitter location and signal parameter estimation," *IEEE Trans. Antennas Propag.*, vol. 34, no. 3, pp. 276–280, Mar. 1986.

[6] R. Roy and T. Kailath, "ESPRIT-estimation of signal parameters via rotational invariance techniques," *IEEE Trans. Acoust., Speech, Signal Processing*, vol. 37, no. 7, pp. 984–995, Jul. 1989.

[7] M. Feder and E. Weinstein, "Parameter estimation of superimposed signals using the EM algorithm," *IEEE Trans. Acoust., Speech, and Signal Processing*, vol. 36, no. 4, pp. 477–489, Aug. 1988.

[8] B. H. Fleury, M. Tschudin, R. Heddergott, D. Dahlhaus, and K. I. Pedersen, "Channel parameter estimation in mobile radio environments using the SAGE

algorithm," *IEEE J. Select. Areas Commun.*, vol. 17, no. 3, pp. 434–450, Mar. 1999.

[9] M. Haardt and J. A. Nossek, "Unitary ESPRIT: how to obtain increased estimation accuracy with a reduced computational burden," *IEEE Trans. Signal Process.*, vol. 43, no. 5, pp. 1232–1242, May 1995.

[10] A. van der Veen, M. Vanderveen, and A. Paulraj, "Joint angle and delay estimation using shift-invariance properties," *IEEE Signal Processing Lett.*, vol. 4, pp. 142–145, May 1997.

[11] M. Zoltowski, M. Haardt, and C. Mathews, "Closed-form 2-D angle estimation with rectangular arrays in element space or beamspace via unitary ESPRIT," *IEEE Trans. Signal Processing*, vol. 44, pp. 316–328, Feb. 1996.

[12] W. Li and Q. Ni, "Joint channel parameter estimation using evolutionary algorithm," in *Proc. 2010 IEEE International Conference on Communications, ICC 2010, Cape Town, South Africa*, May. 2010, pp. 1–6.

[13] W. Li, W. Yao, and P. J. Duffett-Smith, "Improving the SAGE algorithm with adaptive partial interference cancellation," in *Proc. IEEE 13th Digital Signal Processing Workshop and 5th IEEE Signal Processing Education Workshop DSP/SPE 2009*, 2009, pp. 404–409.

[14] C. B. Ribeiro, E. Ollila, and V. Koivunen, "Stochastic maximum likelihood method for propagation parameter estimation," in *Proc. 15th IEEE Int. Symp. Personal, Indoor and Mobile Radio Commun., PIMRC 2004*, vol. 3, Sept. 2004, pp. 1839–1843.

[15] D. Umansky and M. Pätzold, "Design of measurement-based wideband mobile radio channel simulators," in *Proc. 4th IEEE International Symposium on Wireless Communication Systems, ISWCS 2007, Trondheim, Norway*, Oct. 2007, pp. 229–235.

[16] A. Fayziyev and M. Pätzold, "An improved iterative nonlinear least square approximation method for the design of measurement-based wideband mobile radio channel simulators," in *Proc. IEEE Advanced Technologies for Communications, ATC 2011*, Danang, Vietnam, Apr. 2011, pp. 106–111.

[17] M. Pätzold and B. Talha, "On the statistical properties of sum-of-cisoids-based mobile radio channel simulators," in *Proc. 10th International Symposium on Wireless Personal Multimedia Communications, WPMC 2007*. Jaipur, India, Dec. 2007, pp. 394–400.

Appendix G

Paper VII

Title:	An Improved Iterative Nonlinear Least Square Approximation Method of the Design of Measurement-Based Wideband Mobile Radio Channel Simulators
Authors:	**Akmal Fayziyev** and Matthias Pätzold
Affiliation:	University of Agder, Faculty of Engineering and Science, P. O. Box 509, NO-4898 Grimstad, Norway
Conference:	*IEEE International Conference on Advanced Technologies for Communications, ATC 2011*, Da Nang, Vietnam, Oct. 2011.

An Improved Iterative Nonlinear Least Square Approximation Method for the Design of Measurement-Based Wideband Mobile Radio Channel Simulators

Akmal Fayziyev and Matthias Pätzold
Faculty of Engineering and Science, University of Agder,
P.O. Box 509, NO-4898 Grimstad, Norway
E-mails: {akmal.fayziyev, matthias.paetzold}@uia.no

Abstract — **This paper deals with the design of measurement-based simulation models for wideband single-input single-output (SISO) mobile radio channels. We present an improved version of the iterative nonlinear least square approximation (INLSA) method for computing the parameters of measurement-based simulation models. The proposed method aims to fit the temporal-frequency correlation function (TFCF) of the simulation model to that of the measured channel. Unlike the original INLSA method, the proposed approach provides a unique optimal set of estimated model parameters. The proposed iterative procedure involves numerical optimization techniques to determine a set of parameters that minimizes the Euclidian norm of the fitting error. Our investigations show that the proposed method performs well in terms of the goodness of fit to the measured data. The new method is relatively simple and can be used for the design of measurement-based wideband channel simulators, which are important for the performance analysis of mobile communication systems under real-world propagation conditions.**

Index Terms — **Wideband channel modelling, single-input single-output, parameter computation, measurement data, temporal-frequency correlation function, wide-sense stationarity, uncorrelated scattering**

I. INTRODUCTION

With the increasing complexity of wireless communication systems, channel simulation models are becoming indispensable for assessing the system performance. In recent years, considerable efforts have been devoted to the development of channel simulation models precisely characterizing realistic propagation conditions. The result is a variety of relatively simple and accurate channel models [1].

When dealing with wideband channel models, the wide-sense stationary uncorrelated scattering (WSSUS) assumption is often made [2, 3]. The WSSUS assumption allows the characterization of the channel in terms of a mixture of correlation and spectral functions. The common way of developing wideband channel models is to represent the time-variant transfer function (or equivalently the time-variant impulse response) by a finite sum of multipath propagation components [4, 5]. For this kind of modeling approach, the most important question is how to determine the model parameters, which are the path gains, Doppler frequencies, and propagation delays. Involving real-world measurement into the parameter computation process, guarantees the validity of the developed channel model for specific propagation environments. Hence, advanced parameter computation methods are required to precisely obtain the model parameters from the measurements. A number of existing parameter computation methods can be found in [6–10] and the references therein. The space-alternating generalized expectation-maximization (SAGE) algorithm [10], e.g., is widely used for the channel parameter estimation due to its superior performance in most scenarios. However, this algorithm often requires a large number of specular components for the accurate estimation of the channel. Moreover, the SAGE algorithm is very sensitive to the parameter initialization [11]. Various approaches have been proposed in [11–14] to overcome the drawbacks of this algorithm.

The main objective of this paper is to present an accurate and robust iterative approach to determine the parameters of a wideband channel simulation model. Therefore, we improve the INLSA method presented in [15]. In the original INLSA method, there are two variants of optimizing the simulation model parameters. The first variant aims to optimize the path gains together with the Doppler frequencies by modelling the measured temporal autocorrelation function (TACF), and then to obtain the propagation delays from the frequency correlation function (FCF) of the measured channel. This variant of the original INLSA will be referred to as the INLSA-T-F. In the second variant, the path gains are optimized jointly with the propagation delays by using the FCF, whereas the Doppler frequencies are obtained from

the TACF of the measured channel. The second variant of the INLSA method will be called in sequel the INLSA-F-T. The major drawback of the INLSA algorithm is the separate optimization of the simulation model parameters, which may result in erroneous parameter estimations when evaluating the resulting channel simulator with respect to the TFCF. Moreover, the INLSA-T-F and INLSA-F-T approaches result in different sets of estimated parameters for identical measured data. Instead of the TACF and FCF, the proposed method estimates the simulation model parameters by fitting the TFCF of the simulation model to that of the measured channel. The proposed method is called INLSA-TF emphasizing the joint fitting of both the temporal and frequency correlation functions of real-world channels. With the proposed approach, we overcome the major drawback of the original INLSA method associated with the separate optimization of the model parameters and guarantee a very good fitting of the TACF and the FCF at the same time. Unlike the original INLSA method, the proposed INLSA-TF approach always provides a unique set of estimated model parameters. The proposed method involves numerical optimization techniques to determine the simulation model parameters by minimizing the Euclidian norm of the fitting error. To investigate the performance of the INLSA-TF method, computer simulations have been carried out. The results acquired by the proposed approach are compared to those obtained by the two versions of the original INLSA method. The comparisons are made in terms of fitting the TFCF, TACF, FCF, and the scattering function of a measured channel.

The remainder of this paper is organized as follows. In Section II, we introduce the wideband channel simulation model. The design of measurement-based wideband channel simulators is discussed in Section III. Section IV deals with the description of the proposed parameter computation method. Numerical examples and results are presented in Section V. Finally, Section VI concludes this work.

II. The Wideband Channel Simulation Model

In this section, we describe an analytical model for the simulation of real-world wideband mobile radio channels. We introduce conditions guaranteeing that the channel simulator is autocorrelation ergodic and derive the TFCF of the channel simulation model.

The fundamental assumption about multipath propagation is that the transmitted signal travels along a finite number of paths before it reaches the receiver antenna. This assumption allows the representation of the time-variant frequency response (TVFR) of multipath fading channels by a finite sum of N propagation paths as

$$H(f',t) = \sum_{n=1}^{N} c_n e^{j(2\pi f_n t - 2\pi f' \tau'_n + \theta_n)} \tag{G.1}$$

where t and f' are the time and frequency variables, respectively. The propagation paths are characterized by their path gains c_n, propagation delays τ'_n, Doppler frequencies f_n, and the phase shifts θ_n. The elements of the set $\{\theta_n\}$ are independent and identically distributed (i.i.d.) random variables, each having a uniform distribution in the interval $[0, 2\pi)$. The objective of measurement-based channel modelling is to determine the parameter N as well as the sets of parameters $\{c_n\}$, $\{f_n\}$, and $\{\tau'_n\}$ of the channel simulation model, described by (G.1), from a given measured TVFR. The channel simulation model is expected to be autocorrelation ergodic with respect to time t and frequency f'. The ergodicity of the channel simulation model is ensured by imposing on the parameter computation method the following conditions

$$f_n \neq f_m, \tau_n \neq \tau_m, \quad \forall\, n \neq m \tag{G.2}$$

$$E\{e^{j(\theta_n - \theta_m)}\} = 0, \quad \forall\, n \neq m \tag{G.3}$$

where the operator $E\{\cdot\}$ represents the expected value operator. The ergodicity properties of the channel simulation model allow obtaining the TFCF $R(\nu', \tau)$ from a single realization of the TVFR $H(f',t)$ by time and frequency averaging as follows

$$\begin{aligned} R(\nu', \tau) &= \langle H(f',t) H^*(f' + \nu', t + \tau) \rangle \\ &= \sum_{n=1}^{N} c_n^2 e^{j2\pi(\tau'_n \nu' - f_n \tau)} \end{aligned} \tag{G.4}$$

where the notation $\langle \cdot \rangle$ denotes averaging over time and frequency.

From (G.4), we can deduce that $R(\nu', \tau)$ depends on the number of paths N, path gains c_n, propagation delays τ'_n, and Doppler frequencies f_n, but not on the phase shifts θ_n. The TACF $r_t(\tau)$ is obtained from the TFCF $R(\nu', \tau)$ at $\nu' = 0$, i.e.,

$$r_t(\tau) = R(0, \tau) = \sum_{n=1}^{N} c_n^2 e^{-j2\pi f_n \tau}. \tag{G.5}$$

The FCF $r_{f'}(\nu')$ of the simulation model can be determined from the TFCF $R(\nu', \tau)$ by setting $\tau = 0$ as

$$r_{f'}(\nu') = R(\nu', 0) = \sum_{n=1}^{N} c_n^2 e^{j2\pi \tau'_n \nu'}. \tag{G.6}$$

III. Design of Measurement-Based Wideband Channel Simulators

In this section, we formulate the problem of determining the simulation model parameters and discuss the correlation properties of the measured channel.

In practice, the TVFR of the measured channel is usually computed from a single snapshot measurement scenario (realization) at discrete time instances and frequencies. In the following, we consider the TVFR $\check{H}(f',t)$ of a real-world channel measured at discrete frequencies $f'_m = -B/2 + m\Delta f' \in [-B/2, B/2], m = 0, ..., M-1$, and at discrete time instances $t_k = k\Delta t \in [0, T], k = 0, ..., K-1$, where B and T denote the measured frequency bandwidth and the observation time interval, respectively. The time sampling interval Δt and the frequency sampling interval $\Delta f'$ are characteristic quantities of the channel sounder used to collect the measurement data. Consequently, the TVFR $\check{H}(f',t)$ can be presented in the form of a discrete function $\check{H}[f'_m, t_k]$. The discrete TFCF $\check{R}[\nu'_p, \tau_q]$ of the measured channel can be obtained from $\check{H}[f'_m, t_k]$ by averaging over time and frequency as

$$\check{R}[\nu'_p, \tau_q] = \frac{1}{KM} \sum_{k=0}^{K-1} \sum_{m=0}^{M-1} \check{H}[f'_m, t_k] \check{H}^*[f'_m + \nu'_p, t_k + \tau_q] \tag{G.7}$$

where $\tau_q = -(K-1)\Delta t, ..., 0, ..., (K-1)\Delta t$ and $\nu'_p = -(M-1)\Delta f', ..., 0, ..., (M-1)\Delta f'$. The TACF $\check{r}_t[\tau_q]$ and the FCF $\check{r}_{f'}[\nu'_p]$ of the measured channel are obtained from (G.7) by setting $\nu'_p = 0$ and $\tau_q = 0$, respectively.

Accordingly, we can represent the TVFR $H(f',t)$ of the simulation model described by (G.1) at discrete values of t and f' by a discrete TVFR denoted by $H[f'_m, t_k]$. In this case, the discrete TFCF $R[\nu'_p, \tau_q]$ of the simulation model can be derived from (G.4) by replacing ν' and τ by ν'_p and τ_q, respectively. In a similar way, we obtain the discrete TACF $r_t[\tau_q]$ and the discrete FCF $r_{f'}[\nu'_p]$ of the simulation model from (G.5) and (G.6), respectively.

Referring to Equation (G.1), the problem at hand is to determine the set of parameters $\mathbb{P} = \{N, c_n, f_n, \tau'_n\}$ in such a way that the statistical properties of the simulation model match those of the measured channel. Here, the desired statistical properties are described by the TFCF $\check{R}[\nu'_p, \tau_q]$ of the measured channel. The problem of determining the set of parameters $\mathbb{P}$ can now be formulated as follows:

Given is the measured discrete TVFR $\check{H}[f'_m, t_k]$ of a real-world channel. Determine the set of parameters $\mathbb{P}$ of the channel simulation model described by (1), such that the TFCF $R[\nu'_p, \tau_q]$ of the simulation model is as close as possible to the TFCF

$\check{R}[\nu'_p, \tau_q]$ *of the measured channel, i.e.,*

$$\mathbb{P} = \arg\min_{\mathbb{P}} \left\| \check{R}[\nu'_p, \tau_q] - R[\nu'_p, \tau_q] \right\|_2 \tag{G.8}$$

where $\|\cdot\|_2$ *denotes the Euclidian norm.*

As it is pointed out in [15], the problem formulation in (G.8) is valid if the measured channel is autocorrelation ergodic.

IV. The INLSA-TF Algorithm

In this section, we describe the INLSA-TF algorithm proposed for estimating the parameters of the simulation model. Assuming that the discrete TFCF $\check{R}[\nu'_p, \tau_q]$ of the measured channel has been derived according to (G.7) and noticing the problem formulation discussed in Section III, we introduce the object function for determining the simulation model parameters as

$$E(\mathbb{P}) = \|\check{R}[\nu'_p, \tau_q] - \sum_{n=1}^{N} c_n^2 e^{j2\pi(\tau'_n \nu'_p - f_n \tau_q)}\|_2^2. \tag{G.9}$$

With respect to the Euclidian norm described in (G.9), the TFCF $R[\nu'_p, \tau_q]$ of the simulation will be fitted as close as possible to the given TFCF $\check{R}[\nu'_p, \tau_q]$ of the measured channel.

Starting with $N = 1$ and arbitrarily chosen initial values of $f_1^{(0)}$ and $\tau_1'^{(0)}$, we obtain an error function $y_l^{(i)}[\nu'_p, \tau_q]$ for the lth propagation path at every iteration i $(i = 0, 1, 2, ...)$ as

$$y_l^{(i)}[\nu'_p, \tau_q] = \check{R}[\nu'_p, \tau_q] - \sum_{n=1, n\neq l}^{N} \left(c_n^{(i)}\right)^2 e^{j2\pi\left(\tau_n'^{(i)} \nu'_p - f_n^{(i)} \tau_q\right)}. \tag{G.10}$$

The new estimates of the path gains $c_l^{(i+1)}$ and Doppler frequencies $f_l^{(i+1)}$ corresponding to the lth path are obtained from $y_l^{(i)}[\nu'_p, \tau_q]$ as follows

$$\left(c_l^{(i+1)}, f_l^{(i+1)}\right) = \arg\min_{c_l, f_l} \left\| \mathbf{y}_l^{(i)} - c_l^2 e^{j2\pi\left(\tau_l'^{(i)} \nu'_p - f_l \tau_q\right)} \right\|_2^2 \tag{G.11}$$

where $\mathbf{y}_l^{(i)}$ is a column vector containing the stacked values of $y_l^{(i)}[\nu'_p, \tau_q]$ for increasing values of p first and then for q.

For a fixed value of $f_l^{(i)}$, it is straightforward to show that (G.11) is minimized when

$$c_l^{(i+1)} = \sqrt{\frac{\mathrm{Re}\left\{\mathbf{y}_l^{(i)}\right\}^T \mathrm{Re}\left\{\mathbf{s}_l^{(i)}\right\} + \mathrm{Im}\left\{\mathbf{y}_l^{(i)}\right\}^T \mathrm{Im}\left\{\mathbf{s}_l^{(i)}\right\}}{\left(\mathbf{s}_l^{(i)}\right)^H \mathbf{s}_l^{(i)}}} \tag{G.12}$$

where the operators $\{\cdot\}^T$ and $\{\cdot\}^H$ denote the transpose and complex-conjugate transpose, respectively. The symbol $\mathbf{s}_l^{(i)}$ refers to a column vector containing the stacked values of the exponential function $e^{j2\pi\left(\tau_l'^{(i)}\nu_p' - f_l^{(i)}\tau_q\right)}$ for increasing values of p first and then for q. The operator $\mathrm{Re}\{\cdot\}$ designates the real part and $\mathrm{Im}\{\cdot\}$ denotes the imaginary part.

Substituting (G.12) into (G.11) reduces the two-dimensional optimization problem into a one-dimensional one as

$$f_l^{(i+1)} = \arg\min_{f_l} \left\| \mathbf{y}_l^{(i)} - \left(c_l^{(i+1)}\right)^2 e^{j2\pi\left(\tau_l'^{(i)}\nu_p' - f_l\tau_q\right)} \right\|_2^2. \tag{G.13}$$

The propagation delay $\tau_l'^{(i+1)}$ is estimated by using $c_l^{(i+1)}$ and $f_l^{(i+1)}$ as

$$\tau_l'^{(i+1)} = \arg\min_{\tau_l} \left\| \mathbf{y}_l^{(i)} - \left(c_l^{(i+1)}\right)^2 e^{j2\pi\left(\tau_l'\nu_p' - f_l^{(i+1)}\tau_q\right)} \right\|_2^2. \tag{G.14}$$

The iterative estimation procedure described in (G.10), (G.12), (G.13) and (G.14) proceeds as long as the relative change in the object function $E(\mathbb{P})$ is higher than the predefined threshold level ε. When the relative change in $E(\mathbb{P})$ becomes smaller than ε, then the number of propagation paths N is increased by one, i.e., $N+1 \rightarrow N$. By setting the initial values of $f_N^{(0)}$ and $\tau_N'^{(0)}$ equal to zero and using the error function $y_N^{(0)}$, defined as

$$y_N^{(0)}[\nu_p', \tau_q] = \check{R}[\nu_p', \tau_q] - \sum_{n=1}^{N-1} c_n^2 e^{j2\pi(\tau_n'\nu_p' - f_n\tau_q)}, \tag{G.15}$$

we obtain the parameters c_N, f_N, and τ_N' by following the steps given in (G.12), (G.13) and (G.14). After this, the iterative estimation procedure is carried out again. This process is repeated until no further progress can be made by increasing N or the maximum number of paths $N_{\max}$ is reached. It should be pointed out here that setting $\nu_p' = 0$ and $\tau_q = 0$ reduces the proposed INLSA-TF algorithm to the INLSA-T-F [15] and the INLSA-F-T [15], respectively. In case $\tau_q = 0$, the propagation delays $\{\tau_n'\}$ need to be computed before the Doppler frequencies $\{f_n\}$.

The main advantage of the proposed INLSA-TF algorithm over the INLSA-T-F and the INLSA-F-T methods is that the path gains are optimized in combination with the corresponding Doppler frequencies and propagation delays, which result in a unique triple (c_n, f_n, τ'_n). This is in contrast to the INLSA-T-F and INLSA-F-T methods for which we obtain only the unique tuples (c_n, f_n) and (c_n, τ'_n), respectively. The results of a comparative study of these three approaches are demonstrated in the next section.

V. Application to Measurement Data

In this section, we present the results demonstrating the performance of the proposed INLSA-TF algorithm. For the performance analysis, we used the measurement data of a measurement campaign by Elektrobit conducted in an urban environment in the 5.25 GHz frequency band. In this measurement campaign, the transmit antenna was positioned at street level on a trolley, and the receiving antenna was fixed at 19 m height on the rooftop. The measurement has been conducted by using the channel sounder Propsound CS, which is described in detail in [16]. The key parameters of the measurement equipment include:

- Time interval between the snapshots: $\Delta t = 6.3$ ms
- Sampling frequency: $\Delta f' = 97.847$ kHz
- Bandwidth: $B = 100$ MHz

For the purpose of comparison, we demonstrate the channel estimation capabilities of the new and the two original versions of the INLSA method for the same measured data. The parameter ε of the proposed algorithm is empirically set to $\varepsilon = 0.01$ in all simulations. In Fig. G.1, the normalized residual error norm $\|\check{R} - R\|_F / \|\check{R}\|_F$ versus the number of paths N is depicted. Here, $\|\cdot\|_F$ designates the Frobenius norm. As it is readily apparent from the results shown in this figure, the proposed INLSA-TF method performs significantly better than the two original INLSA approaches. The different performance of the INLSA-T-F and INLSA-F-T implies that the estimated set of model parameters is not identical when these methods are used. As an aside, we want to mention that the INLSA-TF algorithm and also the two original versions of the INLSA method are initialization insensitive. This means that independent of the chosen initial values for the Doppler frequencies and path delays, we always get the same graph for the normalized residual error. We also note from the

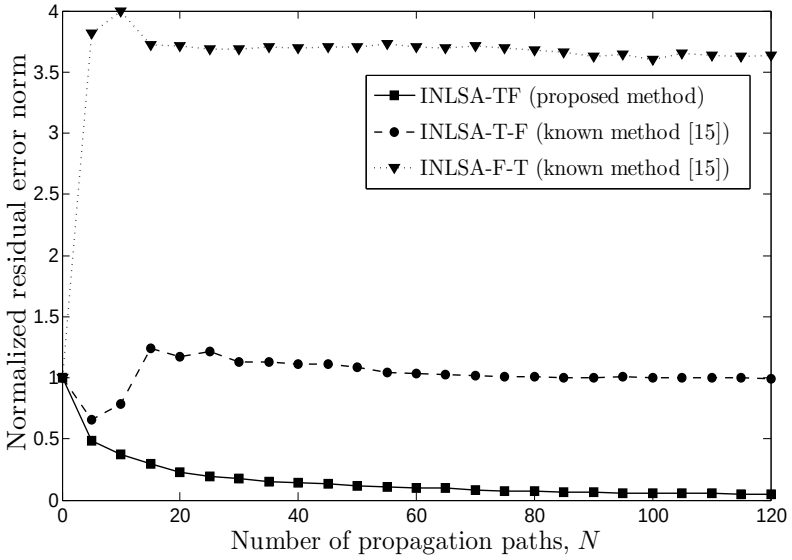

Figure G.1: Normalized residual error norm versus the number of propagation paths N.

inspection of Fig. G.1 that if $N = 60$, the normalized residual error norm is approximately 10%, whereas the error drops below 5% if $N = 120$ when the INLSA-TF method is used. By referring to these results, the number of paths $N_{\max} = 120$ is considered to be sufficient and adopted for further simulations as a stopping criterion in the iterative optimization procedure.

The proposed method has been developed for estimating the model parameters of a simulation model that matches the TFCF of real-world channels, whereas the original INLSA method focuses only on the behavior of the TFCF along the principal axes, i.e., namely the TACF and the FCF. For comparison purposes, we have plotted the figures for the TFCFs of the measured channel and the simulation model by using the INLSA-TF and the INLSA-T-F in Figs. G.2, G.3, and G.4. With reference to Figs. G.2–G.4, we can say that the INLSA-TF method performs significantly better than the original INLSA-T-F in terms of fitting the TFCF of the measured channel. As it has been mentioned above, the separate parameter optimization implemented in the original INLSA algorithm may result in incorrect estimations of the simulation model's parameters. In order to highlight this problem, we have illustrated the performance of two versions of the original INLSA method in Figs. G.5 and G.6. As can be seen from those figures, in case the INLSA-F-T approach is used, the difference between the TACF curves of the simulation model and the measured channel is significant, whereas the FCF of the simulation model closely matches the FCF of

the measured channel. The discrepancy between the FCF curves of the simulation model and the measured channel is relatively small when the INLSA-T-F method is applied. We also note from the inspection of Figs. G.5 and G.6 that the TACF and the FCF of the simulation model are well fitted to the corresponding functions of the measured channel, if the simulation model parameters are estimated by using the proposed INLSA-TF method.

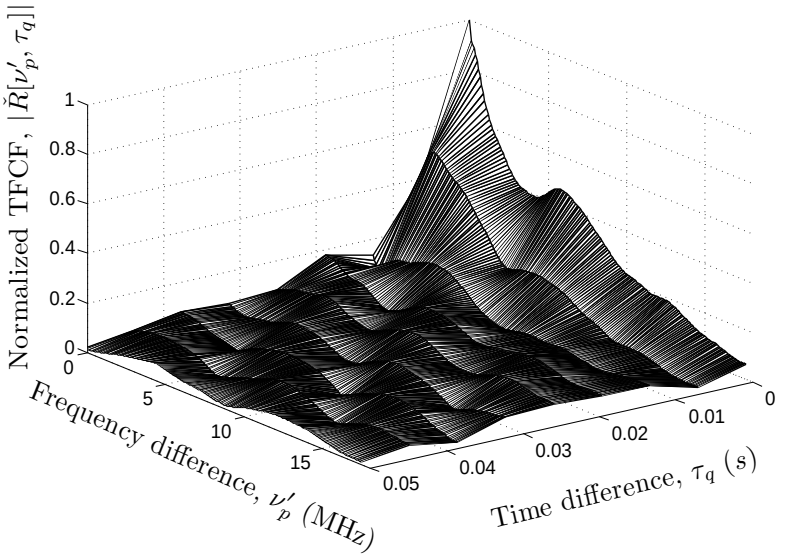

Figure G.2: Absolute value of the normalized TFCF $\check{R}[\nu'_p, \tau_q]$ of the measured channel.

For performance analysis, we have also considered the scattering function $S(\tau', f)$, which is obtained from the two-dimensional discrete Fourier transform of the TFCF $R[\nu'_p, \tau_q]$. We have illustrated the comparison between the scattering functions of the measured channel and those of the simulation models in Figs. G.7 and G.8. An excellent agreement between the measured channel and the simulation models' scattering functions is observed when the proposed INLSA-TF method is used (see Fig. G.7). The results presented in Fig. G.8 demonstrate the poor performance of the INLSA-T-F and the INLSA-F-T methods in terms of fitting the scattering function of the measured channel.

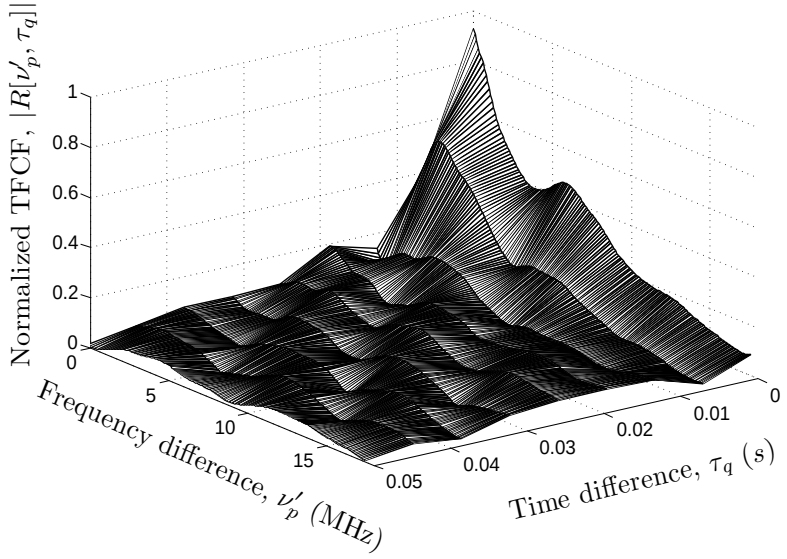

Figure G.3: Absolute value of the normalized TFCF $R[\nu'_p, \tau_q]$ of the simulation model with the parameters estimated by using the proposed INLSA-TF method.

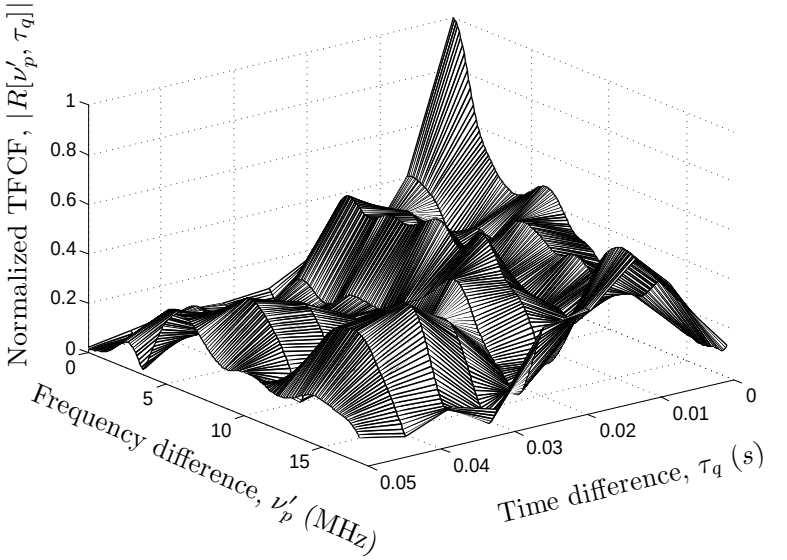

Figure G.4: Absolute value of the normalized TFCF $R[\nu'_p, \tau_q]$ of the simulation model with the parameters estimated by using the INLSA-T-F method.

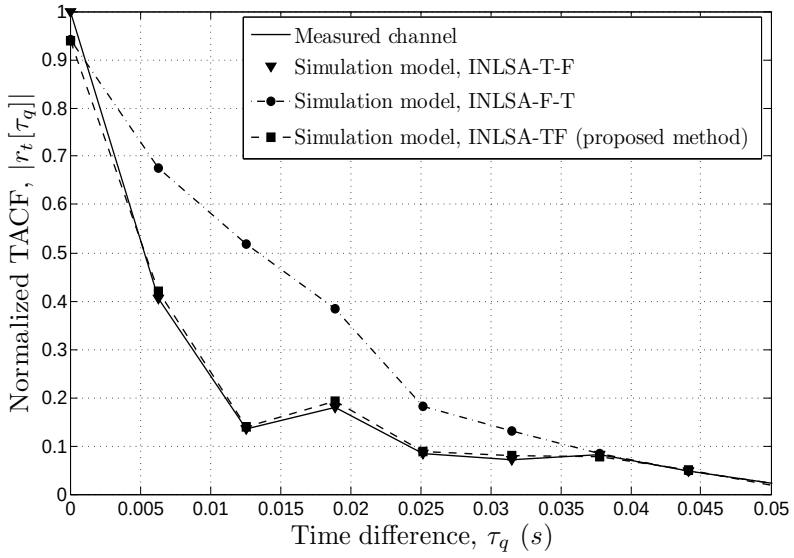

Figure G.5: Examples of estimated TACFs.

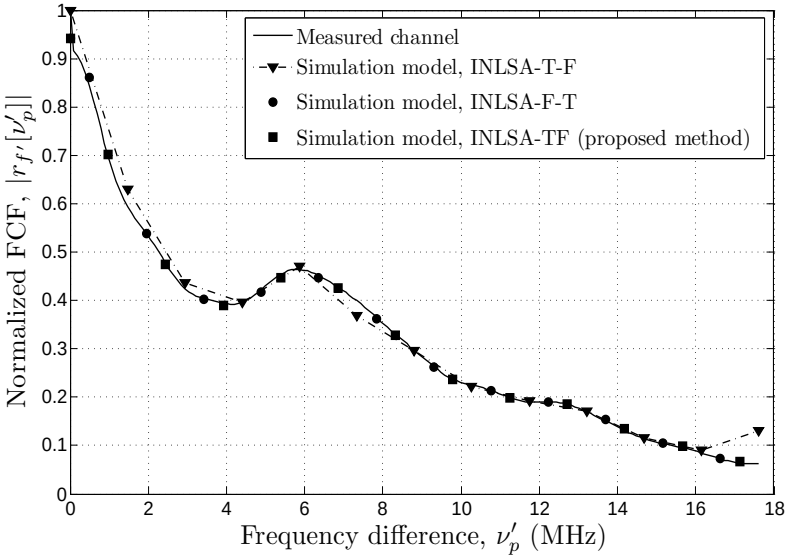

Figure G.6: Examples of estimated FCFs.

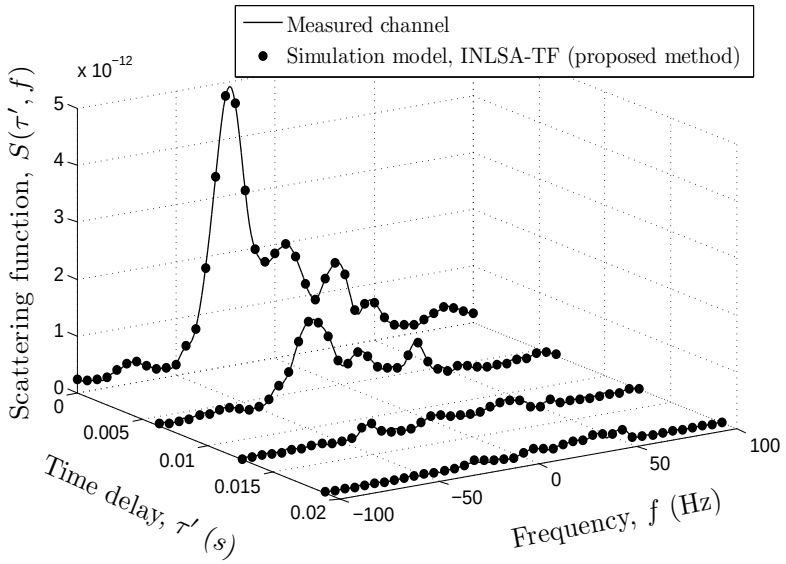

Figure G.7: Comparison between the scattering functions of the measured channel and the simulation model designed by using the INLSA-TF method.

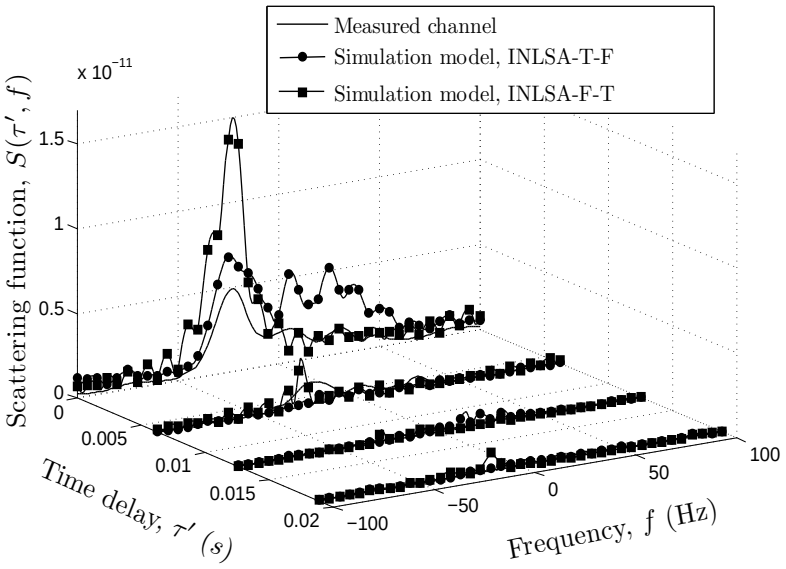

Figure G.8: Comparison between the scattering functions of the measured channel and the simulation model designed by using the original INLSA method.

V. Summary and Conclusions

In this paper, we presented the INLSA-TF method for designing the measurement-based stochastic simulation models. The INLSA-TF method aims to fit the TFCF of the simulation model to that of the measured channel. The proposed method is an extension of the INLSA method. It has been shown that the two original versions of the INLSA method can be described as a special cases of the proposed method.

The proposed INLSA-TF method has been applied on measurement data collected in urban environment to estimate the parameters of the simulation model. The correlation properties of the simulation model have been compared to those of the measured channel. A comparison has also been made with respect to the goodness of fitting the scattering function of the channel simulator to that of a measured channel. The obtained results demonstrated that the proposed INLSA-TF algorithm precisely estimates the simulation model parameters and provides an excellent fitting to real-world channels. Finally, it has been shown that the proposed version of the INLSA method significantly outperforms the original version.

References

[1] P. Almers, E. Bonek, A. Burr, N. Czink, M. Debbah, V. Degli-Esposti, H. Hofstetter, P. Kyösti, D. Laurenson, G. Matz, A. F. Molisch, C. Oestges, and H. Özcelik, "Survey of channel and radio propagation models for wireless MIMO systems," *EURASIP J. Wireless Commun. Net.*, vol. 2007, Article ID: 19070, 2007.

[2] P. Bello, "Characterization of randomly time-variant linear channels," *IEEE Trans. Commun.*, vol. 11, no. 4, pp. 360–393, 1963.

[3] G. D. Durgin, *Space-Time Wireless Channels*. NJ: Prentice Hall, 2003.

[4] R. S. Thomä, D. Hampicke, M. Landmann, A. Richter, and G. Sommerkorn, "Measurement-based parametric channel modelling (MBPCM)," in *Int. Conf. on Electromagnetics in Advanced Applications, (ICEAA 2003)*, Torino, Italia, Sept. 2003.

[5] M. Pätzold and B. O. Hogstad, "A space-time channel simulator for MIMO channels based on the geometrical one-ring scattering model," *Wireless Communications and Mobile Computing, Special Issue on Multiple-Input Multiple-Output (MIMO) Communications*, vol. 4, no. 7, pp. 727–737, Nov. 2004.

[6] R. Schmidt, "Multiple emitter location and signal parameter estimation," *IEEE Trans. Antennas Propag.*, vol. 34, no. 3, pp. 276–280, Mar. 1986.

[7] R. Roy and T. Kailath, "ESPRIT-estimation of signal parameters via rotational invariance techniques," *IEEE Trans. Acoust., Speech, Signal Processing*, vol. 37, no. 7, pp. 984–995, Jul. 1989.

[8] M. Haardt and J. A. Nossek, "Unitary ESPRIT: how to obtain increased estimation accuracy with a reduced computational burden," *IEEE Trans. Signal Process.*, vol. 43, no. 5, pp. 1232–1242, May 1995.

[9] M. Feder and E. Weinstein, "Parameter estimation of superimposed signals using the EM algorithm," *IEEE Trans. Acoust., Speech, Signal Processing*, vol. 36, no. 4, pp. 477–489, Aug. 1988.

[10] B. H. Fleury, M. Tschudin, R. Heddergott, D. Dahlhaus, and K. I. Pedersen, "Channel parameter estimation in mobile radio environments using the SAGE algorithm," *IEEE J. Select. Areas Commun.*, vol. 17, no. 3, pp. 434–450, Mar. 1999.

[11] W. Li and Q. Ni, "Joint channel parameter estimation using evolutionary algorithm," in *Proc. IEEE Int Communications (ICC) Conf*, 2010, pp. 1–6.

[12] B. H. Fleury, X. Yin, K. G. Rohbrandt, P. Jourdan, and A. Stucki, "Performance of a high-resolution scheme for joint estimation of delay and bidirection dispersion in the radio channel," in *Proc. 55th IEEE Veh. Technol. Conf., VTC2002-Spring. Singapore*, May. 2002, pp. 522–526.

[13] C. B. Ribeiro, E. Ollila, and V. Koivunen, "Stochastic maximum likelihood method for propagation parameter estimation," in *Proc. PIMRC*, vol. 3, Sept. 2004, pp. 1839–1843.

[14] W. Li, W. Yao, and P. J. Duffett-Smith, "Improving the SAGE algorithm with adaptive partial interference cancellation," in *Proc. IEEE 13th Digital Signal Processing Workshop and 5th IEEE Signal Processing Education Workshop DSP/SPE 2009*, 2009, pp. 404–409.

[15] D. Umansky and M. Pätzold, "Design of measurement-based wideband mobile radio channel simulators," in *Proc. 4th Int. Symp. Wireless Communication Systems ISWCS 2007*, 2007, pp. 229–235.

[16] L. Hentilä, P. Kyösti, J. Ylitalo, X. Zhao, J. Meinilä, and J.-P. Nuutinen, "Experimental characterization of multi-dimensional parameters at 2.45 and 5.25 GHz indoor channels," in *Proc. 8th International Symposium on Wireless Personal Multimedia Communications, WPMC 2005*, Aalborg, Denmark, Sept. 2005, pp. 254–258.